STRUCTURE, GEOCHRONOLOGY AND GEOCHEMISTRY OF THE KADAVUR DOME, SOUTHERN INDIA.

A thesis presented to the

School of Geology and Geophysics,

University of Adelaide,

by William Teale, 2010

Abstract

An Investigation of the structure of the Kadavur Dome in India's Southern Granulite Terrain has revealed an absence of domal features, and instead evidence for poly-deformational folding and thrusting. Zircon U/Pb analysis by Laser Ablation Inductively Coupled Mass Spectrometry (LA-ICPMS) reveals that the quartzites of the Kadavur Valley in the north of the Madurai Block were deposited between the late Palaeo- and early Neoproterozoic. The depositional age and the detrital zircon populations found in the Kadavur quartzites are analogous to the depositional age and detrital zircon populations found in the Itremo Group of central Madagascar, which has been identified as a part of the former continent Azania. Metamorphic zircon rim analyses of Kadavur quartzites yield dates of ~840ma and ~882 Ma. These rims are interpreted as a result of contact metamorphism induced by the intrusion of nearby anorthositic gabbros, dated in this study at 825 ± 17 Ma. Thermal Ionisation Mass Spectrometry (TIMS) on whole rock samples of the igneous suite present in the Kadavur area reveal negative εNd values, while evidence of crustal contamination has been found by both Sensitive High Resolution Ion Microprobe (SHRIMP) analysis of oxygen isotopes and LA-Multicollector-ICPMS analysis of Lu/Hf isotopes. Thin section analysis reveals that the igneous suite is divided mineralogically into two broad groups. Major, trace and rare earth element (REE) geochemical analysis of these groups shows that they are also divided chemically. Geochemical discrimination plots of these samples suggest an Island Arc Basalt/Tholeiite petrogenesis. Of particular interest is a felsic gneiss sampled in the Kadavur Valley that has been interpreted as either a tuffaceous/volcanoclastic meta-sediment or felsic intrusive. The implication of this sample being a tuffaceous meta-sediment is that its age would date the Kadavur sequence and hence date the Itremo Group.

Acknowledgements

Thanks go to my wonderful partner Jen Pitman for her munificent support throughout my uni career. Thank you to my primary supervisor Alan Collins for making it all possible, and to my secondary supervisor John Foden. The project was funded by an Australian-Indian research grant. Thanks also to the GRI and to Santosh for making our time in India so great. Dad, thanks so much for all your support, guidance and help with this project and with everything else, and Mum thanks for always supporting me and listening to me grumble. Staff at Adelaide Microscopy, particularly Ben Wade and Angus Netting, were extremely helpful. A big thankyou also goes to Mark Fanning for the oxygen isotope work undertaken and for advice given. Thanks to Diana Plavsa for helping with my Hf work and to Justin Payne for all your advice and support. David Bruce was a huge help throughout the TIMS process, thank you. Big thanks also to Ian Pontifex for all your help, especially with photomics, and thanks also to Alan Purvis. Thank you to my field buddies Steph Rowe and Venkata Siva and also to Jade Anderson, Libby Metz, Billy Reid, Alec Walsh and all the honours crew who were generous with advice and encouraging words whenever I needed them. Conversations with Campbell Harvey helped me greatly and kept me (mostly) sane.

Table of contents

1. Introduction

As Gondwana amalgamated during the late Neoproterozoic and into the early Cambrian, Azania, a continent in the Mozambique Ocean that consisted of parts of contemporary Madagascar, East Africa, Arabia and south India, collided with the Congo-Tanzania-Bangweulu Block at ~640 Ma forming the East African Orogeny. This was followed at ~550 - 515 Ma by the Malagasy Orogeny which resulted in the collision of Azania/Africa with India during the final amalgamation of the supercontinent Gondwana (Collins and Pisarevsky 2005). Oceans in the path of the colliding continents and arcs were consumed. The Mozambique Ocean, which separated the Congo/Tanzania/Bangweulu Block from Neoproterozoic India, was one example of this (Santosh *et al*, 2009). The suture zone that marks its closure has been identified in Madagascar and named the Betsimisaraka suture. Madagascar lay directly alongside southern India in eastern Gondwana. The possible continuation of the Madagascan Betsimisaraka suture into India is an issue of debate. It has been suggested that the Palghat-Cauvery shear zone (PCSZ), in places up to 100 km wide, could be the continuation of the suture into India. The PCSZ lies along strike of the Betsimisaraka Suture and forms a high pressure granulite belt which separates crustal domains of different histories (Collins et al, 2007). These differing crustal zones are known as the Dharwar Craton north of the PCSZ and the Southern Granulite Terrain (SGT) south of PCSZ. The Dharwar Craton is largely made up of greenschist to amphibolite grade metamorphism, with common BIF and mafic-ultramafic supracrustal rocks, and rare associated calc-silicates. Conversely the SGT has mainly granulite grade of metamorphism and abundant calc-silicates with rare BIF and mafic-ultramafic supracrustal rocks (Ghosh *et al.*, 2004). The SGT is made up of the Madurai Block in the north and the

Trivandrum Block in the south (Fig. 1). The Blocks are separated by the Achancovil shear zone, which is also a possible suture zone (Cenki and Kriegsman, 2005).

This study focuses on an area in the north of the Madurai Block known as the Kadavur Dome or the Kadavur Valley. The Dome is located at approximately 10°35'03.67"N, 78°11'44.64"E in the state of Tamil Nadu, Southern India (Fig. 1). This places the study area approximately 35 km south of the PCSZ. The supposed Kadavur Dome is formed by the central Kadavur Valley, with gabbro, anorthositic leuco-gabbro and older retrogressed felsic bodies (possible volcanoclastic/ tuffaceous sediment or felsic volcanic) enclosed by quartzite and calc-silicate ridges in a roughly circular shape, as shown in Figure 2. The Dome is approximately 17 km east to west and 12 km north to south. A representative suite of all rock types in the area was collected with the aim of addressing several questions. Firstly, is the Kadavur area part of the Dharwar Craton or is it part of an exotic block such as Azania (relicts of which are now found in Madagascar)? This question also alludes to whether the PCSZ is in fact a suture zone. Secondly, how does the igneous suite fit in to the tectonic evolution of the Kadavur area? And finally the structure of the Dome will be examined. The samples were collected during fieldwork, as was field data such as foliations and lineations. Geochronological data was gathered from Laser Ablation Inductively Coupled Plasma Mass Spectrometry (LA-ICPMS) and Multicollector Inductively Coupled Plasma Mass Spectrometry (MC-ICP-MS) zircon analysis (U-Pb and Lu-Hf respectively). These data were compared with data from Madagascar, specifically with the Itremo Group of central Madagascar, as this has been identified as a likely match by Collins et al. in 2007. The data from this study were also compared with data from the Dharwar Craton and other potential source areas to ascertain whether the northern Madurai block was always joined to the

Dharwar Craton or was in fact part of an exotic block that was consumed by the closure of the Mozambique Ocean during Gondwana amalgamation. Geochemical analysis of all fifteen samples was undertaken by Amdel–Bureau Veritas at Wingfield, South Australia. Geochemical data have been used to make interpretations about petrogenesis and provenance. A comparison of the Kadavur Dome geochemistry with that of Itremo Group geochemistry has been made. Thermal Ionisation Mass Spectrometry (TIMS) Sm-Nd isotopic analysis was also undertaken, as was oxygen isotope analysis by Sensitive High Resolution Ion Microprobe (SHRIMP). This data has been used to make interpretations about the geochemical and geochronological framework of the Kadavur Dome and the northern Madurai Block.

2. Analytical Methods

2.1. Structure and petrology.

Field work was undertaken for seven days in January. This time was spent collecting structural data at locations in and around the Kadavur Dome. Measured structural data consisted mostly of foliation and lineation measurements, but where possible fracture cleavage and bedding measurements were also taken. Data was measured and presented as dip/dip direction. Figures 3 and 4 show more detailed data collected along two short transects. The first transect of approximately 1.6 km cut the eastern edge of the Dome and is referred to as the Poonani Dam transect. A small section (~400m) of this transect was sketched and photographed in detail (Figure 7.1, 7.2 and 7.3). The second transect of approximately 1.5km covered an area on the north western inner slopes of the dome. Further data was collected

wherever access permitted, generally where roads cut through the Dome and into the Kadavur Valley.

In addition to structural data, fifteen samples were collected for geochronological, geochemical and petrographic analysis. These samples were selected as they form a representative suite of samples from the general region. Figure 2 and Table 1 summarise sample locations. Four quartzites were sampled for possible detrital zircon age analysis. A further eleven samples were chosen for geochemical analysis of the igneous suite present within the dome. These samples consisted of five gabbros, three anorthositic gabbros, one gabbro-norite, one felsic gneiss and one hedenbergite-scapolite calc-silicate. Ten samples were probed with the Cameca electron-microprobe at Adelaide Microscopy to identify variants and chemical formulae of plagioclase, hornblende, biotite, clinopyroxene and orthopyroxene (Table 14). The probe data was also collected for geothermometry purposes.

2.2. Geochronology

2.2.1. U/Pb Laser Ablation Inductively Coupled Plasma Mass Spectrometry (LA-ICPMS):

Samples chosen for geochronological analysis included three quartzites, one anorthositic gabbro and one felsic gneiss. Rock samples were crushed in a large steel jaw crusher, a smaller steel jaw crusher and then briefly milled in a tungsten-carbide mill. The resulting crushate was then sieved using 425 µm and 79 µm mesh. The >79 µm and <425 µm fraction was panned for heavy minerals. A neodymium magnet was used to remove magnetic heavy minerals, and the remaining fraction consisted largely of zircons, monazites and residual quartz. This fraction was used for zircon selection. One sample (WTKV13) required the use of methylene iodine

heavy liquids for further separation. A Frantz magnetic separator was not used to avoid possible contamination and to ensure the broadest range of zircons possible. Zircons were handpicked with qualitative analysis in mind (picking a wide selection of the population, no particular age range being sought) using a binocular microscope. The zircons were mounted in epoxy resin and the mounts were then polished to remove approximately a third of each zircon, leaving flat surfaces suitable for imaging. The mounts were then carbon coated by staff at Adelaide Microscopy, and imaged by the author using a Phillips XL20 scanning electron microscope (SEM). Images taken included back scattered electron (BSE) images of the entire collection of mounted grains for use as a map, and cathodoluminescence (CL) images of smaller groups (3-4) of zircons for greater individual study. Zircons were ablated with a New Wave Research UP-213 laser using a spot size of 30µm, frequency of 5Hz and intensity at 75%. Isotopes ($^{206}Pb/^{238}U$, $^{207}Pb/^{235}U$, $^{207}Pb/^{206}Pb$ and $^{208}Pb/^{232}Th$) were measured with the attached Agilent 7500 series Inductively Coupled Plasma Mass Spectrometer (ICP-MS). An internal standard (Plesovice, published $^{207}Pb/^{206}Pb$ age of 339.22 ± 0.25 Ma, $^{206}Pb/^{238}U$ age of 337.13 ± 0.37 Ma) and external standard (GJ, published $^{207}Pb/^{206}Pb$ age of 607.7 ± 4.3 Ma, $^{206}Pb/^{238}U$ age of 600.7 ± 1.1 Ma) were analysed repeatedly throughout the sessions to correct machine drift and ablation data. Over the course of the laser sessions, a total of 228 GJ external standard analyses gave a weighted average $^{207}Pb/^{206}Pb$ age of 608.4 ± 3.7Ma (MSWD = 0.48), and a weighted average $^{206}Pb/^{238}U$ age of 600.68 ± 0.98 Ma (MSWD = 0.75). A total of 112 Plesovice internal standard analyses were made, and gave a weighted average $^{207}Pb/^{206}Pb$ age of 343.6 ± 5.8 Ma (MSWD = 1.2), and a weighted average $^{206}Pb/^{238}U$ age of 336.0 ± 2.7 Ma (MSWD = 11.4).

Data were collected, corrected and filtered in the GLITTER version 3.0 (Van Achterbergh et al. 2001) software package. Concordia diagrams (after Wetherill, 1956) and weighted average age plots were created using ISOPLOT 4.11 for Excel (Ludwig, 2009). Probability distribution plots were created using AgeDisplay for Excel (Sircombe, 2004).

2.2.2. *Sm/Nd model ages*

Methods for TIMS sample preparation and analysis can be found in Section *3.3.2*. of this paper. Results from the TIMS SM/Nd isotope analysis of samples WTKV01, 02, 04, 07 and 09 were used in creation of an Nd isochron. The plots were created using ISOPLOT 4.11 for Excel (Ludwig, 2009).

2.3. Geochemistry

2.3.1. *Major and trace elements:*

Samples were crushed as per preparation of geochronology samples. Samples were then thoroughly milled with a tungsten-carbide mill to a size of < 180 µm. The resulting powder was sent to Amdel analytical laboratories in Wingfield, South Australia for analysis. Four different methods of analysis were chosen. For measuring the major oxides and Cr, V, Sc and Zr a 0.1 g subsample of the powdered material was fused with lithium metaborate followed by dissolution to give a total concentration for any given element. The solution was then analysed using an Inductively Coupled Plasma-Optical Emission Spectroscope (ICP-OES) for determination of element concentrations. The solution from the lithium metaborate fusion process was also analysed with an ICPMS for Ba, Be, Hf, Sn and Ta. To measure the concentrations of Cs, Ga, Zn, Ce, La, Mo, Nb, Rb, Sr, Th, U, and Y a

small subsample of around 0.5 g was digested using an HF/multi acid digest and the solution was then analysed with an ICPMS. Concentrations of Dy, Er, Eu, Gd, Ho, Lu, Nd, Pr, Sm, Tb, Tm and Yb were also measured by ICPMS.

2.3.2. *Sm, Nd and Sr isotopes by Thermal Ionisation Mass Spectrometry (TIMS):*

Sample numbers WTKV01, WTKV04, WTKV07 and WTKV09, were selected on the basis that they represented a range from mafic through to leucocratic gabbroic rock types that may possibly yield an isochron. WTKV02, a quartzite, was also included for TIMS analysis. Samples were crushed and milled as per major and trace element preparation (see 3.2.1. and 3.3.1.). Samples were then weighed into cleaned Teflon flasks. Table 2 shows sample and spike weights. Samples containing zircons (WTKV02 and WTKV09) were weighed into Teflon bombs. Blanks, Internal standard BHVO-2 and international standard JNDi-1 were used as a quality control. Samples were spiked with a known concentration of Sm/Nd/Sr spike to allow low level samples to be detectable. The samples were then dissolved completely using HF and overnight heating at 140° C. Samples in Teflon bombs were encased in steel pressure cylinders to ensure dissolution of refractory minerals. Samples were then evaporated to dryness. The addition of ~1 mL of 7M HNO_3 just prior to dryness reduced the formation of insoluble fluorides. The samples were then dissolved again with a mix of HF and HNO_3, again heating overnight at 140° C. Samples were evaporated to dryness, with the late addition of HNO_3 to prevent insoluble fluoride formation, and then dissolved completely on a hotplate overnight in 6M HCL. Samples were then put in a centrifuge for 5 minutes at 13200 rpm, before being run through Biorad Poly Prep ion exchange columns with 2 mL AG50W X8 200-400 mesh Biorad cation exchange resin to separate Sr, and through separate columns with 2 mL teflon powder impregnated with HDEHP to separate Sm and Nd. Isotopes

($^{143}Nd/^{144}Nd$, $^{150}Nd/^{144}Nd$, $^{147}Sm/^{149}Sm$ and $^{152}Sm/^{149}Sm$ and $^{87}Sr/^{86}Sr$) were measured with a Finnigan MAT 262 thermal ionisation mass spectrometer. Values for ppm concentrations and εNd were calculated with a spreadsheet for excel, as provided by David Bruce of the University of Adelaide. This spreadsheet uses the values for CHUR of Goldstein et al (1984).

2.3.3. *Lu/Hf Isotopes by Laser Ablation Multicollector Inductively Coupled Plasma Mass Spectrometry (LA-MC-ICPMS):*

The zircon mounts prepared for U/Pb LA-ICPMS analysis were also used for Lu/Hf isotopic studies undertaken on the LA-MC-ICPMS at Waite (CSIRO) campus, South Australia. Only grains that U/Pb LA-ICPMS analysis found to be greater than 95% concordant were analysed for Hf with the LA-MC-ICPMS. Laser spots were placed as close as possible to concordant U/Pb LA-ICPMS spots, within the same CL zone. Zircons were ablated with a New Wave UP-193 Excimer laser (193 nm) using a spot size of 50 µm, frequency of 5 Hz, 4ns pulse length and an intensity of ~8-10J/cm2. Zircons were ablated in a helium atmosphere, which was then mixed with argon sample gas upstream of the ablation cell. The attached Thermo-Scientific Neptune Multi Collector measured ^{171}Yb, ^{173}Yb, ^{175}Lu, ^{176}Hf, ^{177}Hf, ^{178}Hf, ^{179}Hf and ^{180}Hf on Faraday detectors with $10^{12}\Omega$ amplifiers. A 0.232 second integration time was used. Methods recommended by Woodhead et al. (2004) for interference and mass bias corrections were followed. Exponential law fractionation correction with a stable isotope ratio of $^{179}Hf/^{177}Hf = 0.7325$ was used to correct Hf mass bias. Isobaric interference of Yb on ^{176}HF was corrected by direct measurement of Yb fractionation using $^{171}Yb/^{173}Yb$ together with the Yb isotopic values of Segal et al. (2003). T (DM) and T (DM) $_{crustal}$ were calculated using ^{176}Lu decay constant after Scherer, et al.,

(2001). Methods for other interference corrections, calibration and confirmation of accuracy are as Justin Payne, pers comm, 2010.

"Yb isobaric interference on 176Hf was corrected by direct measurement of Yb fractionation using $^{171}Yb/^{173}Yb$ coupled with the Yb isotopic values of Segal et al. (2003). The applicability of these values were verified by analysing JMC 475 Hf solutions doped with varying levels of Yb with interferences up to $^{176}Yb/^{177}Hf$= ~0.5. Lu isobaric interference on 176Hf corrected using a 176Lu/175Lu ratio of 0.02655 (Vervoort et al., 2004) assuming the same mass bias behaviour of as Yb. For Yb signals below 10 mV interference corrections were made using an empirically derived 176Yb/173Yb ratio and the Hf mass bias factor similar to the method described by Griffin et al. (2000). This was done as the potential errors involved in the method are outweighed by the significantly greater uncertainty caused by the small Yb beam. In this case an empirically derived ratio of 0.739689 was used. This was derived by analysis of a series of Yb and Hf doped glass beads. Set-up of the system prior to ablation sessions was conducted using analysis of JMC475 Hf solution and an AMES Hf solution. Confirmation of accuracy of the technique for zircon analysis was monitored using a combination of the Plesovice, Mudtank and QGNG standards."

The average value for Plesovice for the analytical session was 0.282496 (2SD=0.000022, n=27). This compares to the published value of 0.282482 +/- 0.000013 (2SD) by Slama et al (2008).

2.3.4. Oxygen isotopes by Sensitive High Resolution Ion Microprobe (SHRIMP)

Analysis of oxygen isotopes was undertaken by Mark Fanning at the Australian National University (ANU) in Canberra, using a Sensitive High Resolution Ion Microprobe (SHRIMP). Only sample WTKV09, an anorthositic gabbro, was analysed. The zircon mount used for geochronology (see 3.2.1.) was sent to Canberra, where it was re-mounted into a “mega-mount” with standard zircons (Temora (3)), and analysed using the SHRIMP. Oxygen isotope ratios were normalised relative to Temora (3) = 7.59 ‰. Uncertainty in the Temora analyses for the analytical session was ± 0.2739 ‰ (2 s.e.). CL images were used to analyse as near as possible to the laser holes made during U/Pb LA-ICPMS while remaining within the same CL zone.

3. Results

3.1. Structure and petrology.

3.1.1. Structure

Based on small scale structural mapping, the Kadavur Dome is likely to have been formed by poly-deformational folding and thrusting rather than the intrusion of gabbroic and anorthositic plutons. Structural transect maps are shown in figures 3 and 4. The Poonani Dam transect (Fig. 3) shows that the dominant foliation at this locality (on the eastern edge of the Dome) plunges predominantly very steeply towards the east *and* west, whereas a true dome should exhibit only foliations that dip (gently) outwards from the centre (Whitney et al., 2004). Lineations (rodding/stretching) for the most part are highly variable, as with measured lineations on the north western transect. Stereonets for these data are shown in Figure 5. North dipping shear faces were also observed. These features can be seen in the

detailed sketch of ~400 m of this transect (Fig 7.1, 7.2 and 7.3) and in photographs taken at the various locations (Figs. 8 - 16). The small transect in the Dome's north west exhibits foliations that dip steeply towards the south, south east and east, shown in Figure 4. Stereonets for this transect are shown in Figure 6.

The highly variable plunge and plunge direction of the dominant lineation present indicates that this lineation has been folded. Foliations have also been subjected to later deformation and folding and this can be observed in outcrop where strong foliation can range from sub-vertical to horizontal (Figs. 8 - 16). The strong foliation is parallel to bedding, termed here S_0. There is some petrological evidence to suggest that this foliation may have been preceded by an earlier event, (e.g. folded sillimanite perpendicular to the strong fabric), but the strong foliation is for this study termed S_1. It is suggested that the Kadavur Dome is related to later folding (F_2/D_2) of this S_1 fabric and is not a domal structure cored by a mafic pluton. The S_1 fabric is at all times parallel to sub-parallel to S_0 suggesting that the earliest observable folding was isoclinal. Evidence for D_2/F_2 folding can be seen in Figures 8-16. Although there is no observable penetrative fabric associated with this folding a fracture cleavage (S_2) has been developed (Figs. 14 and 15). This fracture cleavage, where observed, always trends east west (sub-vertically) and suggests that D_2/F_2 maximum principal stress was north south.

3.1.2. *Petrology*

Detailed petrological and mineragraphic descriptions of the fifteen samples can be found in Appendix 1. Photomicrographs of points of interest are shown in Figures 55 - 79. A summary of the differing rock types follows.

3.1.2.1. Meta-sedimentary samples:

Quartzites and calc-silicates occur in the study area with quartzites dominating (WTKV02, WTKV03, WTKV14 and WTKV15). The quartzites are usually very coarse grained, containing greater than 90% quartz. Sillimanite, both prismatic and fibrolitic can be present up to 7% and is fabric forming, showing a strong preferred orientation. The acicular sillimanite pins quartz growth (Vernon, 1976). In addition to sillimanite the quartzites contain minor pinitised cordierite, oxidised and ragged biotite and ilmenite, magnetite, titan-hematite and ferrian-ilmenite. The titan-hematite exsolves ferrian-ilmenite and vice versa. The exsolved mineral can also contain further exsolution. The presence of these oxidised Fe-Ti oxides also occurs within the igneous rocks sampled (e.g. WTKV08). These minerals in the quartzites are fabric forming and most samples contain highly lenticular quartz grains. Retrograde muscovite is present and can sometimes contain fibrolitic sillimanite. Detrital accessory phases are zircon, monazite, rutile and tourmaline, suggesting a granitic or felsic provenance for the original sediments.

Sample WTKV06 is a polygonal textured hedenbergite-scapolite calc-silicate which is dominated by 91% pale green hedenbergite. Scapolite makes up 5% of this sample, along with 2% prograde carbonate, 1% retrograde ferrohastingsite and trace anorthite, sphene, chalcopyrite and apatite.

Sample WTKV13 is a felsic gneiss, (interpreted as a tuffaceous/volcanoclastic meta-sediment or meta-felsic volcanic). The sample is dominated by quartz (36%), perthitic K-feldspar (32%), plagioclase (17%), deep red/brown biotite (6%, this biotite contains ~4.7% TiO_2 i.e. is high temperature biotite), hornblende (5%), and lesser

magnetite, ilmenite with trace pyrite, zircon and apatite. No pyroxenes are present however the hornblende may be replacing former pyroxenes. The sample also contains two distinct zircon populations which were dated.

3.1.2.2. Igneous suite:

There are two variants of the gabbroic suite. The majority of samples investigated contain a deep to mid green hornblende with plagioclase (Figs. 57, 63, 70 and 72). This variant (WTKV01,05, 08, 09, 10 and 11) also contains from 47% to 79% plagioclase, with lesser deep red-brown biotite, significant quartz, retrograde chlorite, sericite, carbonate, hematite, cummingtonite (?), clinozoisite and apatite. The Fe-Ti oxides are dominated by ferrian-ilmenite and/or titan-hematite with some samples containing rutile. Sample WTKV09 was found to contain zircon which was subsequently dated.

The second variant (WTKV04, 07 and 12) is dominated by both orthopyroxene (Mg# 0.658 – 0.722) and clinopyroxene (Mg# 0.563 – 0.574) and contains only minor, deuteric or retrograde hornblende. They contain approximately 30% plagioclase (labradoritic), negligible quartz, no biotite, trace chalcopyrite and pyrite, ilmenite and negligible to absent apatite. This second variant has higher concentrations of Fe, Mg and Ti oxides as shown by Figure 42 (A), (B) and (C).

3.2. Geochronology

U/Pb LA-ICPMS results are presented in Tables 8 - 12, and in Figures 17 - 41. Images (CL) of some analysed zircons are displayed in Figures 17, 20, 23, 28 and 37. $^{207}Pb/^{206}Pb$ ages are used for detrital zircons older than 1Ga and $^{206}Pb/^{238}U$ ages are used for detrital zircons younger than 1Ga, as there is less uncertainty with $^{207}Pb/^{206}Pb$ ages over 1Ga.

3.2.1. *Meta-sedimentary samples:*

Sample WTKV02: This sample is a quartzite. The detrital zircons from the sample form several distinct populations in terms of age; however their appearance within these age populations varies greatly. Some are elongate with lengths averaging 200µm and clear oscillatory zoning under CL (see Fig. 17, (C)). Other zircons have been partially or completely recrystallised and show no real zoning such as those in Figure 17 (A), (B) and (D). Some contain small inclusions within them and/or xenocrystic cores (Fig. 17 (D)). There are smaller round grains with very low CL responses, and also those that are metamict or fractured. Most have very thin, bright rims as seen in the aforementioned figures, which may be Th-rich.

Seventy six analyses were made on seventy zircons (Table 8). This meant the chance of missing a provenance component was less than five percent (Fedo *et al.*, 2003). Sixty five percent of grains were between 90-110% concordant. Only nine grains were less than 80% concordant, with only one grain over 105%. Being detrital zircon grains, ages were spread over several regions of the concordia curve with discernable populations lying on radiogenic lead loss lines towards the origin from around 2100 Ma and 2400 Ma (Fig. 18). These populations are made clearer in the probability density distribution plot (PDD) which shows clear peaks at ~2050 Ma and

~2450 Ma, with lesser peaks at ~2175 Ma and ~2700 Ma (Fig. 19). The oldest analysis yielded a $^{207}Pb/^{206}Pb$ age of 3309.1 ±15.71 Ma (92% concordant, 1σ error) from analysis number WTKV02_73 (Fig. 17 (C)). The maximum depositional age for this quartzite is 1969 ± 19 Ma (93% concordant, 1σ error), based on the youngest concordant zircon analysed, WTKV02_29 (Fig. 17 (A)). The thin, bright rims were too thin for laser ablation to be successful.

Sample WTKV03: This sample is also a quartzite with a wide range of zircon morphologies and textures. The elongate zircons present in WTKV02 are not present in this sample. Zircons in this sample are generally sub-rounded. Oscillatory zoning is well defined in most cases. Several grains in this sample are fractured. A few grains exhibit irregular concentric zoning, convolute zoning or inclusions (Fig 20 (A) – (D)). Several display bright CL rims, however most of these rims were too small for laser ablation analysis.

Seventy six analyses were made on sixty six zircons (Table 9); again sufficient to reduce chances of missing a provenance component to less than five percent. This sample contained a great deal of discordant ages, with 55% of grains being less than 80% concordant. The concordia plot for these zircon analyses shows two relatively clear populations lying on separate radiogenic lead loss lines towards the origin from ~2100 Ma and ~2450 Ma (Fig. 21). The probability distribution plot also shows groupings at ~2100 Ma and ~2450 Ma, as well as at ~2300 Ma and ~2700 Ma (Fig. 22). The maximum depositional age for the sample is 2040 ± 23 Ma (102% conc., 1σ error) based on the most concordant of the younger zircons (WTKV03_09). The oldest analysis was 3218 ± 18 Ma ($^{207}Pb/^{206}Pb$ age, 1 σ error, WTKV03_42, see Fig. 20 (C)) but the analysis was only 83% concordant. The oldest concordant zircon was 3021 ± 16 Ma ($^{207}Pb/^{206}Pb$ age, 92% conc., 1 σ error). Analysis WTKV03_10

was of a rim and gave a $^{206}Pb/^{238}U$ age of 882.3 ±13.21 Ma with concordancy of 92% (Fig 20 (B)). This is interpreted as being related to new zircon growth during contact metamorphism instigated by the intrusion of nearby gabbros, anorthosites and norites. This also provides a minimum depositional age of this quartzite.

Sample WTKV14: This sample is a quartzite with detrital zircon populations of mixed appearance. Most zircons are sub-rounded, and many contain xenocrystic cores up to 200µm in diameter, surrounded by broad (up to 200µm), homogenous rims (see WTKV14_14, Fig. 23 (C)). Many of the zircons in this sample, such as WTKV14_44 in Fig. X, have been completely recrystallised and their ages reset. Recrystallisation is often reasonably homogenous. Zircons with CL visible zoning are rare; WTKV14_13 is one exception, with zoning running parallel to the long axis of the well rounded grain (Fig. 20 (D)).

Eighty two analyses were made on 59 zircons. Thirty five of the eighty two analyses were above 90% and below 105% concordant. While twenty three of the remaining analyses were above 80% concordant, a further twenty four were below 80%. This discordance is interpreted as being a result of radiogenic lead loss which likely occurred during a metamorphic event at around ~800 - 840 Ma. A concordia plot for the concordant core analyses is shown in Fig. 26. The PDD plot (Fig. 24) shows there are a spread of ages from approximately 1750 Ma to approximately 2700, with clear peaks of concordant data at ~2000, ~2400 and ~2700 Ma. A peak is also visible at ~800 Ma, which is from rim analyses. Rim analyses of 24 metamorphic rims show a clear episode of metamorphic growth. Fourteen rims show Neoproterozoic ages, with 90 – 100% concordant analyses giving a $^{207}Pb/^{206}Pb$ weighted average age of 840 ± 21 Ma (MSWD = 0.28, n=6, see Fig 25). A concordia plot for these more concordant younger rims gives an age of 831±25 Ma (MSWD =

1.2, see Fig. 27). This is within error of the event recorded in sample WTKV09 and WTKV13. The remaining 10 rim analyses were all discordant, likely due to lead loss from the ~ 840 Ma event, and returned $^{207}Pb/^{206}Pb$ ages from 1290.7 ± 21.93 Ma (70 % conc.) to 2320.5 ± 1761 Ma (67% conc.). The oldest zircon analysed was WTKV14_45 (Fig. 23 (A)), which yielded a $^{207}Pb/^{206}Pb$ age of 3252 ± 15 Ma (83% conc., 1 σ error). The oldest *concordant* zircon yielded a $^{207}Pb/^{206}Pb$ age of 2876.6 ± 17 Ma (100% conc. 1 σ error), and maximum depositional age is 1996 ± 17 Ma (97% conc., 1 σ error), given by the most concordant of the younger zircon cores.

Sample WTKV13: This sample is a felsic gneiss (tuffaceous/volcanoclastic meta-sediment or meta-felsic volcanic) and contains the assemblage quartz-perthitic K-feldspar-plagioclase-biotite-hornblende. The zircons in this sample were of various morphologies. There were abundant elongate grains, some with zoning parallel to the long axis of each grain, some with convolute zoning and some with rounded or broken terminations (Fig 28 (A) and (D)). Several grains appear to be of igneous origin, such as the grain in Figure 28 (A), with clear zoning. Equant grains are also present, and have similar zoning features to the elongate grains. In terms of CL response, there are two distinct groups. One group has a relatively dark CL appearance, and these are the largely elongate to equant zircons. The second group is very bright, mostly irregularly shaped, almost all of which appear quite homogeneously textured. See Fig. X (A)-(D) for examples of typical morphologies for this sample. There are rare grains with bright CL responses that show oscillatory zoning (Fig. 28 (C)). This CL response difference correlates with age populations. Zircons with a bright CL response yielded Neoproterozoic ages ~790 Ma and the darker CL zircons yielded Palaeoproterozoic ages.

Seventy two analyses were made on 69 zircons (Table 11). Over sixty percent of grains were between 90 and 105% concordant. There were three highly discordant $^{207}Pb/^{206}Pb$ analyses of 2753.9 ± 35.53 Ma, 3439.9 ± 27.99 Ma and 3499.9 ± 24.63 Ma (1 σ error, 36%, 36% and 34% concordant respectively). These analyses gave $^{206}Pb/^{238}U$ ages of 1004 ± 15, 1230 ± 18 and 1206 ± 17 Ma (1 σ error), which are more in line with the bulk of analyses. The rest of the analyses fell into two distinct age groups, clearly visible on the probability density plots and the concordia plots (Fig. 29 and 30 respectively). Cores greater than 95% concordant returned ages between 1727 ± 18 Ma and 1836 ± 26 Ma. Based on concordia interpretation the zircons were divided into age groups. The first group returned a weighted average $^{207}Pb/^{206}Pb$ age of 1779 ± 15 Ma (95 - 100% conc., n = 34, MSWD = 2.6). The second group is 789 ± 33 Ma ($^{207}Pb/^{206}Pb$ age, 95 – 100% conc., 1 σ error, n = 7, MSWD = 0.36), which is within error of the crystallisation age of anorthositic gabbro WTKV09. The emplacement of this intrusion is interpreted as the likely cause of lead loss in the older zircons, and is likely to have reset the ages of this younger population to ~800. One discordant, bright CL rim analysis yielded a $^{207}Pb/^{206}Pb$ age of 1814 ± 39 Ma, but a $^{206}Pb/^{238}U$ age of 808 ± 11 Ma, and is likely to have grown during contact metamorphism.

3.2.2. *Igneous sample:*

Sample WTKV09: This sample is a metamorphosed anorthositic gabbro dominated by elongate zircons of ~200µm in length, many of which have sub-rounded terminations. These are uncharacteristic gabbroic zircons, appearing more like detritals. Oscillatory zoning is uncommon, in most cases zoning seems to have been

overprinted by recrystallised or new growth zones. One unusually large zircon is WTKV02_21/22/23 which is ~200µm wide and ~300µm in length and exhibits oscillatory zoning overprinted in parts with recrystallisation (Fig. 37 (A)). Some zircons contain large, homogeneously recrystallised zones such as WTKV09_19 (Fig. 37 (B)). Inclusions are quite common in this zircon population (Fig. 37 (C)).

Fifty analyses were made on forty three zircons (Table 12). Thirty of the fifty analyses were between 90-110% concordant, with seven being inversely discordant. When plotted on a conventional Concordia diagram (Fig. 38) the 95-105% concordant data lie on a discordia with an upper intercept at 802 ± 30 Ma (MSWD = 0.55) and a lower zero intercept. When only the analyses that yielded ages within 5% of Concordia are considered, a weighted mean of the $^{207}Pb/^{206}Pb$ ages yields a value of 825 ± 17 Ma (MSWD=0.66, n=21, Fig. 41). Due to the possibility of undetected common Pb dispersing some of the less concordant data, this weighted mean age is interpreted as being the best estimate of the time of crystallisation of the gabbroic anorthosite.

In summary the U/Pb geochronological data show: Quartzites in the Kadavur Dome area were deposited between 1969 ± 17 Ma (youngest zircon core, sample WTKV02) and 840 ± 21 Ma (metamorphic rim analyses from sample WTKV14). Detrital zircon populations were most prominent at ~2100 Ma and ~2450 Ma with several lesser peaks at between ~1900 and ~2500, ~2700 Ma and from ~3000 - 3200 Ma. Metamorphic zircon rim analyses from two of the three quartzite samples (WTKV03 and WTKV14) revealed metamorphic rim growth at ~840 - 882 Ma. Zircon rims in the third quartzite sample were too thin for laser ablation to be successful. Anorthositic gabbro WTKV09 was crystallized at 825 ± 17 Ma, within error of the even recorded in the rims of sample WTKV14. This ~800 Ma event is also recorded

in sample WTKV13, a felsic gneiss. The latter sample contained two distinct zircon populations. One population yielded a weighted average age of 789 ± 33 and the second population yielded an age of 1779 ± 15 Ma.

The plotted Sm/Nd isochron gave an age of 1171 Ma with a large error of ± 1800 Ma (see Figure 56). The data appear to form two sub-parallel isochrons. These isochrons were plotted using duplicated data and yielded ages of 1245.6±8.8 Ma and 1231±14 Ma. These ages are tenuous at best as they are only two point isochrons.

3.3. Geochemistry

3.3.1. Trace and major elements

The 15 samples are a representative suite of rocks from the Kadavur Dome area. Samples included four quartzites, three meta-gabbros, two layered gabbros, two gabbroic anorthosites, one felsic gneiss, one anorthosite, one gabbro-norite and one hornblende scapolite meta-sediment. Major, trace and rare earth element (REE) data received from Amdel Laboratories are presented in Tables 3 and 4 and figures 42 – 52.

3.3.1.1. Intrusive samples:

As shown by chondrite normalised REE plots in figures 43 and 44, the intrusive rocks are divided chemically into two groups. Samples WTKV04 and WTKV07 (layered gabbros), WTKV11 (meta-gabbro) and WTKV12 (layered gabbro-norite) each exhibit a positive europium anomaly. Of this group only WTKV11 shows petrological signs of being metamorphosed (refer to thin section descriptions,

Appendix 1). The second group consists of samples WTKV01 (meta-gabbro), WTKV05 (layered anorthositic gabbro), WTKV08 (meta-gabbro), WTKV09 and WTKV10 (anorthositic gabbros), each of which displays a relatively flat REE pattern (Fig. 43). The differences in chondrite normalised Eu may be explained by the different variants and abundances of plagioclase feldspars within each sample. Samples dominated by Opx and Cpx (WTKV04, 07, 11) contain mostly labradorite (e.g. WTKV11: $An_{54.051}$). The Hbl/Pl dominated samples (WTKV01, 05, 08, 09, 10, 12) also contain labradorite but more prevalent is bytownite (e.g. WTKV01: $An_{82.56}$-$An_{83.41}$, etc). The more calcic plagioclase in the Hbl/Pl gabbros may contain significant Eu when compared to the less calcic plagioclase in the Opx/Cpx gabbros. Eu, like Sr, is partitioned into calcic plagioclase. Also the Hbl/Pl gabbros are strongly oxidised and this may also account for the observed patterns. The two gabbro variants also display differing spidergram plots, seen in Figure 46 and 47. Sample WTKV11 is an Hbl/Pl dominated gabbro, but has been plotted with Opx/Cpx gabbros as its signature is more akin to those samples.

Two pyroxene geothermometry for sample WTKV04, one of the Opx/Cpx gabbros, was undertaken with data obtained from microprobe analysis. Table 13 summarizes the FeO and MgO values, and calculated temperatures. Temperatures calculated are possibly a too high, ranging from 1251°C to 1478°C. Data collected from the Microprobe are presented in Table

As seen in the ternary plot of FeO (total)/MgO/(Na_2O + K_2O) (after Irvine and Baragar, 1971. Figure 48), the three Opx/Cpx dominated gabbros plot in tholeiitic series space and samples dominated by Hbl/Pl plot in calc-alkaline space, with the exception of sample WTKV11 which plots on the border of each series. The three Opx/Cpx dominated gabbros are slightly less siliceous than the other gabbros, as

seen in Figure 49, a binary plot of SiO_2 versus $Na_2O + K_2O$ after Middlemost (1985). Further classification plots for the gabbroic samples (Figs. 50-52) show that the Opx/Cpx gabbros plot in, or just outside island arc tholeiite/basalt space, as do samples WTKV05 and 11 from the Hbl/Pl dominated group. A ternary plot of $MnO/TiO_2/P_20_5$ (Fig.50, after Mullen, 1982) also shows this trend, as do binary plots of Zr versus Zr/Y after Pearce & Norry (1979) (Fig. 51) and Ti versus Zr after Pearce and Cann (1973) (Fig.52).

3.3.1.2. Meta-sedimentary samples:

Sample WTKV13, a felsic gneiss (tuffaceous/volcanoclastic meta-sediment or meta-felsic volcanic) dominated by K-feldspar, quartz, plagioclase and high-Ti biotite, shows a very similar chondrite normalised REE pattern to the Hbl/Pl dominated gabbro samples, perfectly “capping” the group as though it were the most felsic member of a volcanic suite (Fig. 44). The 4 quartzite samples as expected have relatively flat REE plots as shown by Fig. 45. Sample WTKV06, a hornblende scapolite meta-sediment shares a similar rare earth pattern to the quartzites although it stays relatively level right into the lighter REEs whereas the quartzites tend to drop off slightly. The latter sample is also plotted in Figure 45.

3.3.2. *Sm, Nd and Sr isotopes by Thermal Ionisation Mass Spectrometry (TIMS):*

The isotopic data collected from analysis of samples WTKV 01, 02, 04, 07 and 09 includes Sm and Nd concentrations, $^{143}Nd/^{144}Nd$ and $^{147}Sm/^{144}Nd$ ratios and calculated εNd and T(DM). These data are summarised in Table 5. Values for εNd

were all negative, ranging from -6.04 to -18.85 for gabbroic samples down to -29.95 for WTKV02, a quartzite. Model ages obtained from isochron plots are reported in section 3.2.2 of this paper.

3.3.3. *Lu/Hf Isotopes by Laser Ablation Multicollector*

Inductively Coupled Plasma Mass Spectrometry (LA-MC-ICPMS):

The Lu/Hf isotopic data obtained are displayed in Table 6. The plot of epsilon Hf(t) versus age seen in Figure 53 displays data for both meta-igneous and meta-sedimentary samples. Zircons from the five samples analysed fall chiefly in negative epsilon space with only six zircons yielding positive εHf(t). This suggests that the primary sources of the detrital zircons in the meta-sedimentary samples contained a significant amount of older crustal components and that the anorthositic gabbro sample was crustally contaminated. The six zircons that yielded positive εHf(t) indicate ages of possible crustal growth as follows: Sample WTKV14 had two zircons with positive εHf(t) which yielded ages of 2401 ± 17 Ma and 2026 ± 18 Ma ($^{207}Pb/^{206}Pb$, 96% and 95% conc. respectively, 1 σ error). Sample WTKV02 also had two zircons with positive εHf(t) with ages of 2424 ± 17 Ma and 2470 ± 18 Ma. The remaining two positive εHf(t) values were in sample WTKV03 which yielded $^{207}Pb/^{206}Pb$ ages of 2424 ± 17 Ma and 3021 ± 16 Ma (95% and 98% conc., 1 σ error). In summary positive values were found for zircons of ages ~2000, ~2400 and ~3000 Ma. The anorthositic gabbro WTKV09 showed a crustal residence time ($TDM_{crustal}$) of 2.27 - 2.49 Ma.

3.3.4. *Oxygen isotopes by Sensitive High Resolution Ion Microprobe (SHRIMP):*

Zircons from sample WTKV09, the anorthositic gabbro dated at 825 ± 17 Ma, were analysed at ANU for oxygen isotopes. Values yielded by SHRIMP analyses are presented in Table 7. The values for $\delta^{18}O$ were between 5.8165 ‰ and 6.7400 ‰. These values are all crustal, above or just above the 5.3 ± 0.3 ‰ of mantle (Valley, 2003), suggesting that the zircons were crustally derived. This is supported by zircon morphology more characteristic of detrital zircons than gabbroic zircons, as described in section *4.2.2.* The $\delta^{18}O$ values showed no correlation with age, as can be seen in Figure 54.

4. Discussion

Structural evidence shows that the Kadavur Dome is not in fact a domal structure but rather the result of poly-deformational folding. The following events have been identified in the Kadavur area:

- S_0 - Refers to original sedimentary bedding.
- S_1 - Strong fabric forming event. Some evidence exists for earlier event(s) (i.e. folded sillimanite perpendicular to the strong fabric) but for the purposes of this study the strong fabric is termed S_1.
- F_2 / D_2 - isoclinal folding (shown by S_1 always being parallel to S_0)

  - This event is likely related to formation of the Kadavur structure.

  - Maximum principal stress for this event was N-S, suggested by:

- S_2 - Fracture cleavage, trends E-W, sub vertically.

The Itremo Group of central Madagascar was deposited in shallow marine, continental margin or intracontinental basin conditions between ~833 and ~1700-1855 Ma (Cox et al., 1998, 2004). Itremo Group quartzites and calc-silicates have dominant detrital populations which cluster at 1850 Ma and 2500 Ma, with lesser peaks at ~2200 Ma, 2700 Ma and 2900-3300 Ma. Similarly the quartzites in the Kadavur Dome series were deposited in shallow water between 840 ± 21 Ma and 1969 ± 17 Ma, quite possibly at ~1780 Ma if WTKV13 is in fact a volcanoclastic/tuffaceous meta-sediment and dates the sequence (further discussion of this follows below). Figure 55 compares the detrital population PDDs of Kadavur Dome meta-sedimentary samples and Itremo group samples analysed by Cox et al. (1998), and plotted by Fitzsimons and Hulscher (2005). The striking similarity is clear. Kadavur Dome's quartzitic sediments contain a detrital suite (monazite, zircon, rutile, and tourmaline) that indicates that it was derived from a weathered granitic provenance. The absence of feldspars and presence of sillimanite suggest also that the provenance was probably highly weathered with sillimanite forming from clays associated with the original quartz sand. The abundance of primary hematite in the quartzites may also indicate an originally highly oxidised provenance.

The Itremo Group was intruded by granitoids and gabbros for a period of ~25 Ma between ~804 and 779. This paper dates gabbroic intrusion in the Kadavur Dome area at 825 ± 17 Ma (anorthositic gabbro WTKV09). Intrusion related (contact) metamorphism is also recorded in two of the quartzites at ~840 and ~882 Ma, and in felsic gneiss sample WTKV13 at 789 ± 33 Ma. Geochemical analysis of the igneous suite present in the Kadavur Valley reveals two distinct groups of gabbroic rocks.

One group dominated by orthopyroxene and clinopyroxene displays positive Eu anomalies, while the second group has a flat REE signature. The difference in Eu is probably related to different variants of plagioclase present in each group. Negative epsilon Hf values yielded from WTKV09 suggest crustal contamination of these intrusives, and crustal residence times of 2.27 - 2.49 Ma. Further evidence for crustal contamination comes from the $\delta^{18}O$ values (Table 7). It could be that the Opx/Cpx dominated gabbros were mafic sills at ~1780 Ma. The chondrite normalised rare earth element plot for these samples shows that WTKV13 sits neatly on top of each of these samples (Fig. 43), just as the most felsic variant will sit on top of a volcanic sequence in REE plots. The Itremo Group contains mafic igneous layers, often close to the contact with the quartzites; however these are very thin (one to five metres) and rare (Cox et al., 1998). The geochemical classification plots for the suite indicate the Opx/Cpx gabbros as well as two of the Hbl/Pl gabbros have an island arc basalt/tholeiite petrogenesis.

Calc-silicates and dolomitic rocks present in the Itremo group are a possible counterpart for hedenbergite-scapolite calc-silicate sample WTKV06. The dominance of hedenbergite (and thus significant Ca, and Mg) and scapolite (more Ca) in sample WTKV06 mean that, prior to metamorphism, it could have been a calcite/dolomitic rock similar to the “sandy carbonate” described by Cox et al. (1998). When geochemical data reported for calc-silicates of the Itremo group by Cox et al. (1998) is compared to sample WTKV06 a striking similarity is seen. Further comparison of trace and rare elements is needed.

Two main interpretations of felsic gneiss sample WTKV13 have been made, one that the sample was a tuff deposit or volcanoclastic sediment, the other that the sample was a felsic intrusion. The CL zircon images are somewhat equivocal, but there are

certainly many zircons with a more igneous appearance than detrital. There are many zircons with remnant or ghost oscillatory zoning. Several are elongate with clear zoning (e.g. Fig. 28 (A)). The distinctive age PDD has two clear peaks of concordant data at 1779 ± 15 and 789 ± 33 Ma, as does the concordia plot of concordant data. Given the ~800 Ma intrusives nearby, it is quite possible that the younger peak represents ~1780 Ma zircons that have been reset by contact metamorphism to ~800 Ma, and that prior to this event this sample contained a single population of zircons of ~1780 Ma age. This interpretation has important implications. If the rock was in fact a tuffaceous deposit, the 1779 ± 15 Ma age can be considered as the age of the sequence. It follows that if this sample is formerly part of the Itremo Group, the sample may in fact date the Itremo group sequence of central Madagascar.

The second alternative for felsic gneiss WTKV13 is that the rock is in fact meta-igneous, and represents a granitic/charnockitic intrusion emplaced at ~1780, followed by metamorphic growth due to contact metamorphism at ~800 Ma when gabbros intruded nearby. The older analyses could then be interpreted as inherited detrital grains from the country rock that were caught up in the granitic intrusion or felsic volcanic. There are no other recorded intrusions in the area with ages of ~1780, making this a riskier interpretation. Investigation of Th/U versus age plots (Figs. 34 - 36) reveals a relatively large diversity of Th/U ratios which is indicative of detrital zircons, however the ratios are for the most part greater than 0.2 which suggests the zircons were grown from an igneous melt.

5. Conclusion

Structurally, the Kadavur Dome should no longer be referred to as a dome as the structure is in fact a result of poly-deformational folding and thrusting. The quartzites that form the valley's walls and ridges were deposited in the Proterozoic between 1969 ± 17 Ma and 840 ± 21 Ma in shallow water. Detrital zircon age peaks are most prominent at ~2100 Ma and ~2450 Ma with several lesser peaks at between ~1900 and ~2500, ~2700 Ma and from ~3000 - 3200 Ma. Metamorphic zircon rim analyses of quartzites revealed metamorphic rim growth at ~840 - 882 Ma. These rims have been interpreted as being associated with the intrusion of anorthositic gabbros, one of which this study dated at 825 ± 17 Ma. This event is also recorded in sample WTKV13, a felsic gneiss interpreted as either a tuffaceous/volcanoclastic meta-sediment or felsic intrusive. If WTKV13 represents a tuffaceous sediment, its age of 1779 ± 15 Ma can be used to date the sedimentary sequence present in the Kadavur Valley. When data from this study is compared to data from central Madagascar's Itremo Group the similarities are undeniable. Further, more detailed geochemical comparisons of Kadavur Valley quartzites, calc-silicates and intrusive suite could confirm the interpretation of these two suites having been deposited together. From the assumption that the Kadavur quartzites are a relocated fragment of the Itremo Group, and that sample WTKV13 is a tuffaceous sediment, it follows that the sample dates the deposition of the Itremo Group at 1779 ± 15 Ma. It can also be deduced that the Kadavur area, and thus the northern Madurai Block, was indeed a part of the former continent Azania, and that the PCSZ may well represent the suture that resulted from the final closure of the Mozambique Ocean.

6. References

Amdel Ltd, 35-37 Stirling Street, Thebarton, South Australia 5031

Anders and Grevesse, 1989. Abundances of the elements: meteoric and solar. *Geochimica et Cosmochimica Acta,* 53, pp 197-214

Cenki, B. and Kriegsman, L.M., 2005. Tectonics of the Neoproterozoic Southern Granulite Terrain, South India*. Precambrian Research,* 138, pp 37-56.

Collins, A.S., Clark, C., Sajeev, K., Santosh, M., Kelsey, D.E. and Hand, M., 2007. Passage through India: the Mozambique Ocean Suture, high-pressure granulites and the Palghat-Cauvery shear zone system. *Terra Nova*, 19, No. 2, pp 141-147.

Collins, A.S. and Pisarevsky, S.A., 2005. Amalgamating eastern Gondwana: The evolution of the Circum-Indian Orogen*. Earth Science Reviews,* 71, pp 229-270.

Collins, A.S., Santosh, M., Braun, I. and Clark, C., 2007. Age and sedimentary provenance of the Southern Granulites, South India: U-Th-Pb SHRIMP secondary ion mass spectrometry*. Precambrian Research,* V 155, pp 125-138.

Cox, R., Armstrong, R.A. and Ashwal, L.D., 1998. Sedimentology, geochronology and provenance of the Proterozoic Itremo Group, central Madagascar, and it's implications for pre-Gondwana palaeogeography. *Journal of the Geological society, London*, V 155, pp 1009-1024.

Cox, R., Coleman, D.S., Chokel, C.B., DeOreo, S.B., Wooden, J.L., Collins A.S., De Waele, B. and Kröner, A., 2004. Proterozoic Tectonostratigraphy and Palaeogeography of Central Madagascar Derived from Detrital Zircon U-Pb Age Populations*. The Journal of Geology*, V 112, pp 379 – 399.

Fedo, C.M., Sircombe, K.N. and Rainbird, R.H., 2003, Detrital Zircon Analysis of The Sedimentary Record, *Reviews in Mineralogy and Geochemistry,* V 53, No.1, pp 277-303.

Fitzsimons, I.C.W. and Hulscher, B., 2005. Out of Africa: detrital zircon provenance of central Madagascar and Neoproterozoic terrane transfer across the Mozambique Ocean. *Terra Nova*, V 17, pp 224 – 235.

Gosh, J. G., de Wit, M. J., and Zartman, R. E., 2004. Age and tectonic evolution of Neoproterozoic ductile shear zones in the Southern Granulite Terrain of India, with implications for Gondwana studies, *Tectonics*, V 23.

Goldstein, S.L., O'Nions, R.K. and Hamilton, P.J., 1984. A Sm-Nd isotopic study of atmospheric dusts and particulates from major river systems. *Earth and Planetary Science Letters*, V 70, No.2, pp 221-236.

Irvine, T.N. and Baragar, W.R.A., 1971. A guide to the chemical classification of the common volcanic rocks. *Canadian Journal of Earth Sciences*, V 8, pp 523-548.

Ludwig, K.R., 2009. Isoplot Ver:3.0.

Pearce, J. A. & Norry, M. J., 1979. Petrogenetic implications of Ti, Zr, Y, and Nb variations in volcanic rocks. *Contributions to Mineralogy and Petrology,* V 69**,** pp 33–47.

Santosh, M., Maruyama, S. and Sato, K., 2009. Anatomy of a Cambrian suture in Gondwana: Pacific-type orogeny in southern India? *Gondwana Research,* V16, pp 321-341.

Middlemost, E. A. K., 1985. Naming materials in the magma/igneous rock system*. Earth-Sciences Reviews,* V 37**,** pp 215–224.

Mullen, E.D., 1983. MnO/TiO2/P2O5: a minor element discriminant for basaltic rocks of oceanic environments and its implication for petrogenesis. *Earth and Planetary Science Letters*, V 62, pp 53-62.

Pearce, J. A. & Cann, J. R., 1973. Tectonic setting of basic volcanic rocks determined using trace element analyses. *Earth and Planetary Science Letters* V 19, pp 290–300.

Scherer, E., Münker, C. & Mezger, K., 2001. Calibration of the lutetium-hafnium clock. *Science*, V 293, pp 683-687.

Segal, I., Halicz, L. and Platzner, I.T., 2003. Accurate isotope ratio measurements of ytterbium by multi-collector inductively coupled plasma mass spectrometry applying erbium and hafnium in an improved double external normalisation procedure*. J. Anal. At. Spectrom.* V 18, pp 1217-1223.

Sircombe, K.N., 2004. AgeDisplay: an EXCEL workbook to evaluate and display univariate geochronological data using binned frequency histograms and probability density distributions. *Computers & Geosciences,* V 30, pp 21-31.

Siivola, J. and Schmid, R., 2007. Recommendations by the IUGS Subcommission on the Systematics of Metamorphic Rocks: List of mineral abbreviations. Web version 01.02.07. (http://www.bgs.ac.uk/scmr/docs/papers/paper_12.pdf) *IUGS Commission on the Systematics in Petrology.*

Slama, J., Kosler, J., Condon, D.J., Crowley, J.L., Gerdes, A., Hanchar, J.M., Horstwood, M.S.A., Morris, G.A., Nasdala, L., Norberg, N., Schaltegger, U., Schoene, B., Tubrett, M.N., and Whitehouse, M.J., 2008. Plesovice zircon - A new natural reference material for U-Pb and Hf isotopic microanalysis. *Chemical Geology*, V 249, pp 1-35.

Goldstein, S.L., O'Nions, R.K. and Hamilton, P.J., 1984. A Sm-Nd isotopic study of atmospheric dusts and particulates from major river systems. *Earth and Planetary Science Letters*, V 70(2) 221-236.

Tanaka, T. et al., 2000. JNdi-1: a neodymium isotopic reference in consistency with LaJolla neodymium. *Chemical Geology*, V168, No3-4, pp 279-281.

van Achterbergh, E., Ryan, C.G., Griffin, W.L., 2001. GLITTER version 4. *Macquarie Research Ltd.*

Vernon, R.H., 1976. Metamorphic Processes; Reactions and Microstructure Development. *George Allen and Unwin Ltd. Publishers*.

Valley, J., 2003. Oxygen Isotopes in Zircon. *Reviews in Mineralogy and Geochemistry,* V 53, No.1, pp 343-385.

Wetherill G. W. (1956) Discordant uranium-lead ages. *Trans. Am. Geophys. Union* V 37, pp 320–326.

Whitney, D.L., Teyssier, C. and Siddoway, C.S., 2004. Gneiss Domes and Crustal Flow*. Geological Society of America, Special Paper* 380.

Wilson, S.A., 1997, Data compilation for USGS reference material BHVO-2, Hawaiian Basalt, U.S. *Geological Survey Open-File Report*.

Woodhead, J.D., Hergt, J.M., Shelley, M., Eggins, S. and Kemp, R., 2004. Zircon Hf-isotope analysis with an Excimer laser, depth profiling, ablation of complex geometries, and concomitant age estimation. *Chemical Geology*. V 209, pp 121-135

7. Figures and Tables List.

8. Figures and Tables:

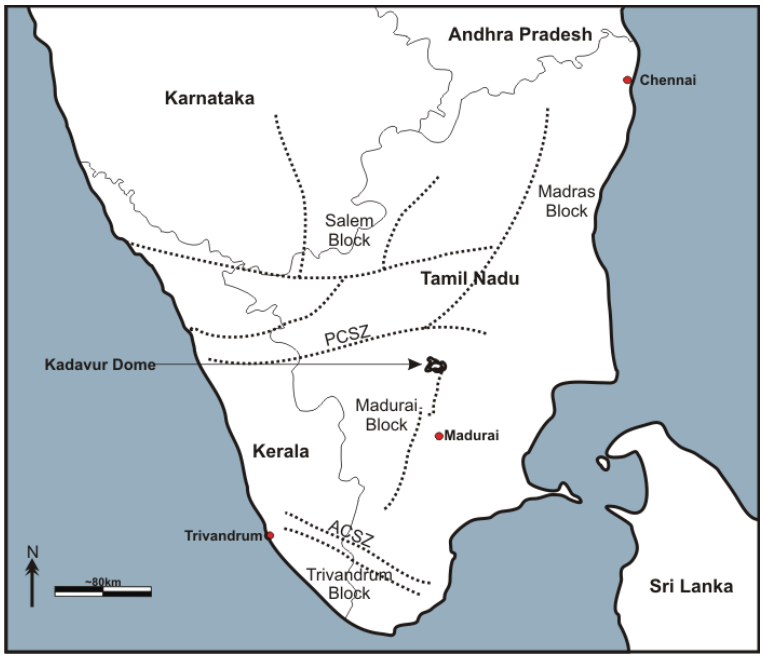

Figure 1. Map showing location of Kadavur Dome within southern India. Dotted lines represent shear zones, thin unbroken lines are state borders. PCSZ is the Palghat Cauvery Shear Zone, ACSZ is Achankovil Shear Zone. The Kadavur Dome is indicated with the arrow.

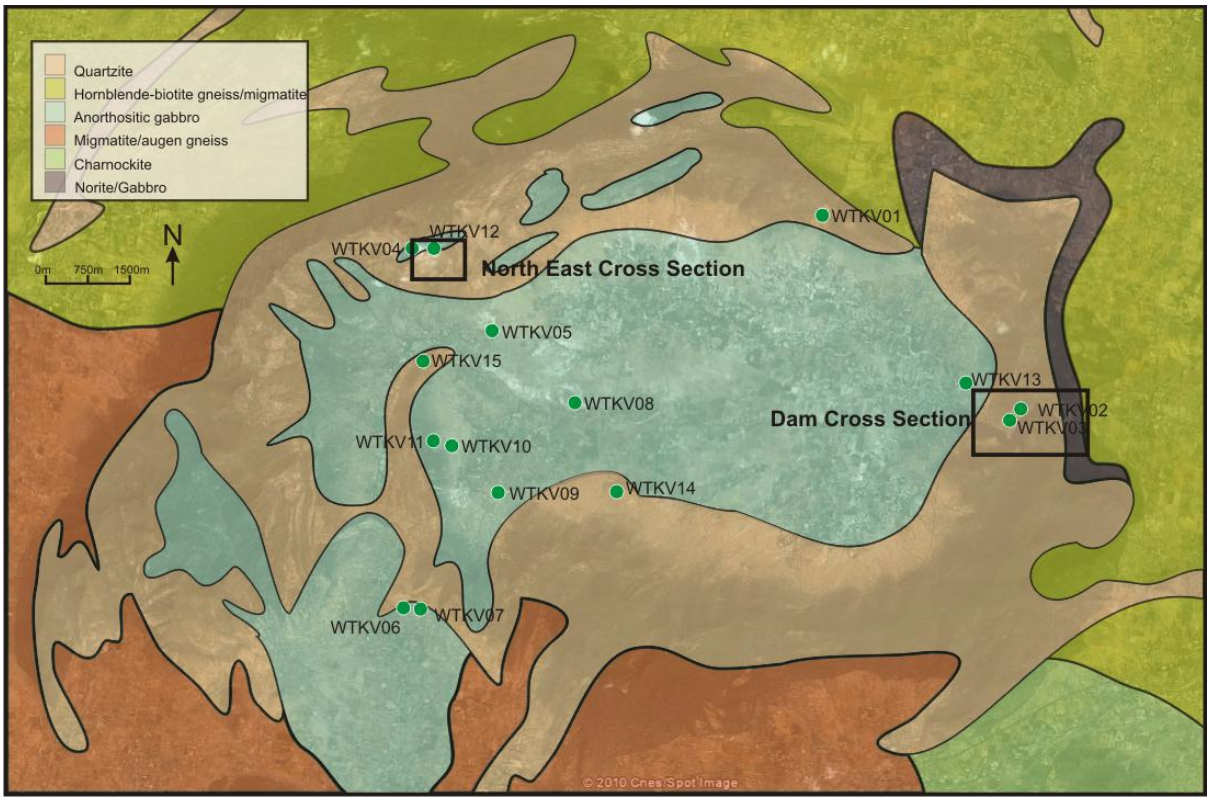

Figure 2. Location of samples and detailed transects (shown in Fig 3 and 4) within the Kadavur Dome. Geology based on Geological Society of India (GSI) map sheet. Sample locations are also summarised in Table 1.

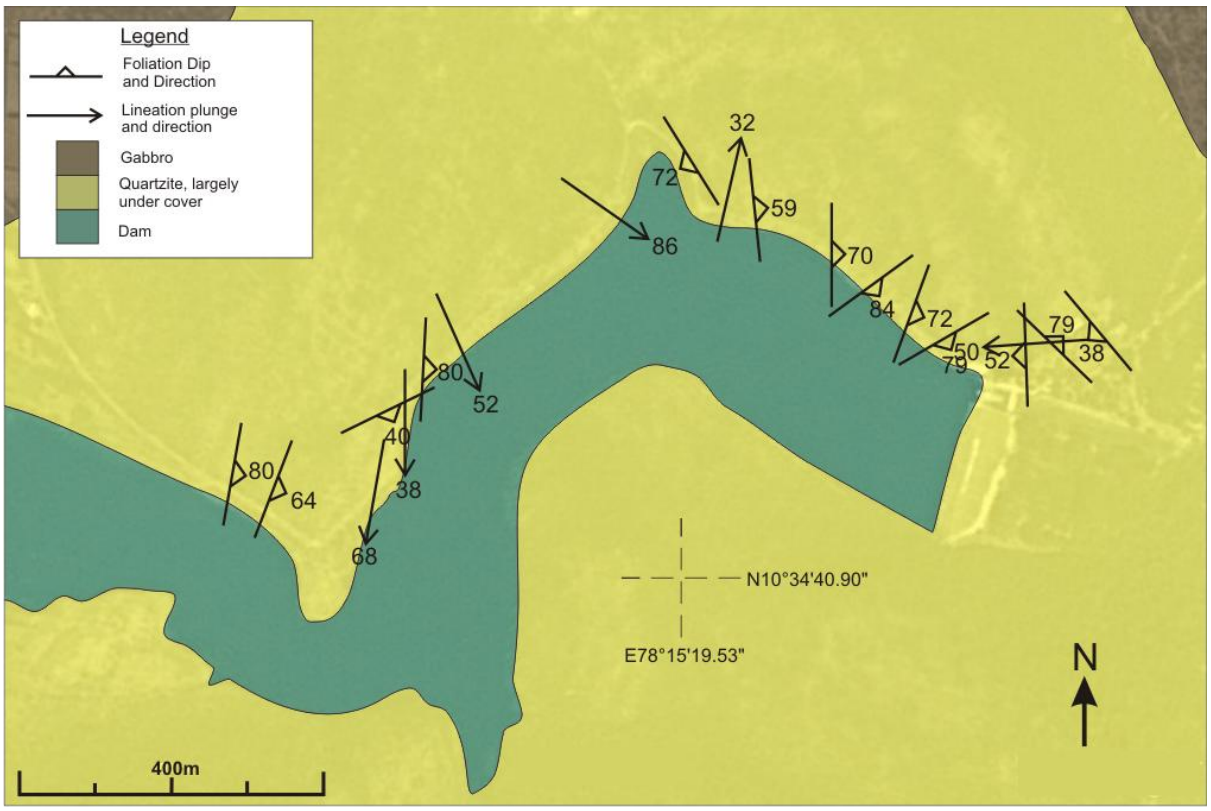

Figure 3. Structural map of Poonani Dam transect. All measurements are expressed as dip/dip direction in degrees.

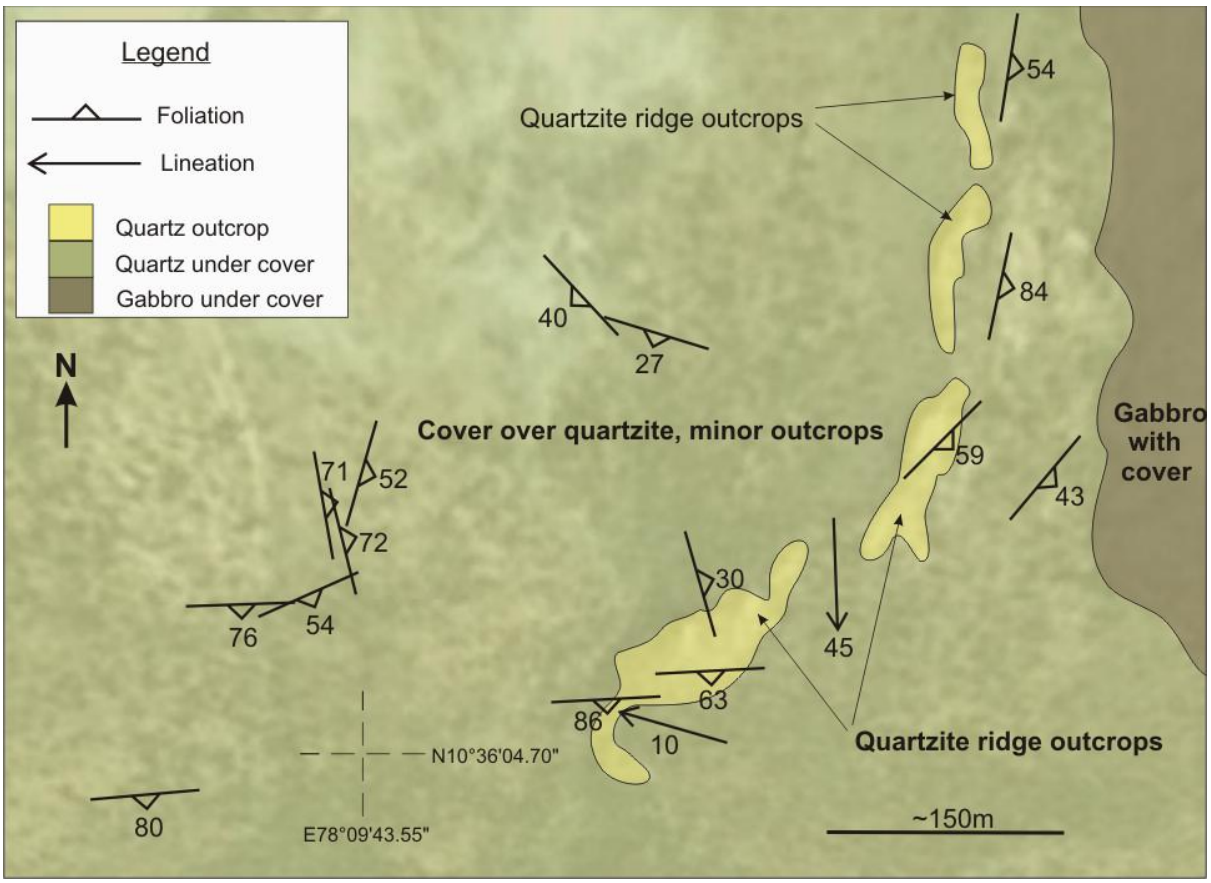

Figure 4. Structural map of NW transect. Measurements are Dip/dip direction.

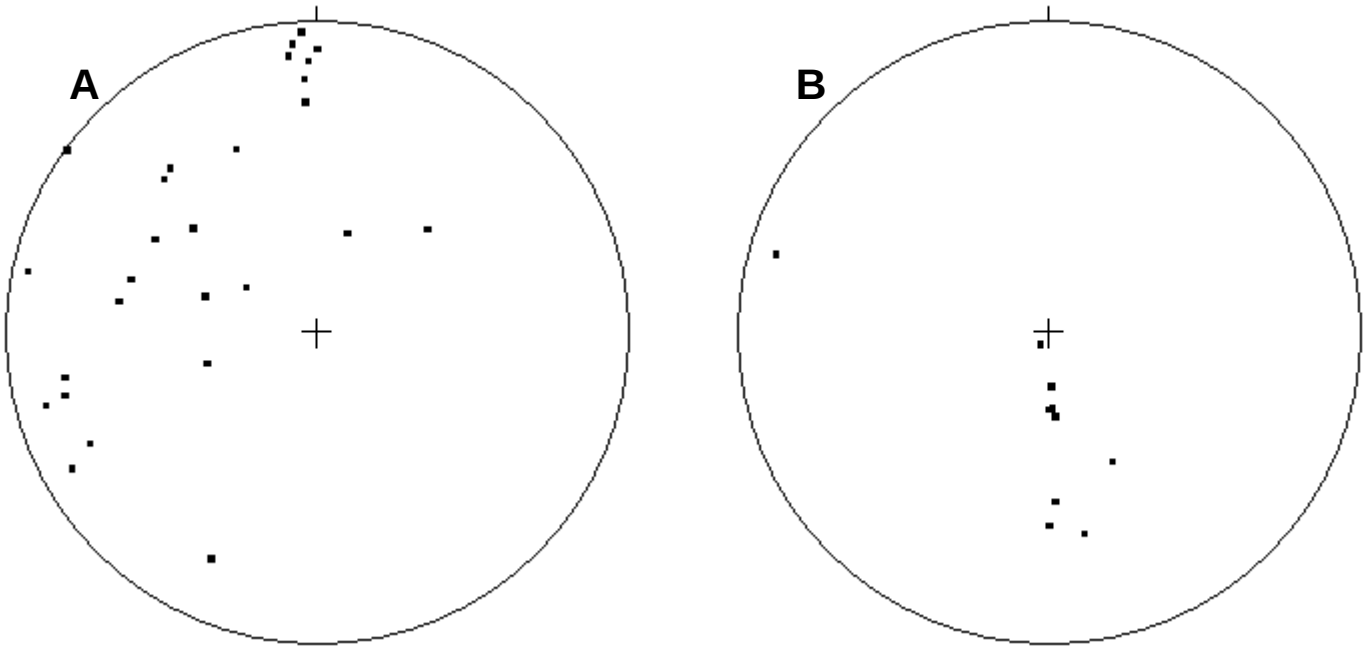

Figure 5. (A) Foliations measured on the NW structural transect, shown as poles to foliation. (B) Lineations measured on the NW structural transect.

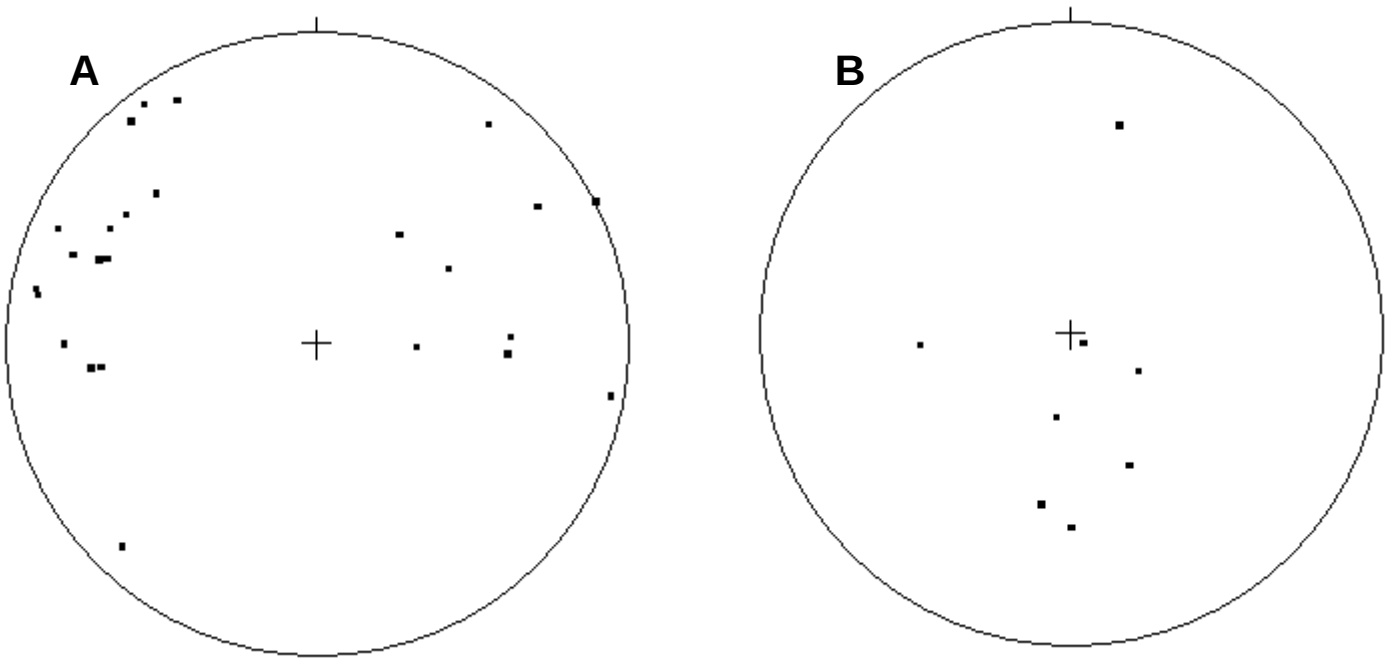

Figure 6. (A) Foliations measured on the Poonani Dam structural transect, shown as poles to foliation. (B) Lineations measured on the Poonani Dam structural transect.

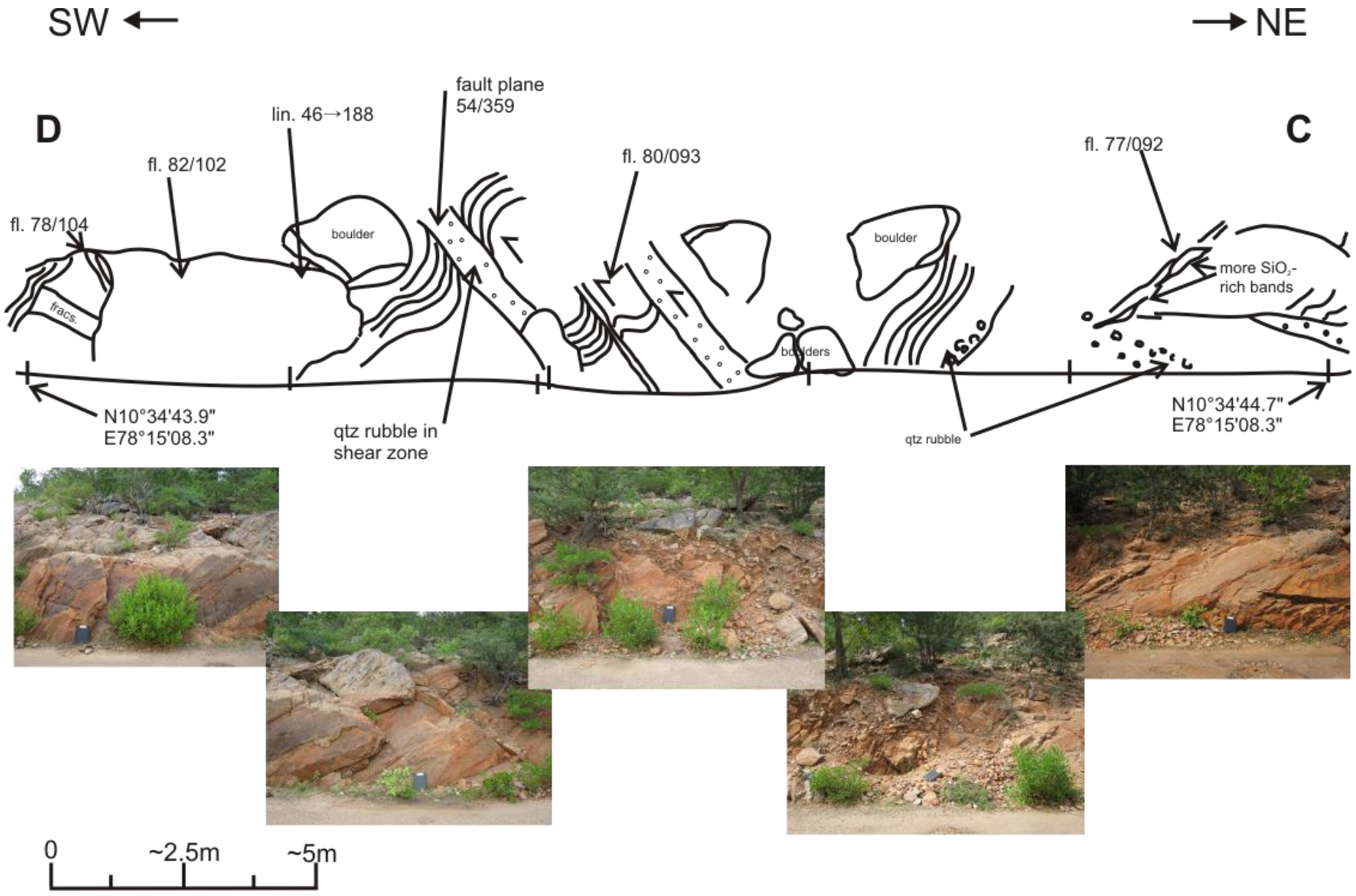

Figure 7.1. (Part 1 of 3) Structural sketch of part of Poonani Dam transect. fl. = foliation, lin. = lineation, fracs. = fractures. All measurements are expressed as dip/dip direction in degrees.

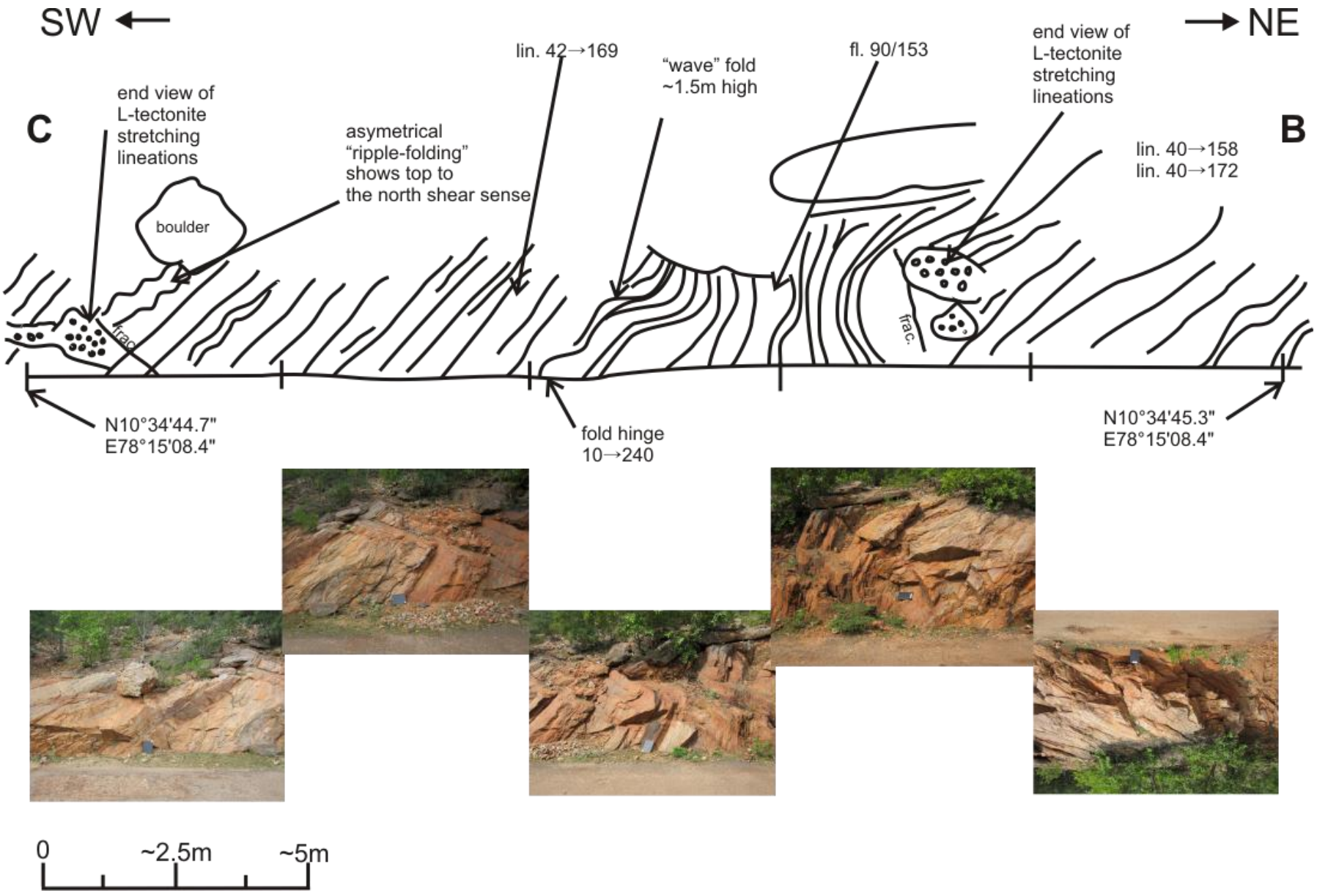

Figure 7.2. (Part 2 of 3) Structural sketch of part of Poonani Dam transect. fl. = foliation, lin. = lineation, fracs. = fractures. All measurements are expressed as dip/dip direction in degrees.

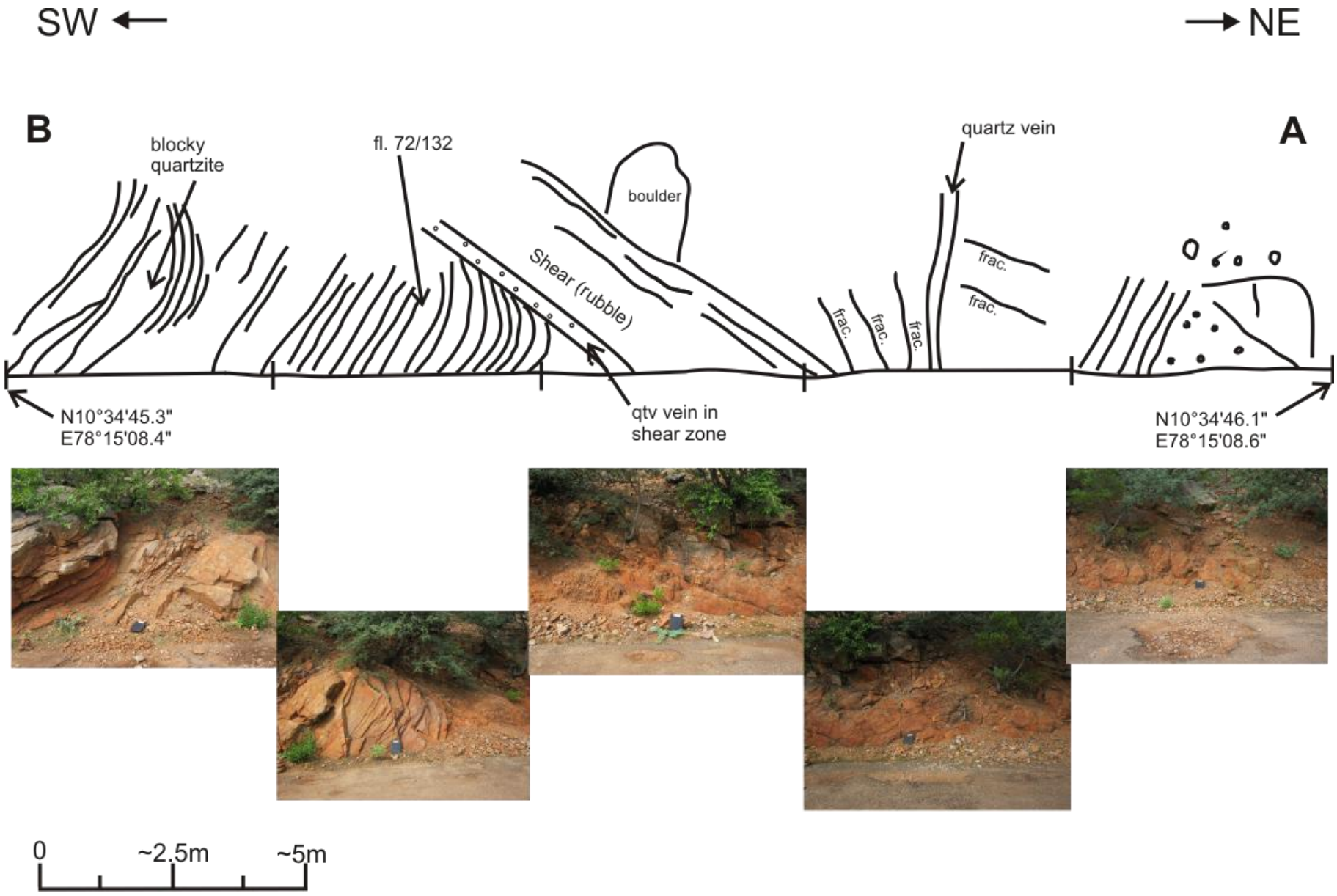

Figure 7.3. (Part 3 of 3) Structural sketch of part of Poonani Dam transect. fl. = foliation, lin. = lineation, fracs. = fractures. All measurements are expressed as dip/dip direction in degrees.

Figure 8. Photo taken by Poonani Dam, facing west-south-west. Red dotted line highlights folding of foliation (S_1) during D_2, and blue arrow shows strong lineation plunge and plunge direction, 42°→150°

Figure 9. “Rodding” lineation which is folded is highlighted with red dashed line. Photo taken facing north east from approximately N10°34’50.3”, E78°15’30.7”.

Figure 10. Photo taken in the Dome's north west, facing west at N10°36'12.0", E78°09'47.8". Visible here is a strong fabric development (red dotted line) which is parallel to heavy mineral laminations (just below dotted line) which gives bedding, indicating S_0 is parallel to sub-parallel to foliation (S_1), measured here as 52°/270°. Notice sub-horizontal orientation.

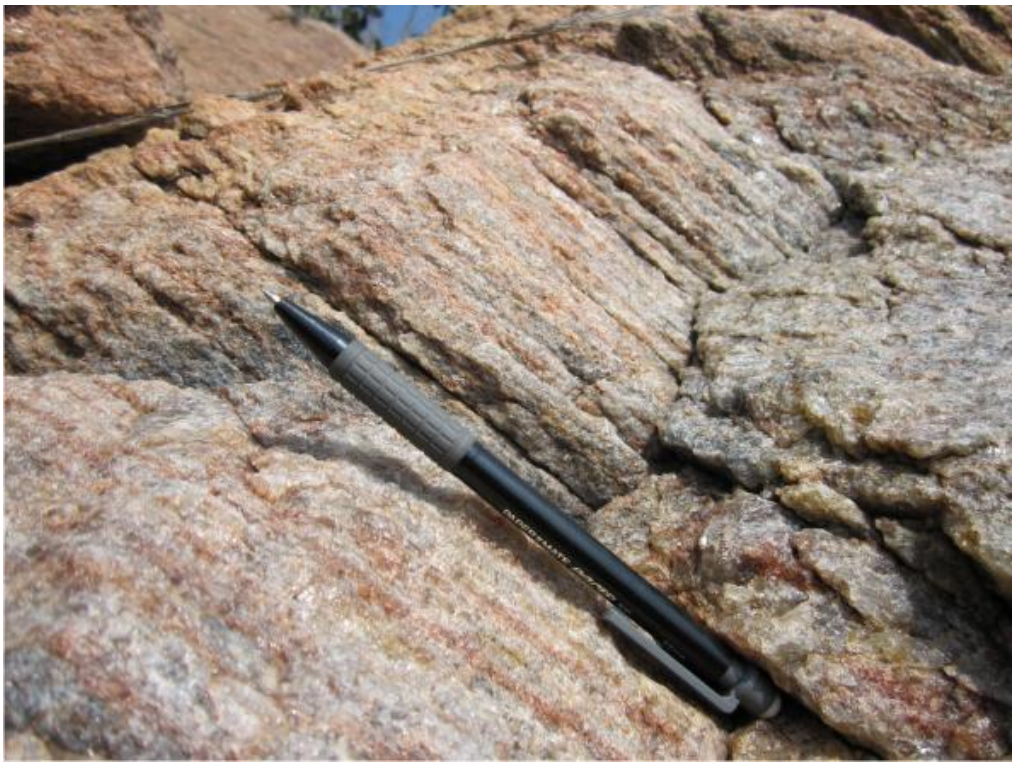

Figure 11. Very strong lineation (rodding 68°→176°) in quartzite, pencil shows direction. Photo taken at N10°36'08.8", E78°09'43.7" looking east.

Figure 12. Photo taken at N10°36’04.0”, E78°09’48.4” shows lineation now approximately sub-vertical.

Figure 13. Photo showing tight folding of foliation/bedding (S_1/S_0) in a quartzite boulder at N10°35’16.5”, E78°09’33.2”.

Figure 14. Photo taken at N10°36’14.9”, E78°09’55.8”, shows S_1 parallel to S_0 near the top of the photo; red dotted line indicates heavy mineral banding in the quartzites; A more siliceous “bed” within the quartzite unit sits just below the heavy mineral layer; also visible (green dotted lines) is the fracture cleavage (D_2/S_2), perpendicular to S_1 and S_0. This fracture cleavage is always sub-vertical and east-west.

Figure 15. Photo taken at N10°36’08.7”, E78°09’56.6” facing east. Clearly visible is the sub-vertical fracture cleavage (D_2/S_2), measured here as 88°/358° and highlighted with green dotted line. Red dotted line highlights foliation (S_1). Original bedding (S_0) is parallel to foliation here, as seen by presence of more SiO_2 rich bands and heavy mineral bands.

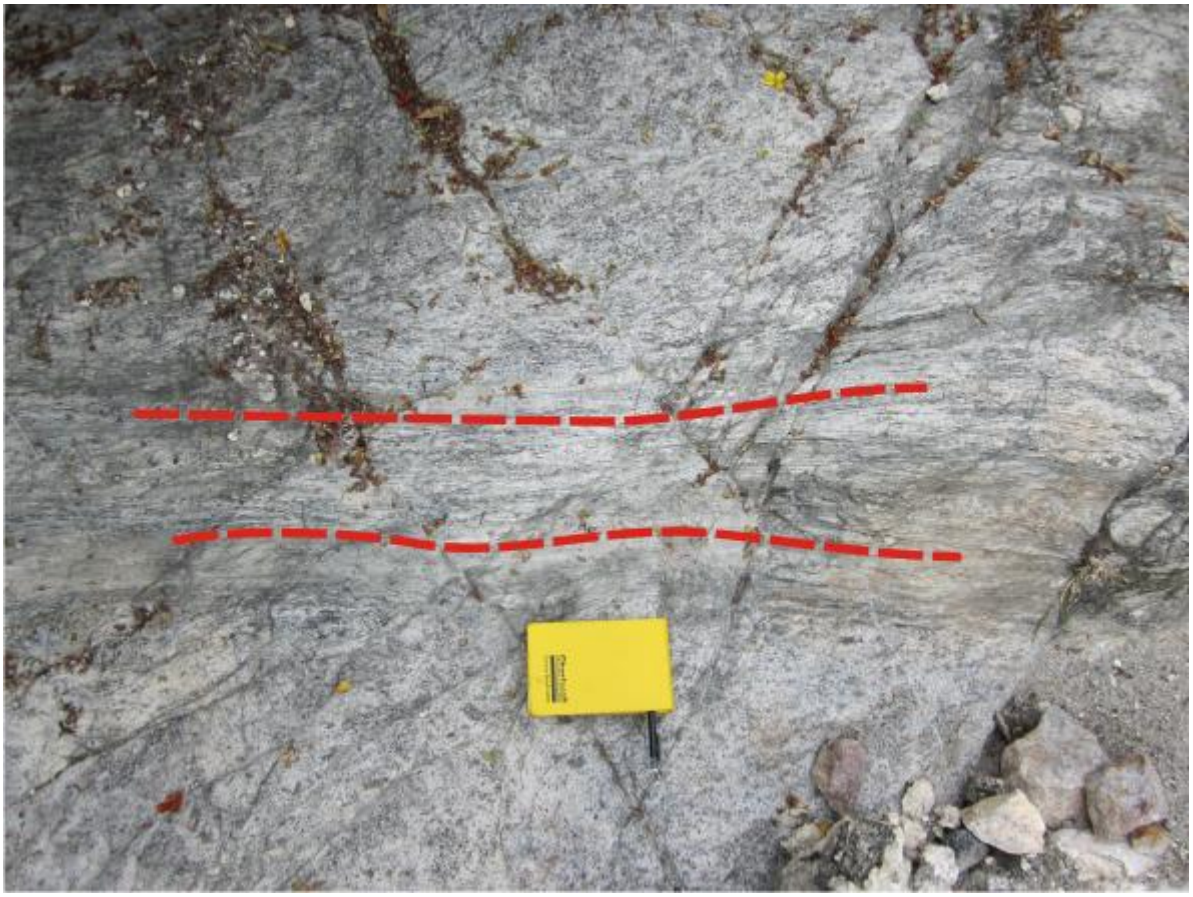

Figure 16. Photo taken at N10°34’10.4”, E78°09’47.8”, shows a deformed zone in an anorthositic leuco-gabbro. The foliation within the zone is 52°/308°. Sample WTKV10 was taken approximately 100m south of this photo in the same rock unit.

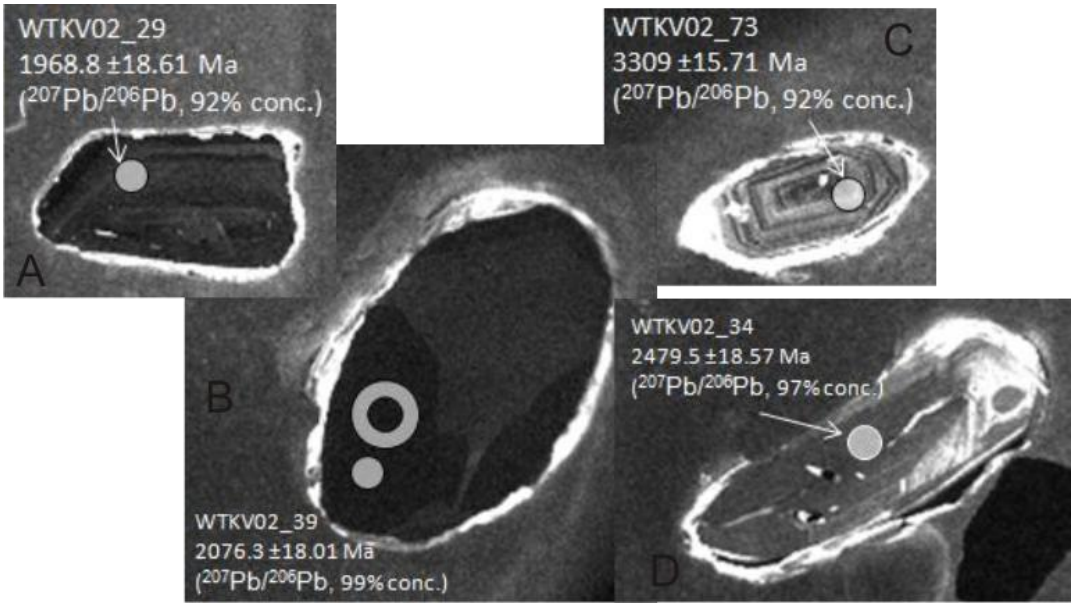

Figure 17. Zircons from sample WTKV02. Small filled spots are locations of U/Pb analysis and are 30µm; large hollow spot is Hf analysis point and is 50µm. (A) Youngest zircon, with $^{207}Pb/^{206}Pb$ age of 1969 ± 19 Ma. (B) Homogeneous recrystallisation. (C) Oldest Zircon, $^{207}Pb/^{206}Pb$ age of 3309 ± 16 Ma. Note oscillatory zoning. (D) Small inclusions, homogeneous recrystallisation.

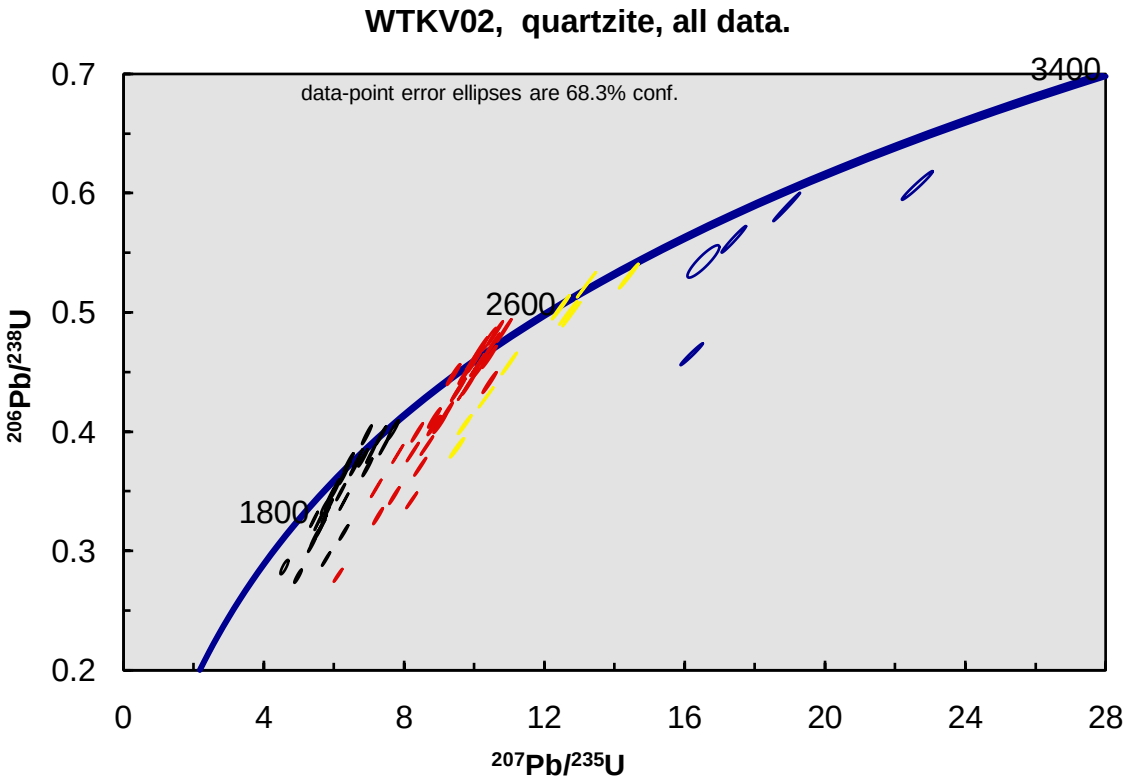

Figure 18. Concordia plot for quartzite sample WTKV02 with all data plotted. Different colours have been used to highlight approximate population groups (black, red and yellow), and older analyses (blue).

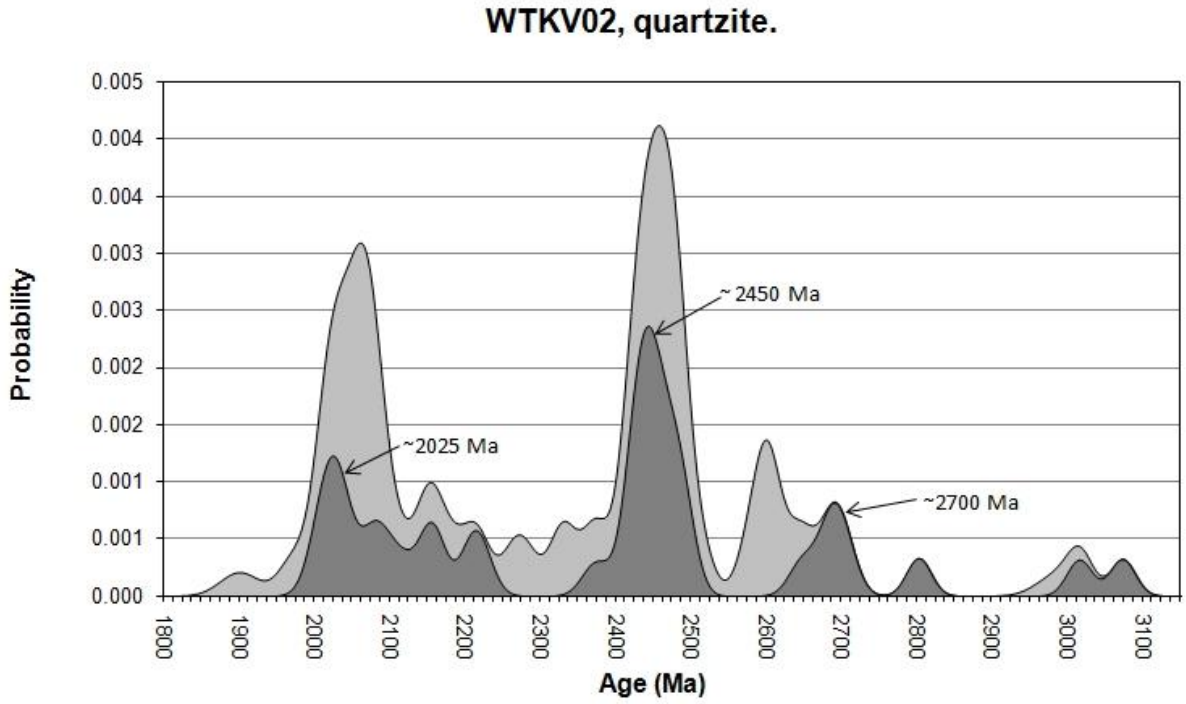

Figure 19. Probability density distribution plot of $^{207}Pb/^{206}Pb$ ages for sample WTKV02, a quartzite. Dark grey shaded area is 95-105% concordant data, light grey shaded area is all data. Note detrital spread of ages.

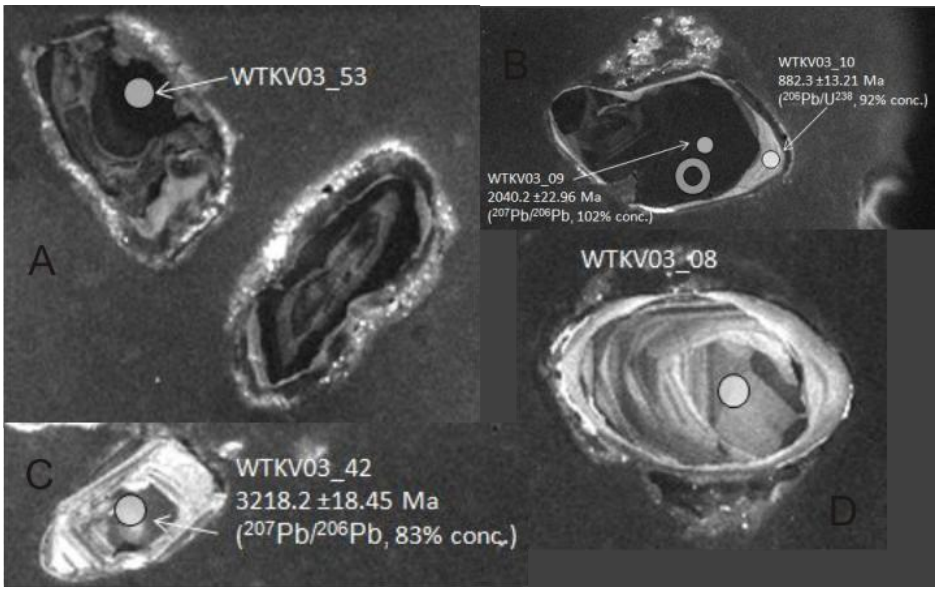

Figure 20. CL images of zircons from sample WTKV03. Small filled spots are locations of U/Pb analysis and are 30µm; large hollow spot is Hf analysis point and is 50µm. (A) Irregular and convolute zoning. (B) Detrital zircon dated at 2040 ± 23 Ma with a rim of 882 ± 13 Ma ($^{207}Pb/^{206}Pb$ ages, 102% and 92% conc. respectively, 1 σ error). (C) This well zoned zircon yielded the oldest age for this sample at 3218 ± 18 Ma but was only 83% concordant. (D) Irregular zoning in a well abraded and rounded zircon.

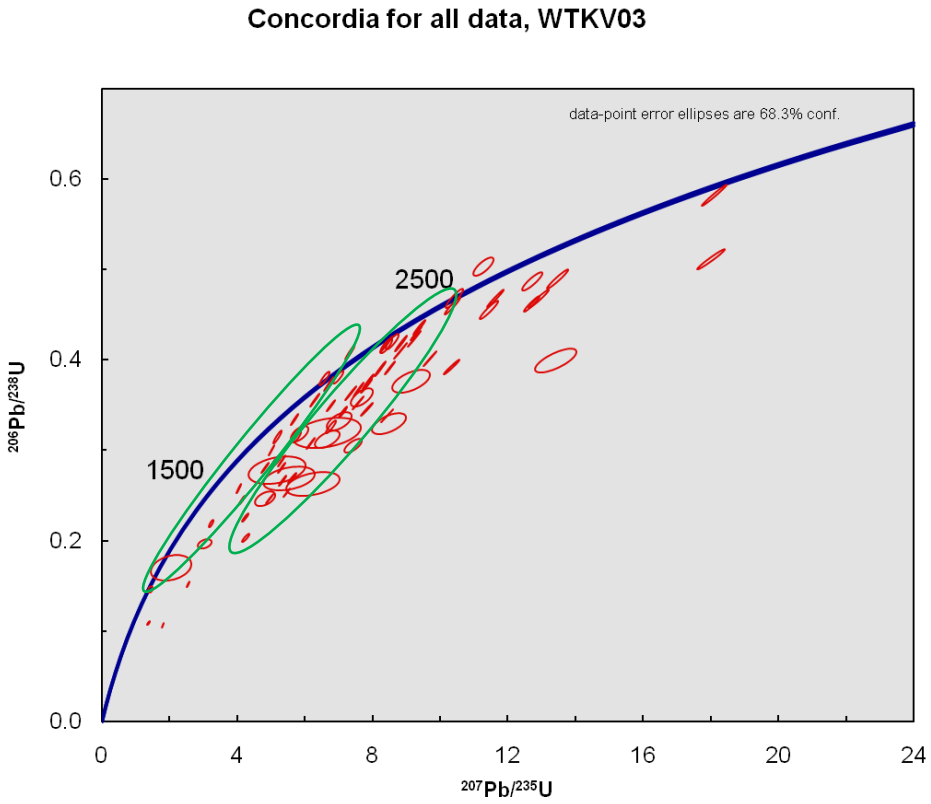

Figure 21. Concordia plot for quartzite sample WTKV03 with all data plotted. Green ellipses have been used to highlight the two most obvious zircon populations.

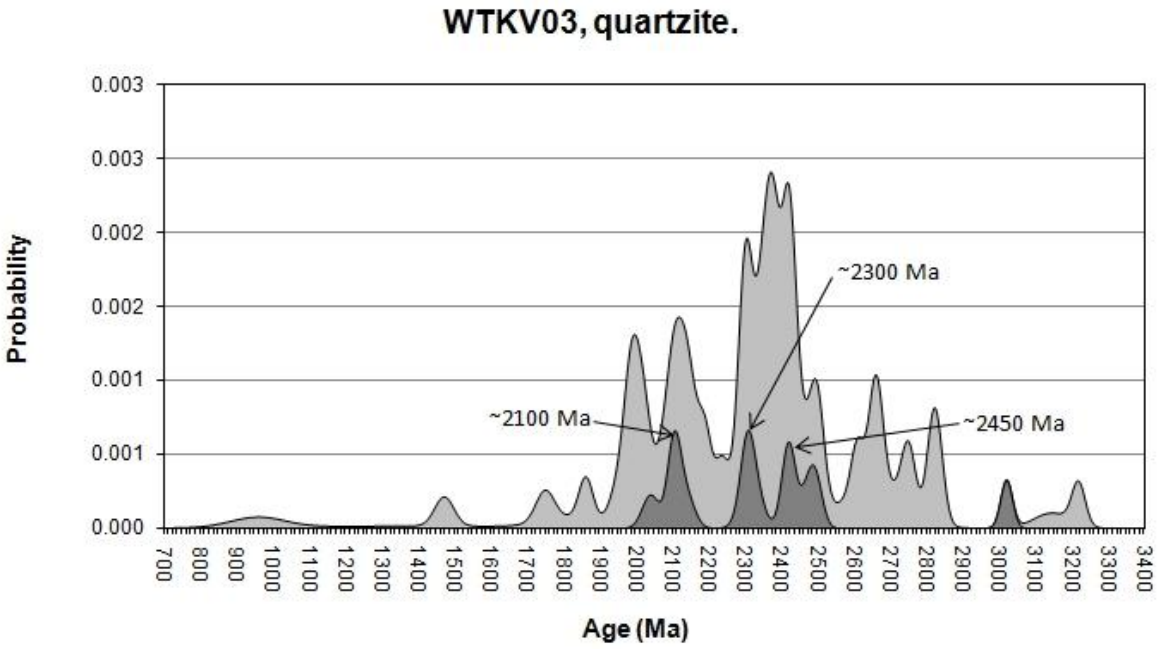

Figure 22. Probability density distribution plot of $^{207}Pb/^{206}Pb$ ages for sample WTKV03, a quartzite. dark grey shaded area is 95-105% concordant data, light grey shaded area is all data. Note the spread of detrital ages.

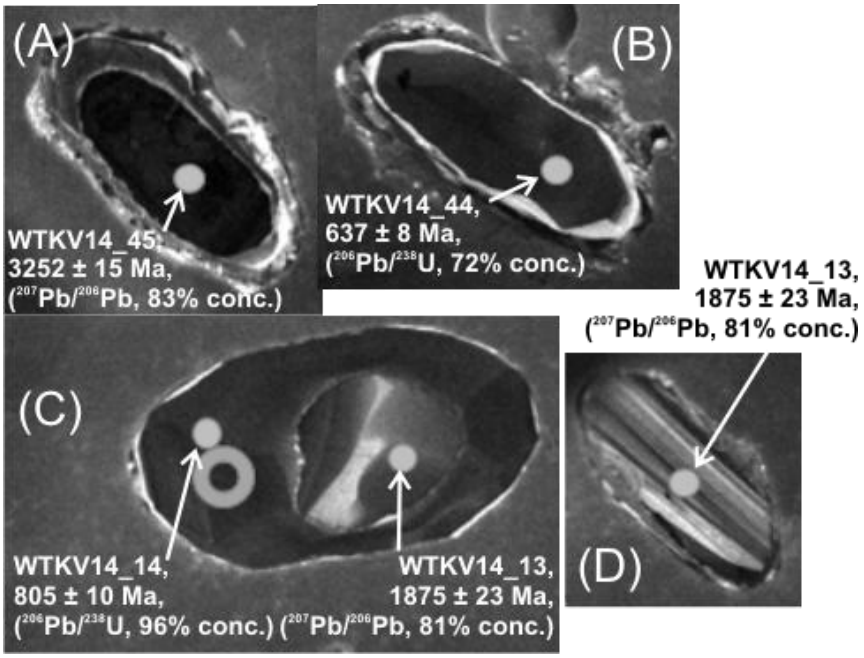

Figure 23. CL images of zircons from sample WTKV14, a quartzite. Small filled spots are locations of U/Pb analysis and are 30µm; large hollow spot is Hf analysis point and is 50µm. (A) The oldest zircon analysed, WTKV14_45, yielded a $^{207}Pb/^{206}Pb$ age of 3252 ± 15 (83% concordant, 1 σ error). (B) Discordant zircon WTKV14_44 has undergone recrystallisation of its core, which has reset its $^{206}Pb/^{238}U$ age to 637 ± 8 Ma (72% concordant, 1 σ error). (C) WTKV14_14 has a particularly large rim. Rim $^{206}Pb/^{238}U$ age is 805 ± 10 Ma (96% conc., 1 σ error). Partially recrystallised, discordant, xenocrystic core $^{207}Pb/^{206}Pb$ age is 1875 ± 23 Ma (81% conc., 1 σ error). (D) Older zircon with zoning running parallel to long axis of the grain.

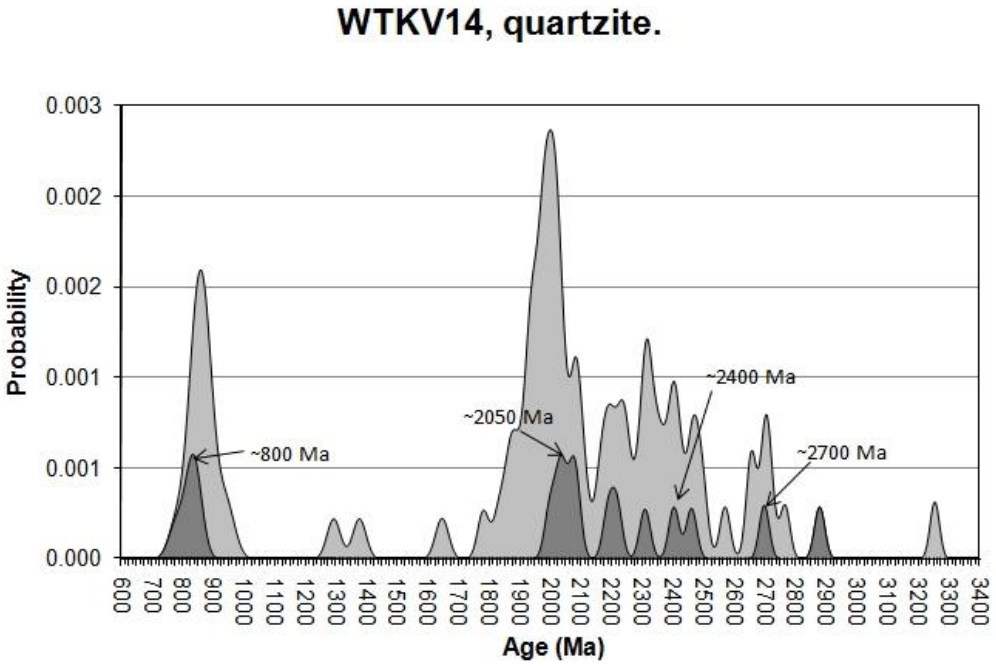

Figure 24. Probability density distribution plot for sample WTKV14, a quartzite. Dark grey shaded area is 95-105% concordant data, light grey shaded area is all data. Note spread of detrital ages, and the peak from rim analyses at ~840 Ma.

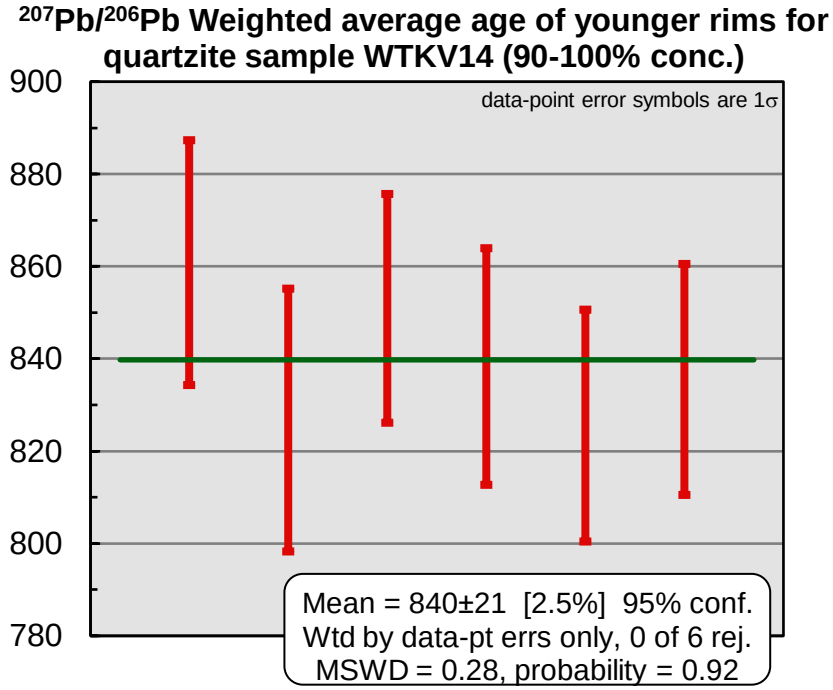

Figure 25. Weighted average $^{207}Pb/^{206}Pb$ age (90-100% conc.) for younger rims in WTKV14.

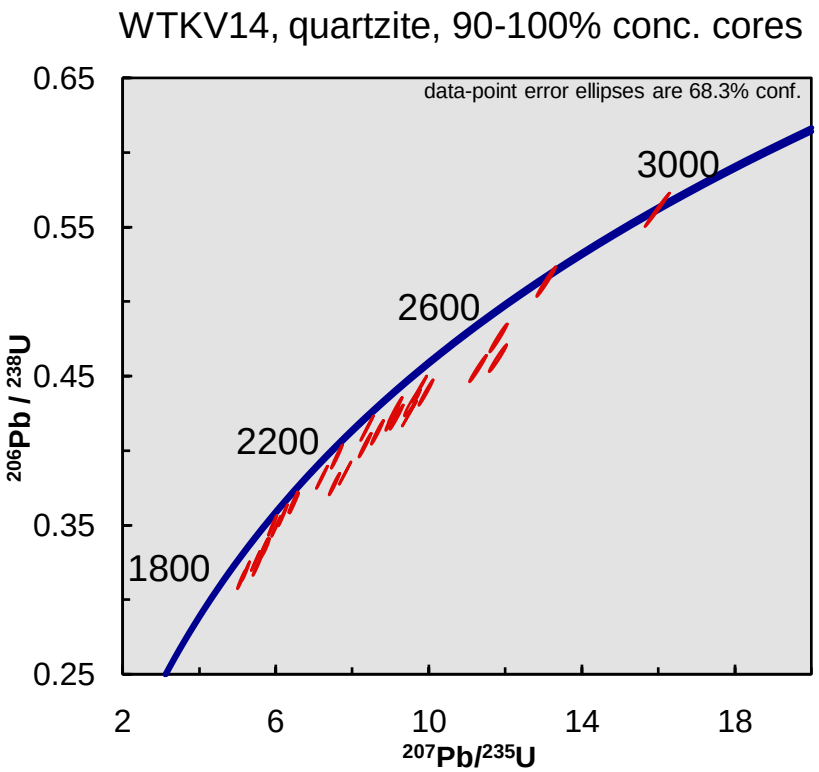

Figure 26. Concordia plot of 90-100% concordant cores for sample WTKV14

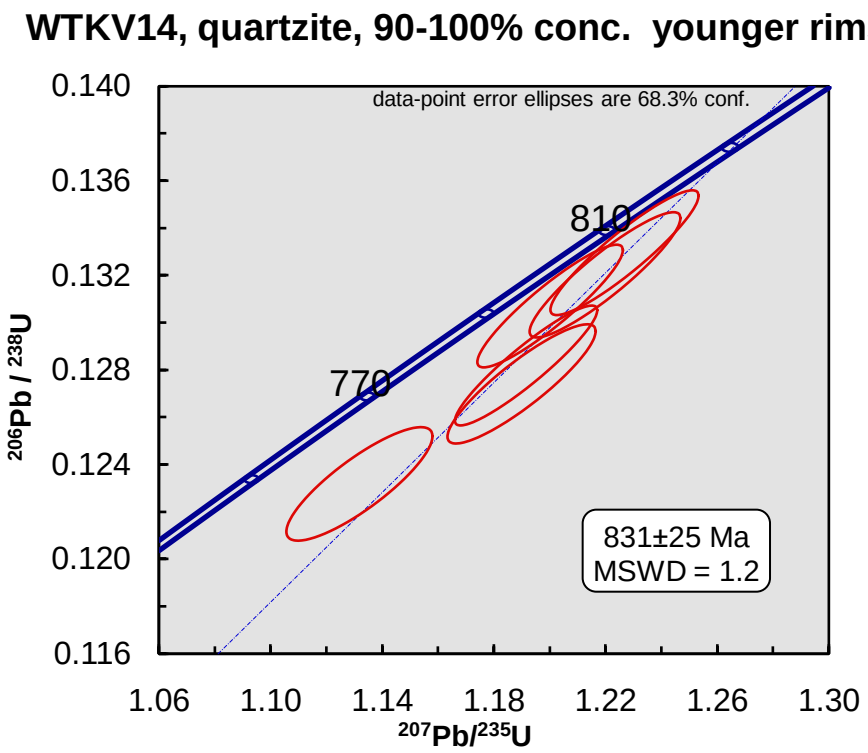

Figure 27. Concordia plot of 90-100% concordant data from younger rim analyses in sample WTKV14.

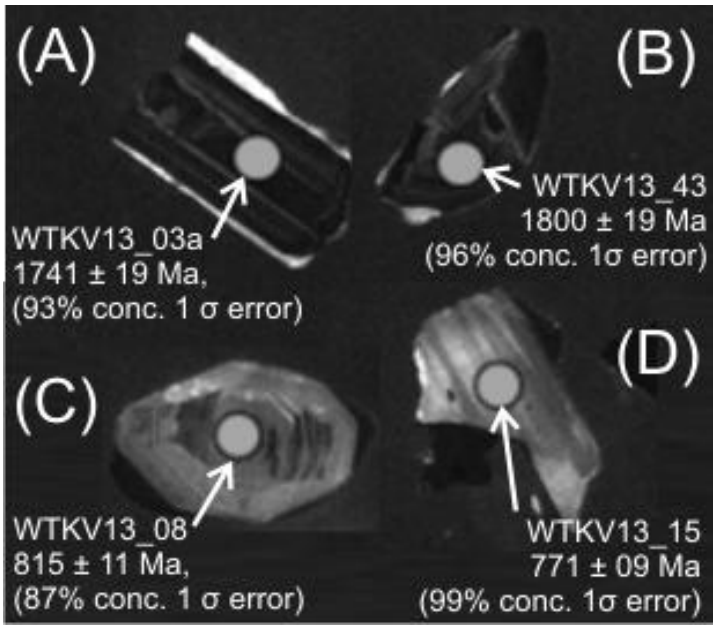

Figure 28. CL images of zircons from sample WTKV13, a felsic gneiss. Small filled spots are locations of U/Pb analysis and are 30µm. (A) Broken and rounded terminations present on this zircon of igneous appearance are common on many of the zircons in this sample. The dark CL response of this zircon is typical of the ~1750 Ma zircon population in WTKV13. (B) This zircon is a typical example of the morphology of the ~1750 Ma zircons. (C) "Ghost" Oscillatory zoning of bright CL response zircons was rare in this sample. WTKV13_08 was an exception. (D) This zircon is typical of the light CL response zircons of ~790 Ma $^{206}Pb/^{238}U$ age.

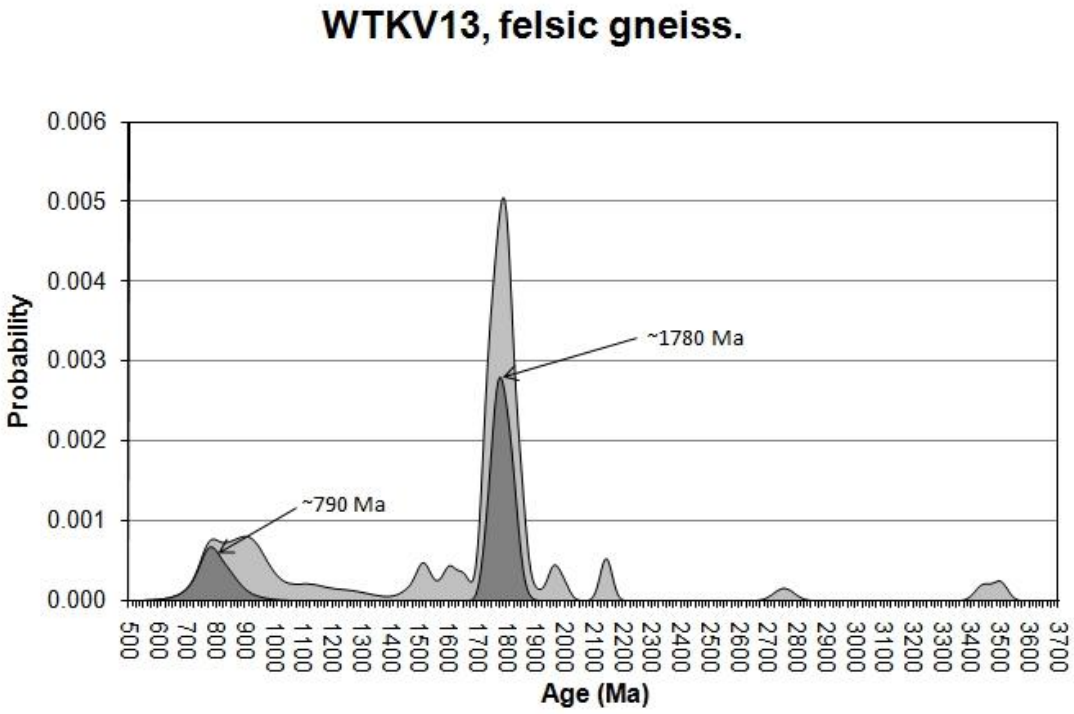

Figure 29. Probability density distribution plot of $^{207}Pb/^{206}Pb$ ages for sample WTKV13, a felsic gneiss (two feldspars-quartz-biotite-hornblende). Dark grey shaded area represents 95-105% concordant data, light grey shaded area represents all data. Two possible interpretations of this rock are made. One is that it is a meta-felsic volcanic that intruded at approximately 1779 Ma and that older, discordant analysis are zircons from country rock caught up during intrusion. The second interpretation is that this is a volcanoclastic or tuffaceous meta-sediment and the few older analyses are simply older detrital zircons incorporated into it. Note two clear populations; one at ~840 and one at ~1800 Ma.

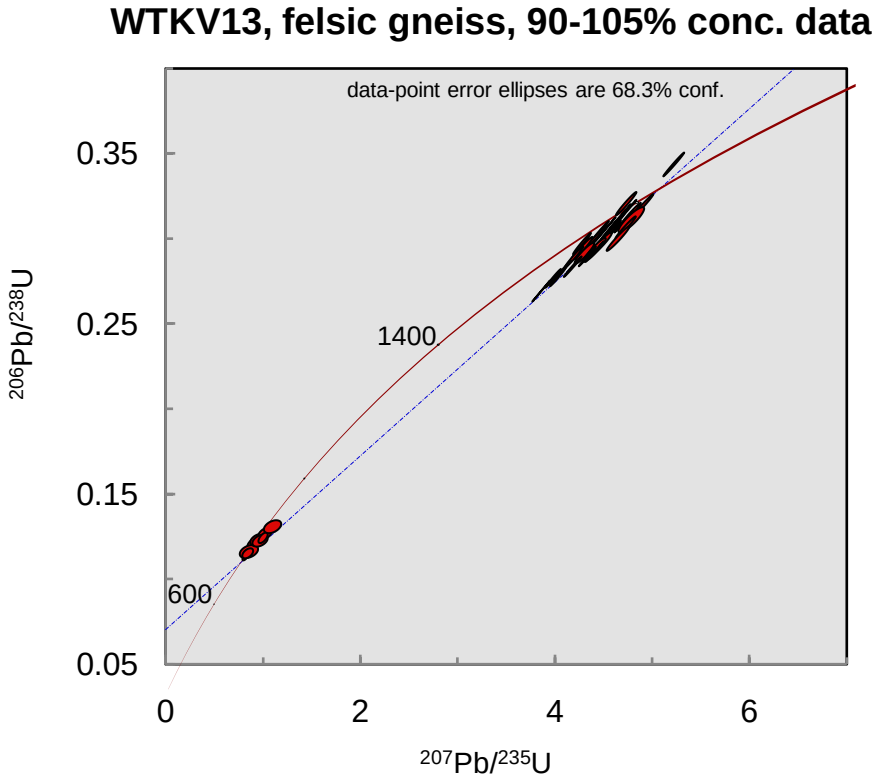

Figure 30. Concordia plot of 90-105% concordant data for sample WTKV13, a felsic gneiss.

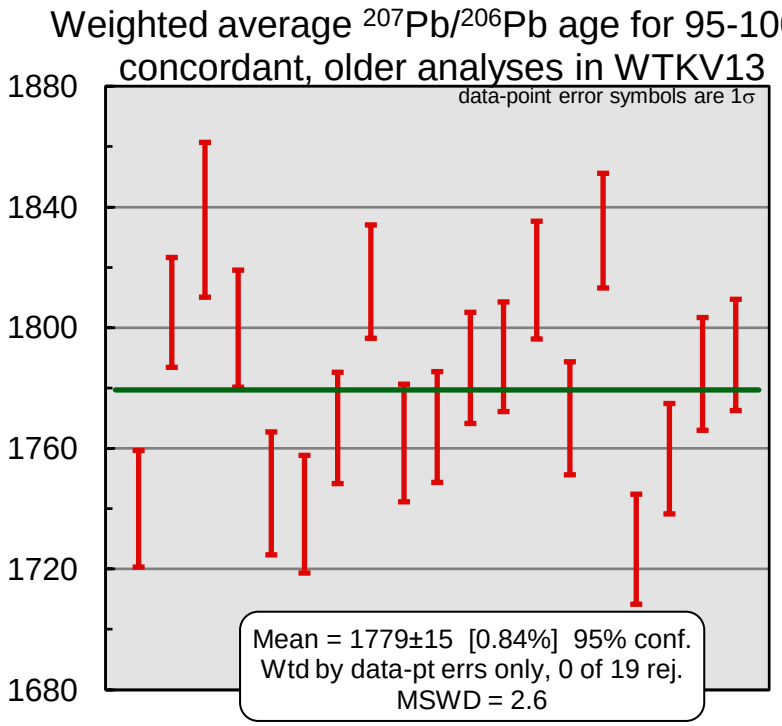

Figure 31. Weighted average $^{207}Pb/^{206}Pb$ age for older, 90-100% concordant data for sample WTKV13, a felsic gneiss.

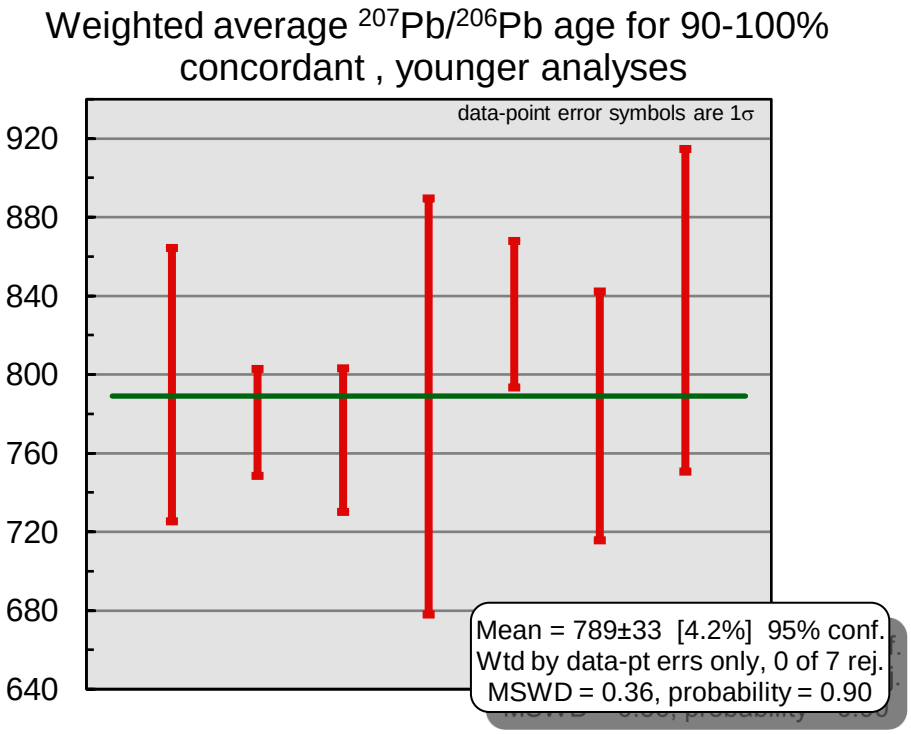

Figure 32. Weighted average $^{207}Pb/^{206}Pb$ age for younger, 90-100% concordant data for sample WTKV13.

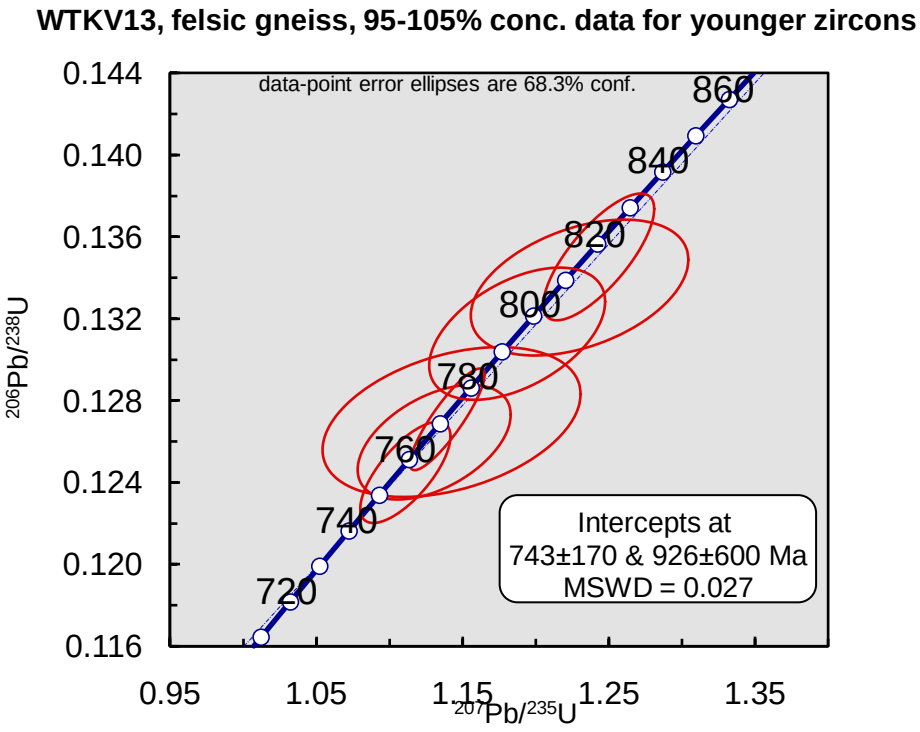

Figure 33. Concordia plot for 95-105% concordant data, for the younger population of zircons in sample WTKV13.

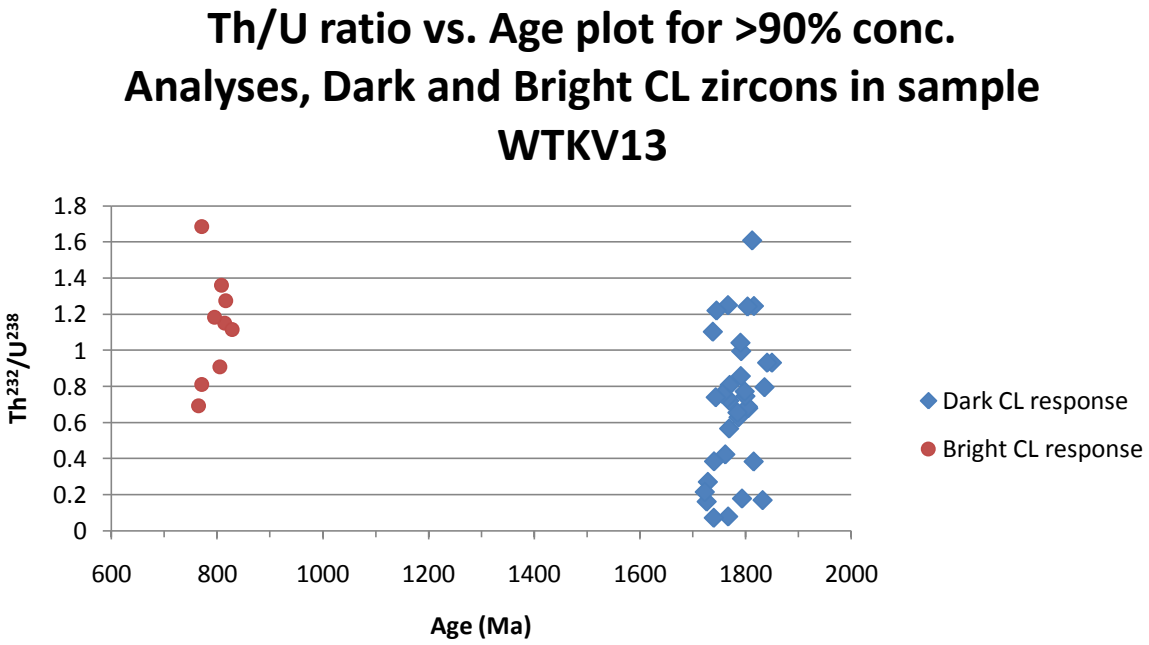

Figure 34. U/Th ratio versus age plot for both dark (~1720 - 1850 Ma) and bright (~800 Ma) CL response zircons.

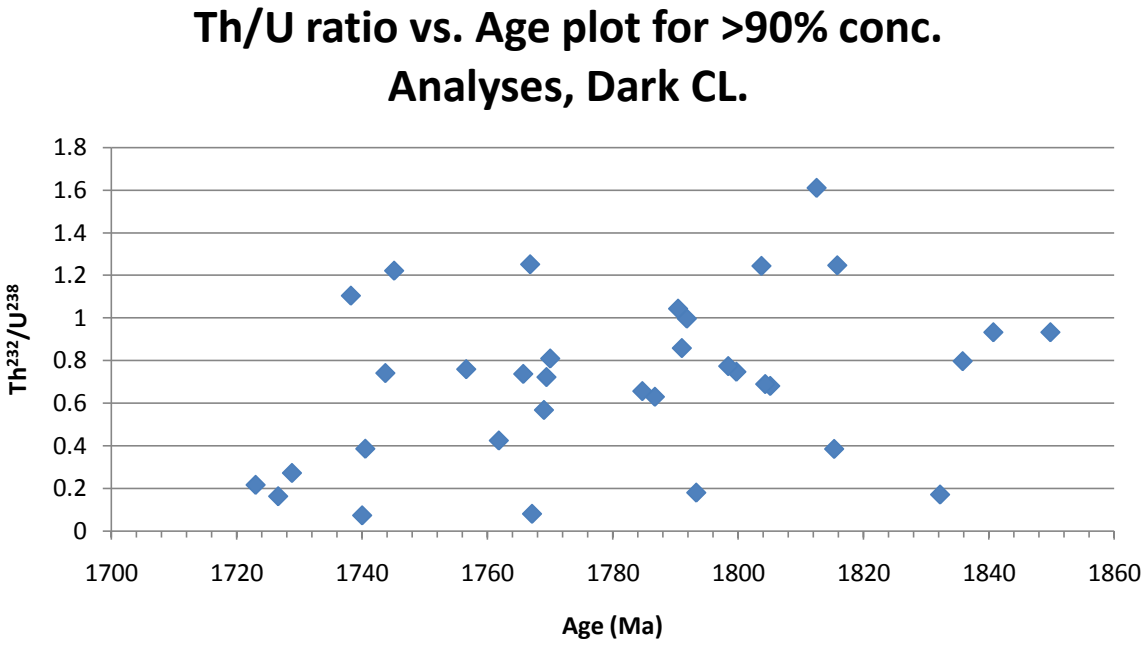

Figure 35. U/Th ratio versus age plot for dark CL response, older zircons.

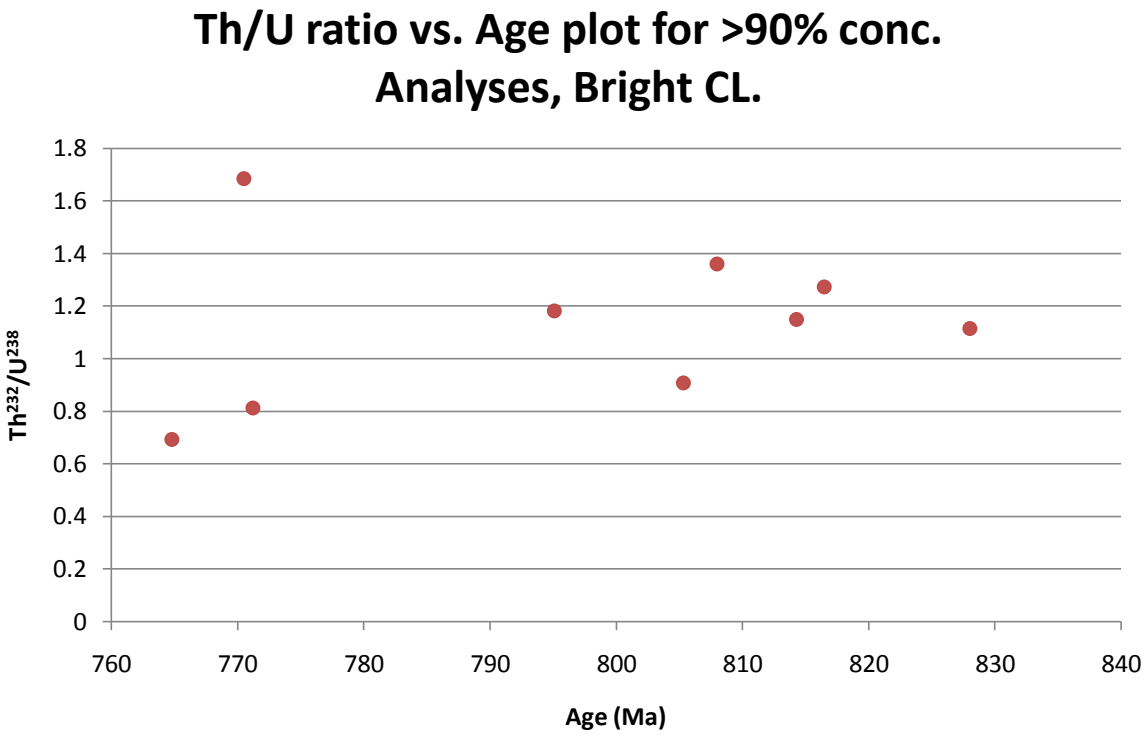

Figure 36. U/Th ratio versus age plot for bright CL response, younger zircons.

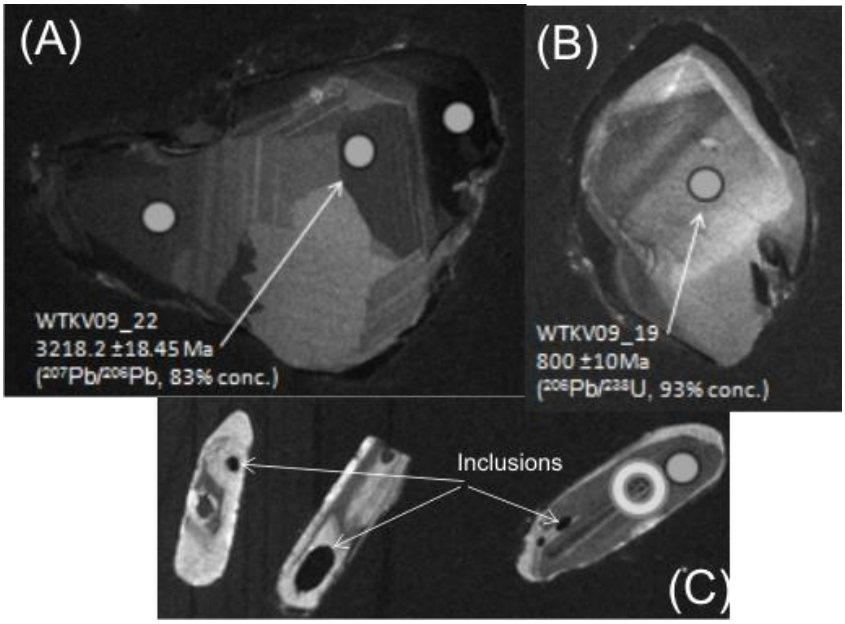

Figure 37. CL images of zircons from sample WTKV09, an anorthositic gabbro. Small filled spots are locations of U/Pb analysis and are 30µm; large hollow spot is Hf analysis point and is 50µm. (A) An unusually large zircon, with a core analysis of 3218 ± 18 Ma ($^{207}Pb/^{206}Pb$ age, 83% conc. 1σ error). (B) Homogenous recrystallisation is evident in this zircon. (C) Inclusions were common in this sample, indicated by the arrows.

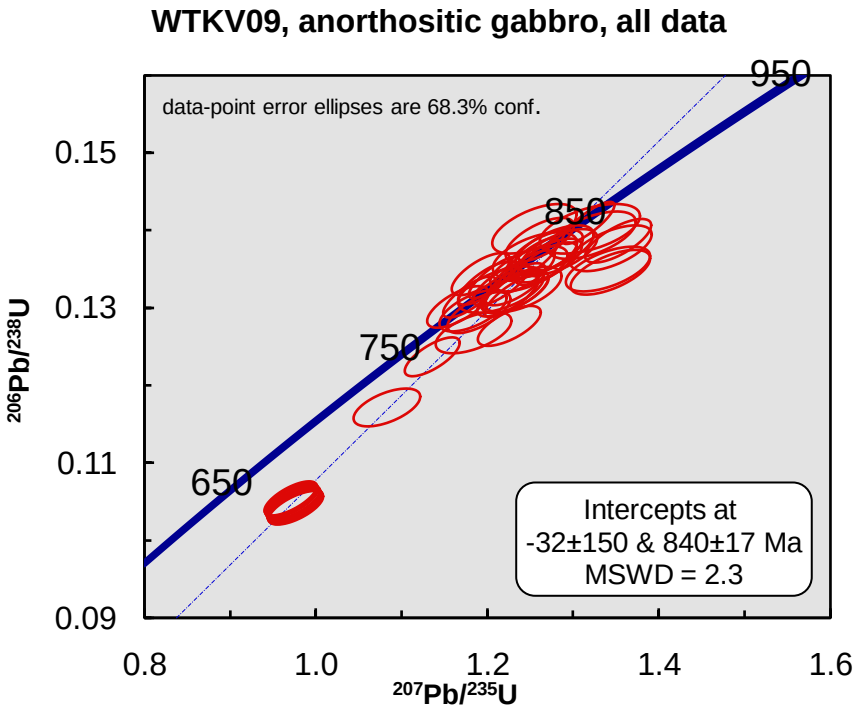

Figure 38. Concordia plot of all data for anorthositic gabbro sample WTKV09.

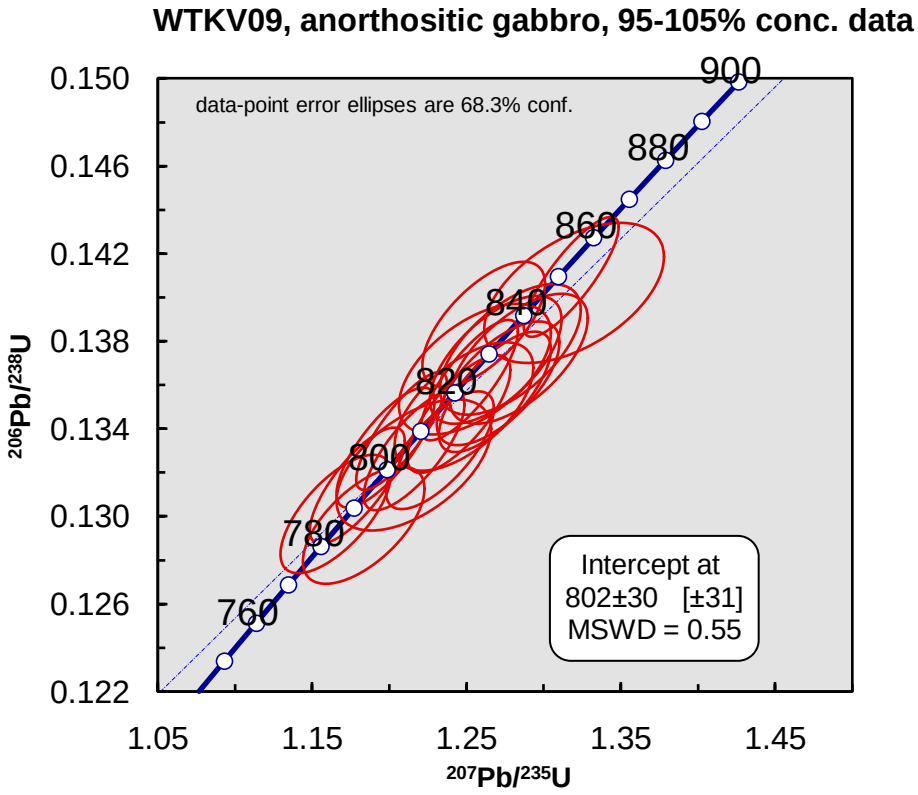

Figure 39. Concordia plot of 95-105% concordant data for the anorthositic gabbro sample WTKV09.

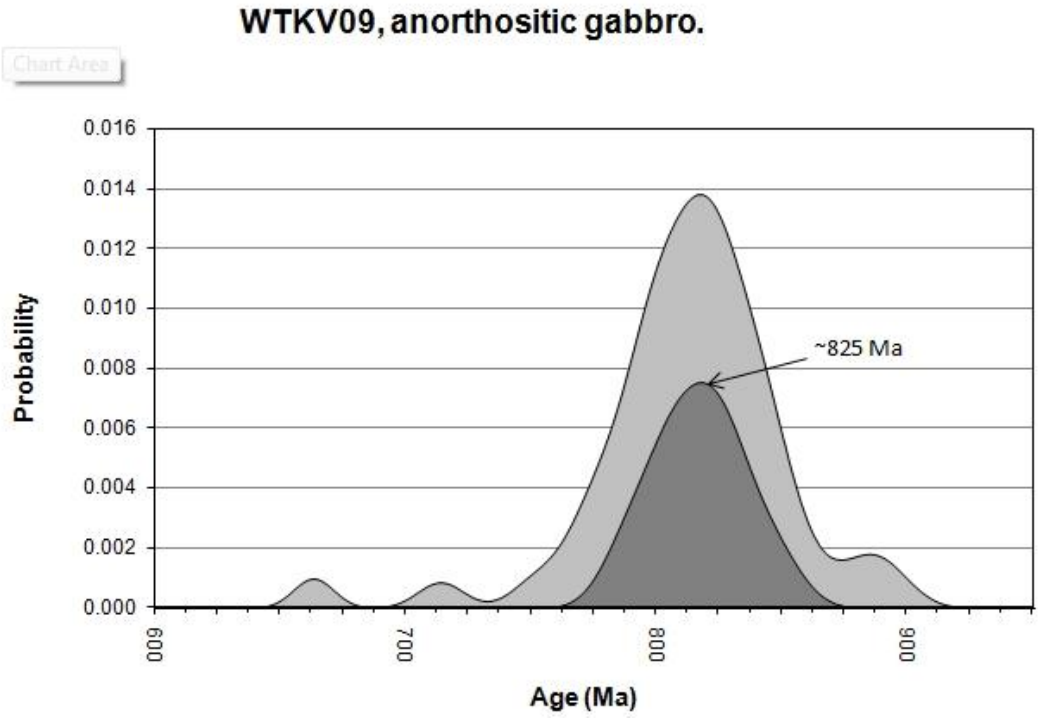

Figure 40. Probability density distribution plot of $^{206}Pb/^{238}U$ ages for sample WTKV09, an anorthositic gabbro. Dark grey shaded area represents 95-105% concordant data, light grey shaded area represents all data.

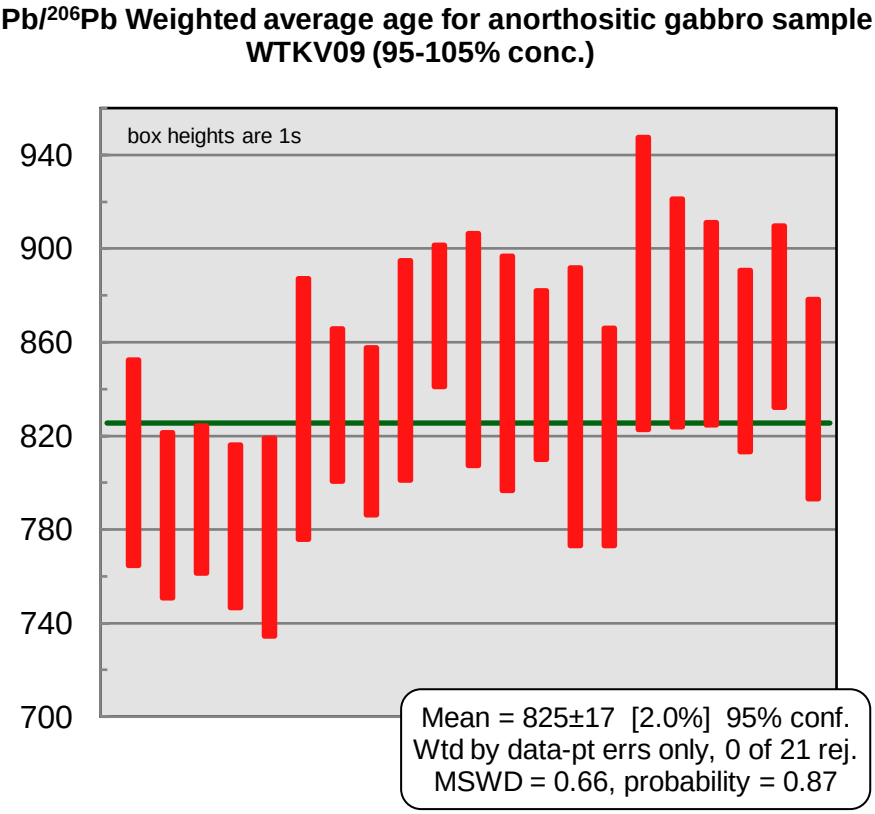

Figure 41. ^{207}Pb/^{206}Pb weighted average age plot of 95-105% concordant data for anorthositic gabbro WTKV09.

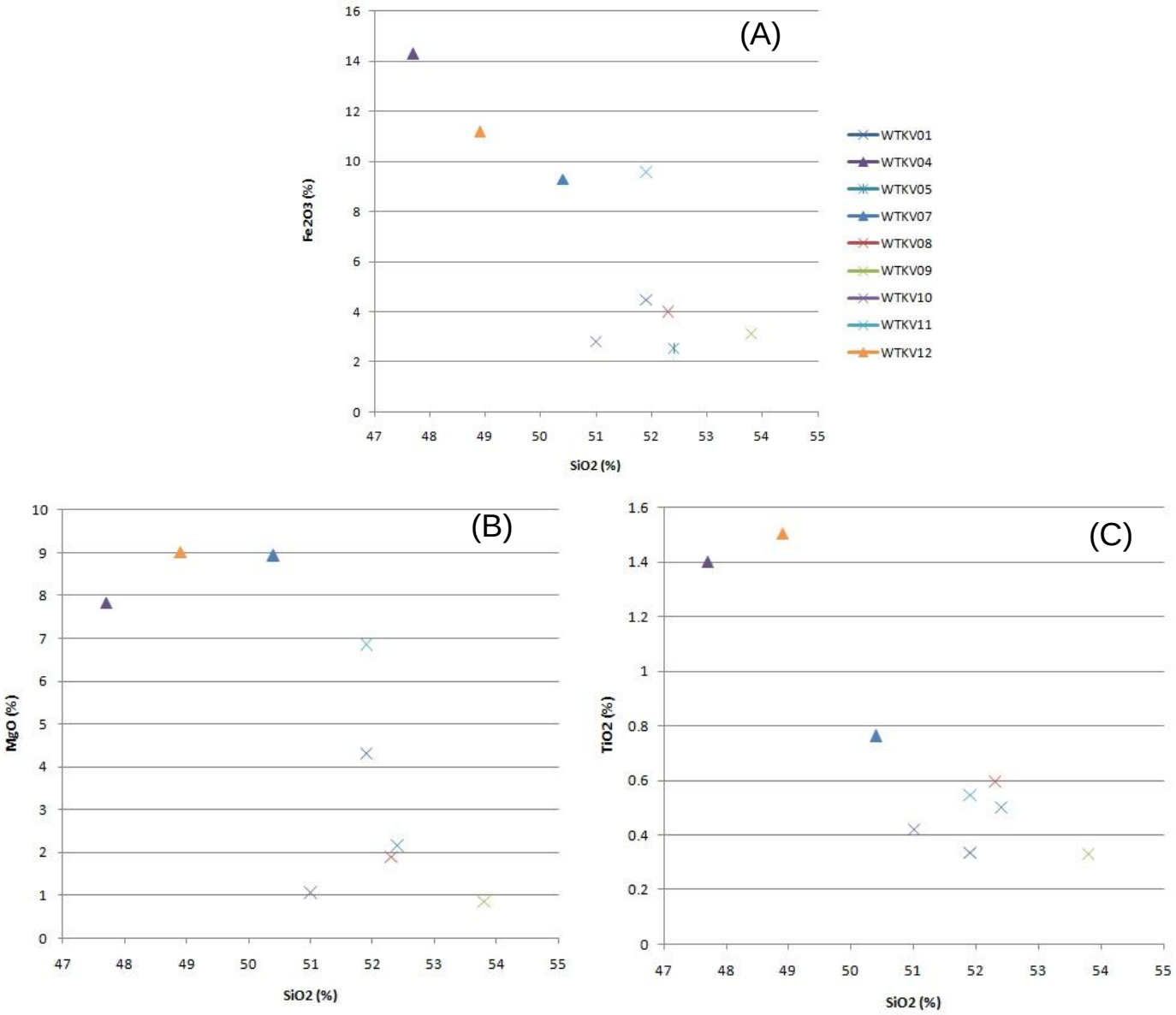

Figure 42. Binary plots of SiO2 versus Fe2O3, MgO and TiO2 for anorthositic/gabbroic/noritic samples. The legend shown for (A) applies to each plot. Hbl/Pl dominated samples are marked with a cross, while Opx/Cpx dominated samples are marked with a triangle. Note higher levels of each oxide in the Opx/Cpx gabbros.

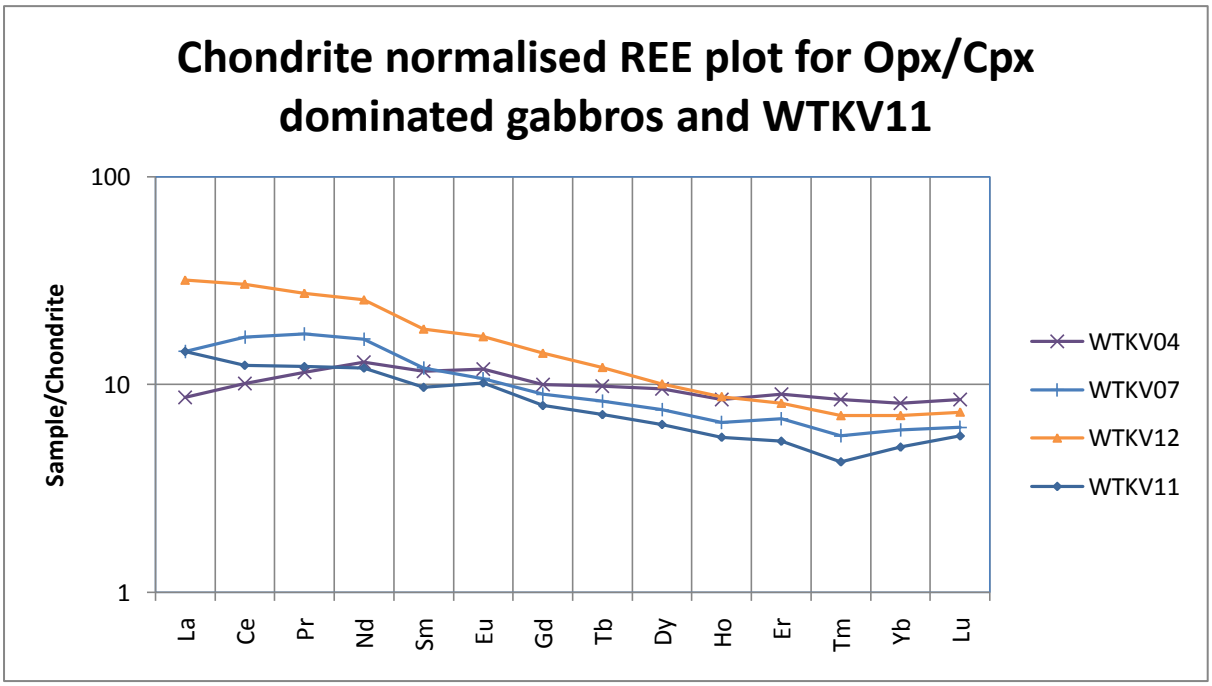

Figure 43. Chondrite normalised rare earth element plot for the igneous samples without a positive europium anomaly. Samples WTKV04, 07 and 12 are each dominated by ortho- and clinopyroxene, while WTKV11 is more like the samples on the plot below and is dominated by plagioclase and hornblende. Note relatively flat pattern. Value for chondrite from Anders and Grevesse, 1989.

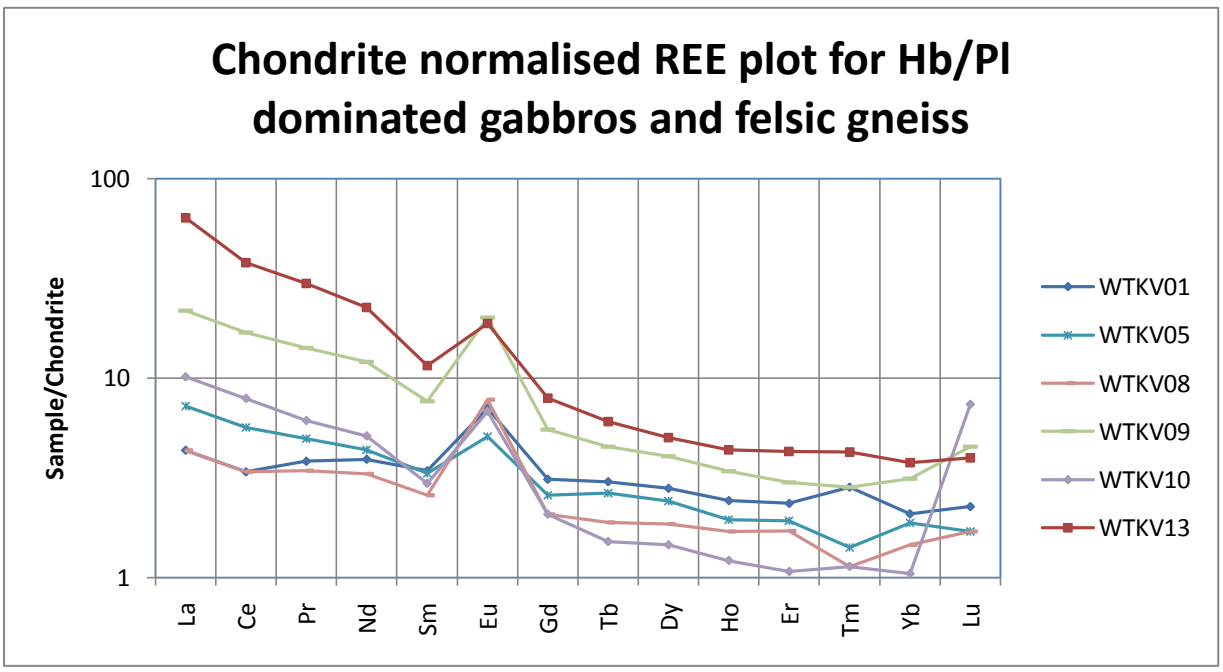

Figure 44. Chondrite normalised rare earth element plot for igneous samples with a positive europium anomaly. Each sample is dominated by plagioclase and hornblende, with the exception of sample WTKV13, a felsic gneiss (tuffaceous/volcanoclastic meta-sediment or meta-felsic volcanic) dominated by quartz, K-feldspar and plagioclase. Value for chondrite from Anders and Grevesse, 1989.

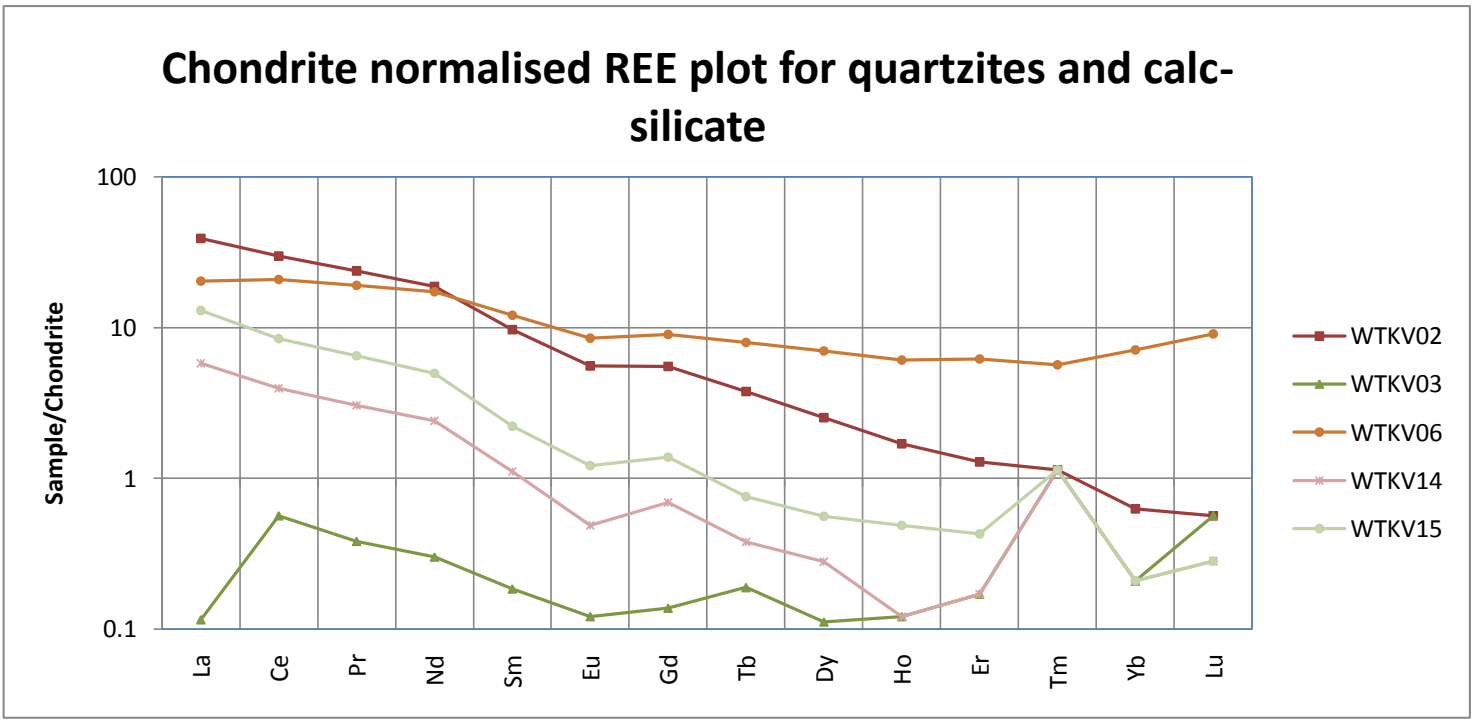

Figure 45. Chondrite normalised rare earth element plot for meta-sedimentary samples. WTKV02, 03, 14 and 15 are quartzites, WTKV06 is a hedenbergite-scapolite calc-silicate. Value for chondrite from Anders and Grevesse, 1989

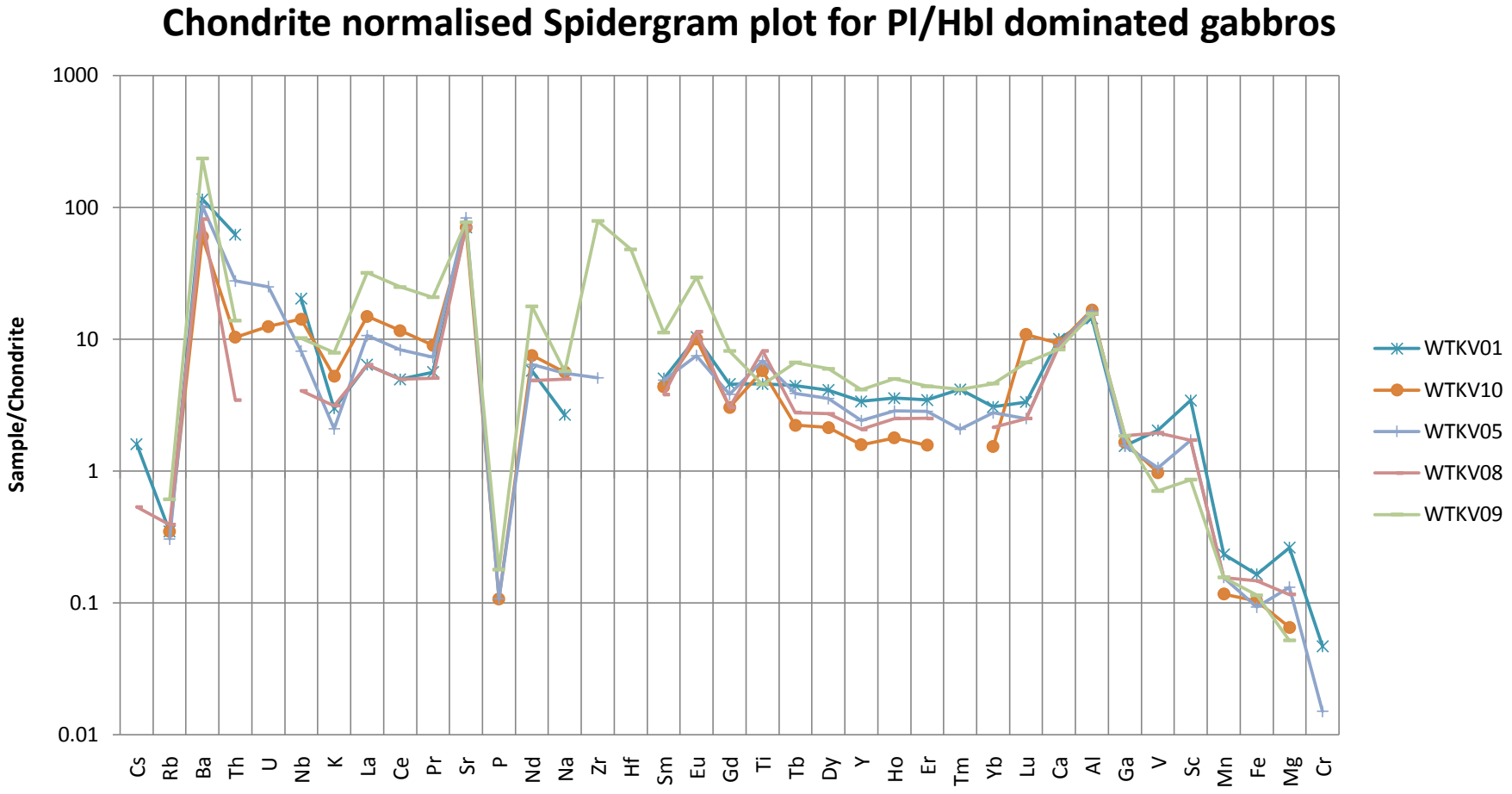

Figure 46. Spidergram plot for the plagioclase-hornblende dominated gabbros.

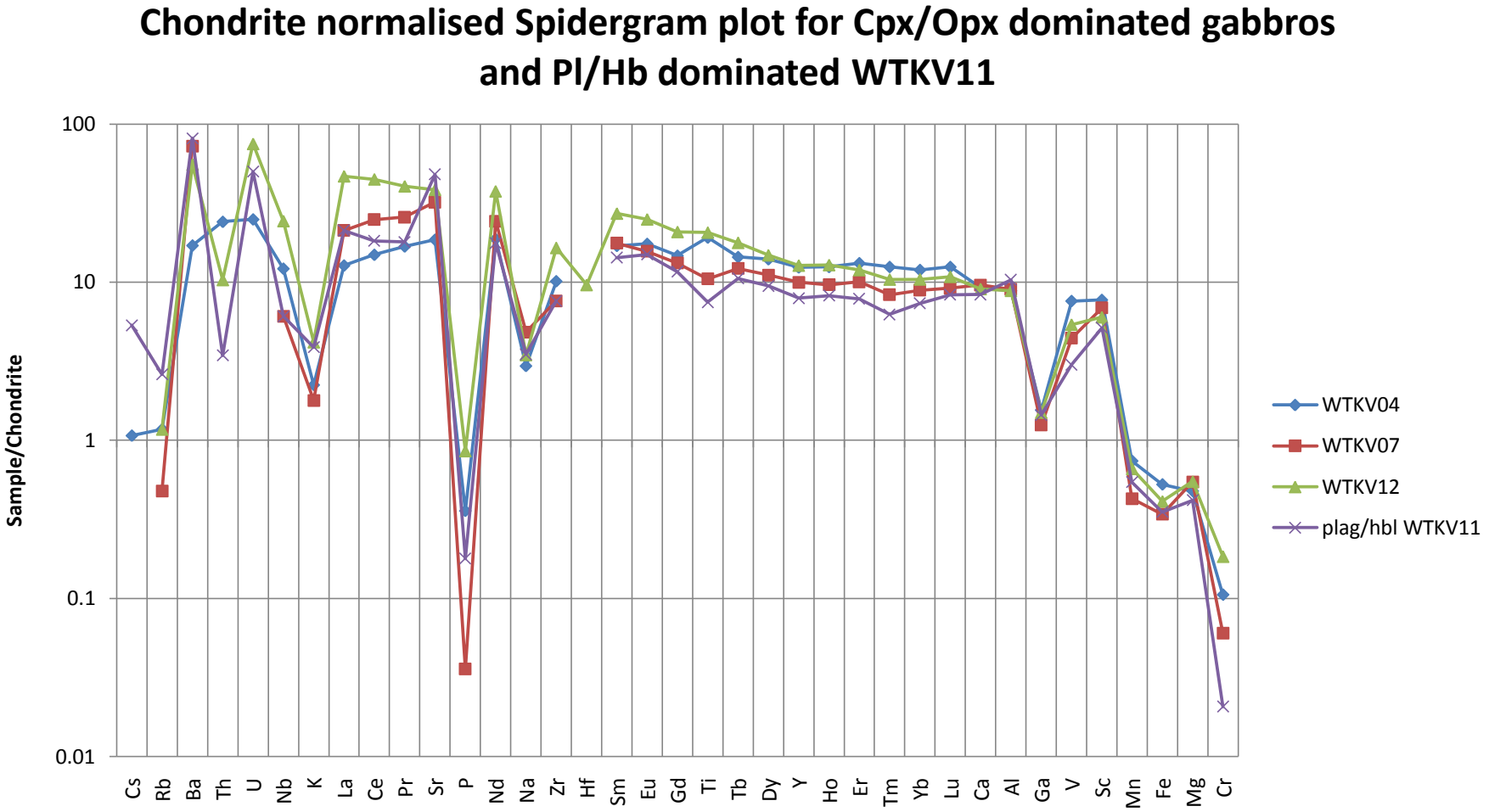

Figure 47. Spidergram plot for the ortho- and clinopyroxene dominated gabbros, and the plagioclase-hornblende dominated gabbro, WTKV11. WTKV11 has been included with this plot as its signature is very similar to the other samples on this plot.

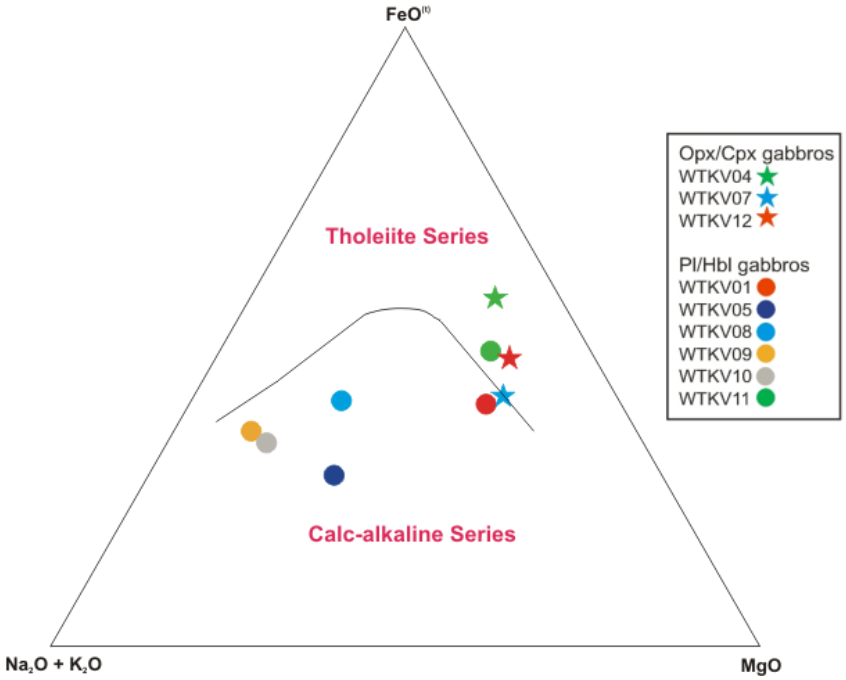

Figure 48. Ternary plot of FeO (total) – MgO – $Na_2O + K_2O$ after Irvine and Baragar (1971).

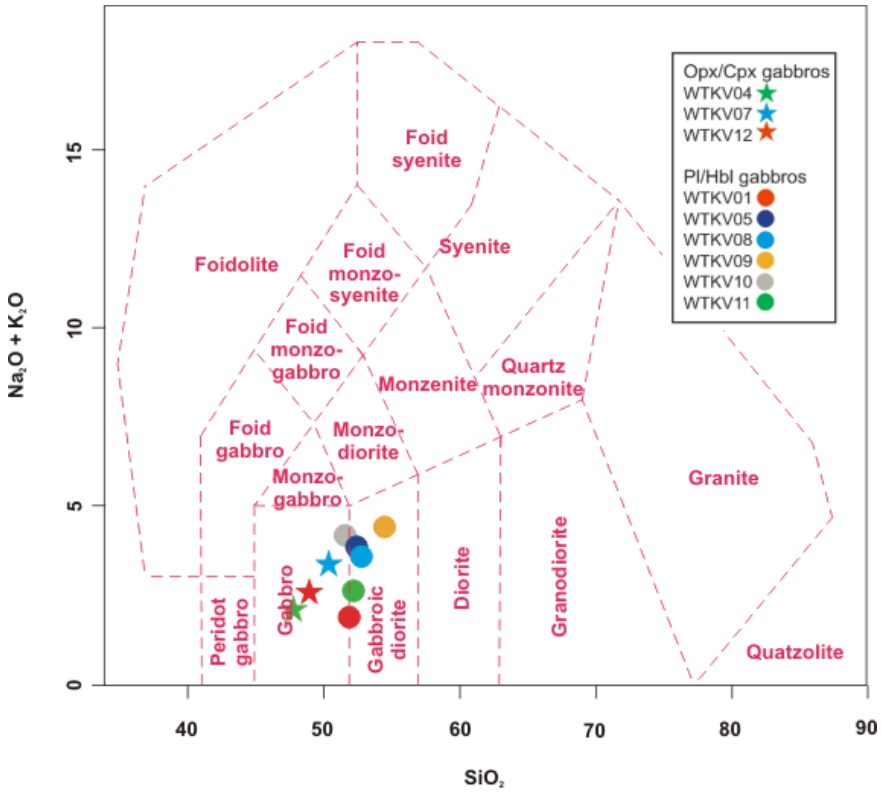

Figure 49. Binary Plot of SiO_2 versus $Na_2O + K_2O$ after Middlemost (1985). All three ortho- and clinopyroxene dominated gabbros plot in the gabbro field, and the plagioclase/hornblende dominated gabbros plot as gabbro-diorites very near the gabbro field.

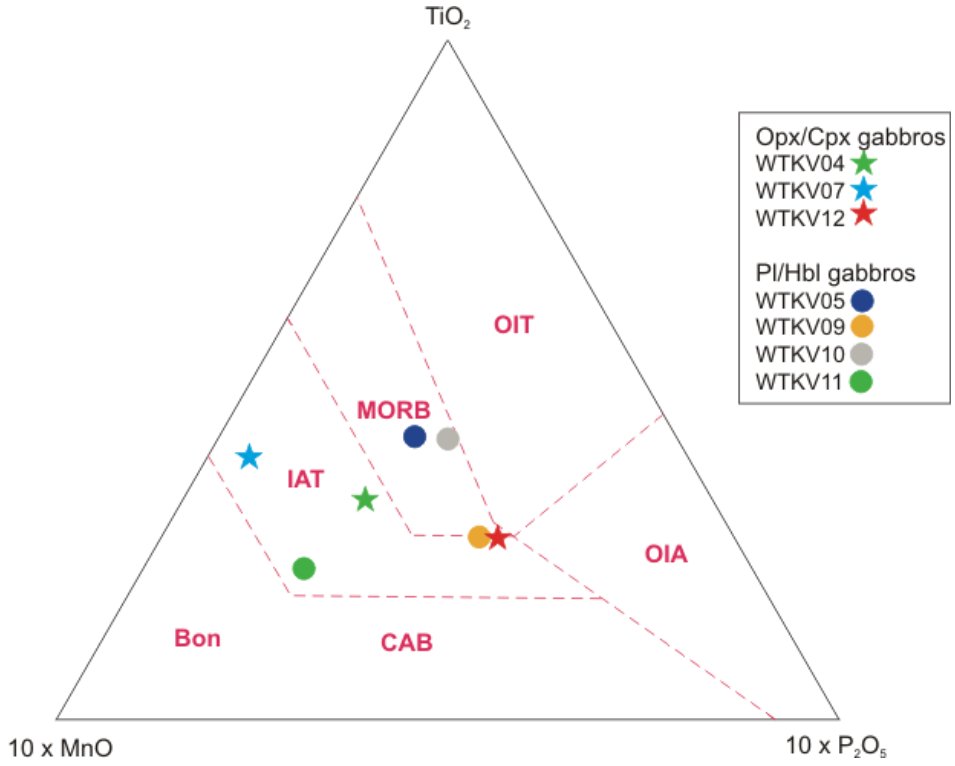

Figure 50. Ternary plot of TiO_2 – 10 x MnO – 10 x P2O5 after Mullen (1983). MORB = Mid Ocean Ridge Basalt, IAT = Island Arc Tholeiite, CAB = Island Arc Calc-Alkaline, OIA = Seamount Alkalic, OIT = Seamount Tholeiite, Bon = Boninite

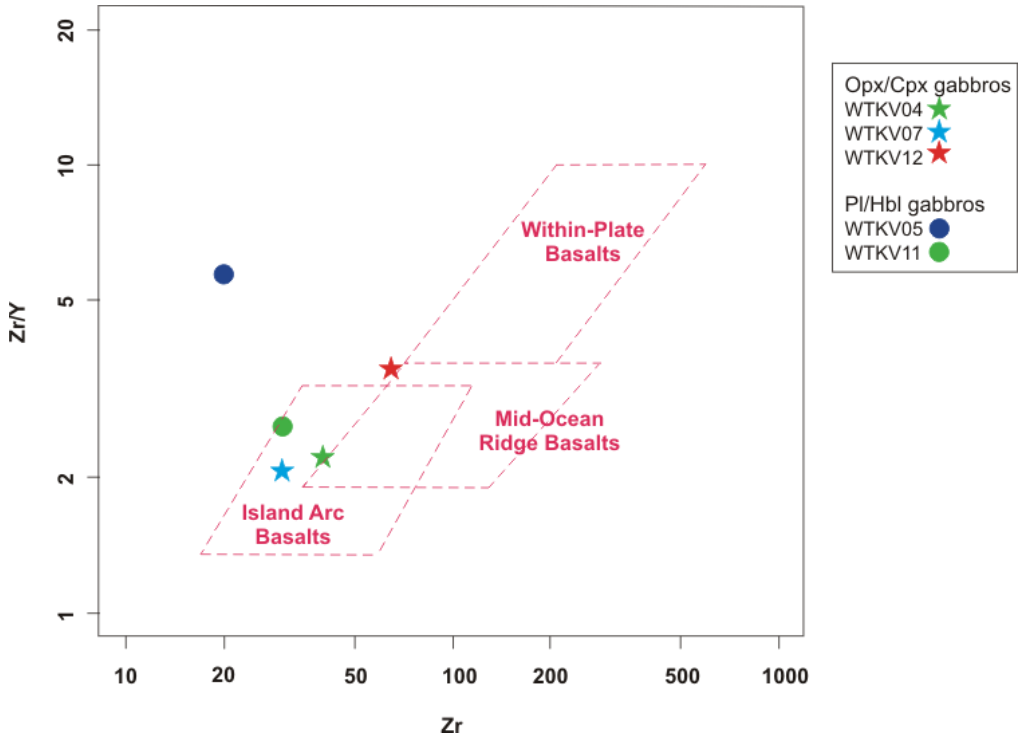

Figure 51. Plot of Zr versus Zr/Y after Pearce & Norry (1979).

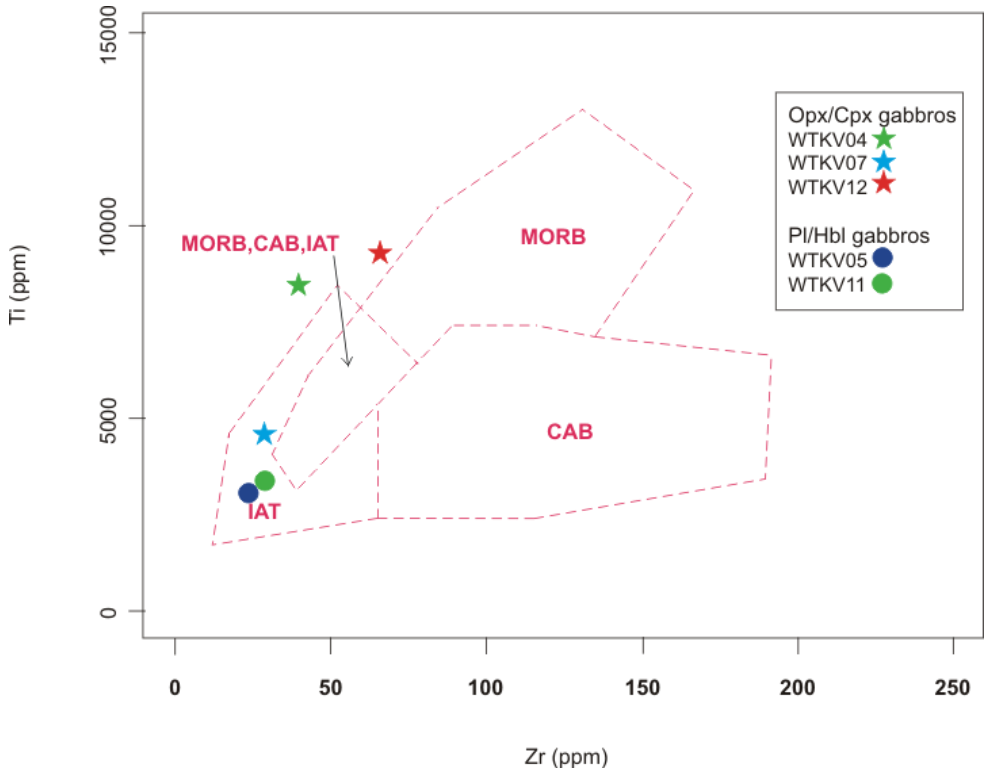

Figure 52. Ti versus Zr plot after Pearce and Cann (1973). MORB = Mid Ocean Ridge Basalt, CAB = Island Arc Calc-Alkaline, IAT = Island Arc Tholeiite.

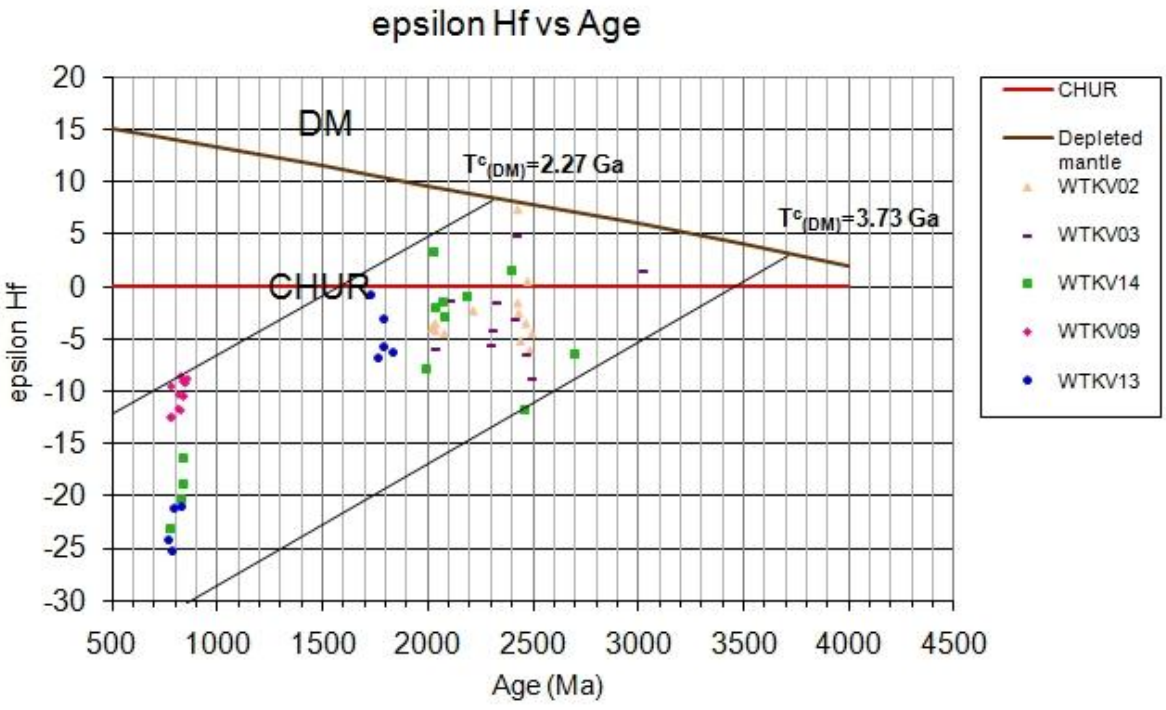

Figure 53. Epsilon Hf (*T*) vs. age plot of concordant detrital zircon analyses for quartzite samples (WTKV02, 03 and 14), anorthositic gabbro (WTKV09) and felsic gneiss (WTKV13). The majority of analyses yielded negative εHf values. Only the three quartzites show any positive εHf values, mostly clustered at ~2500Ma.

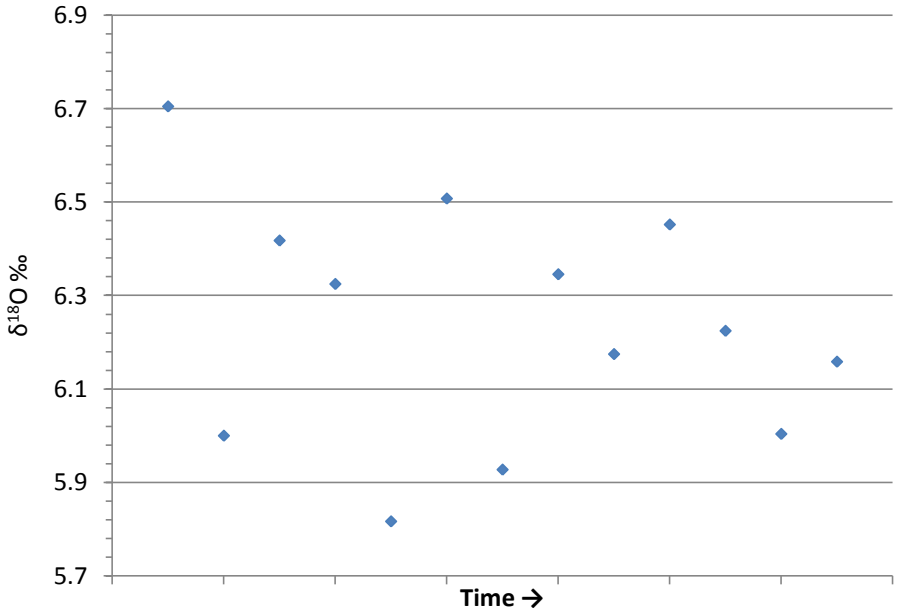

Figure 54. Plot of $\delta^{18}O$ versus time, with oldest analysis on the left (~750 Ma) and youngest on the right (~840 Ma). Further analysis of rocks in the area is needed.

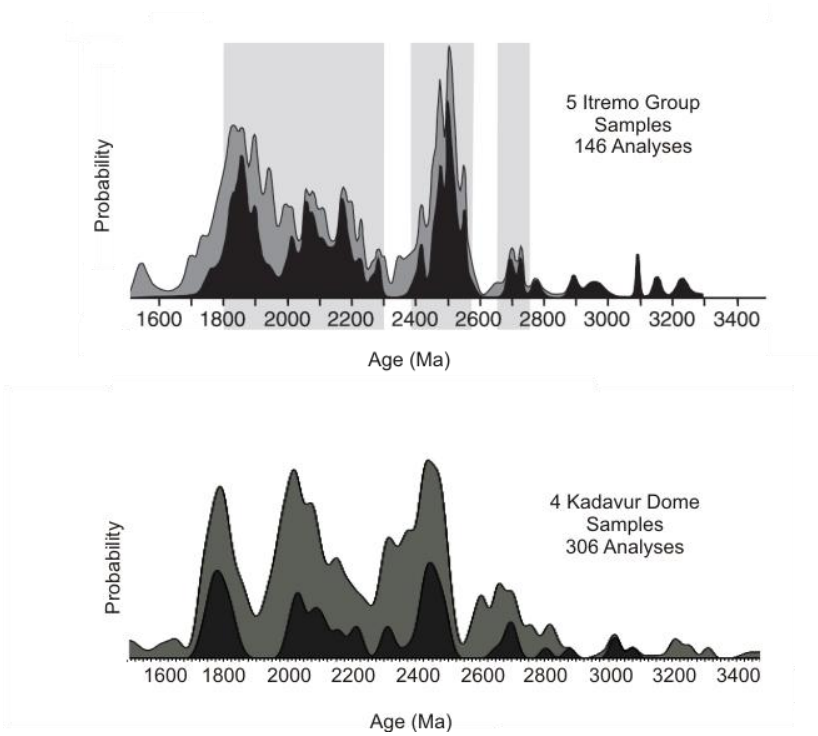

Figure 55. Probability density distribution of detrital zircon ages for the Itremo Group, Madagascar (top) and for the Kadavur Dome (bottom), (Itremo plot modified from Fitzsimons and Hulscher, 2005). Note close match of peaks. Itremo Group also has a younger population of 700 – 850 Ma grains not shown on this plot, as does the Kadavur Dome.

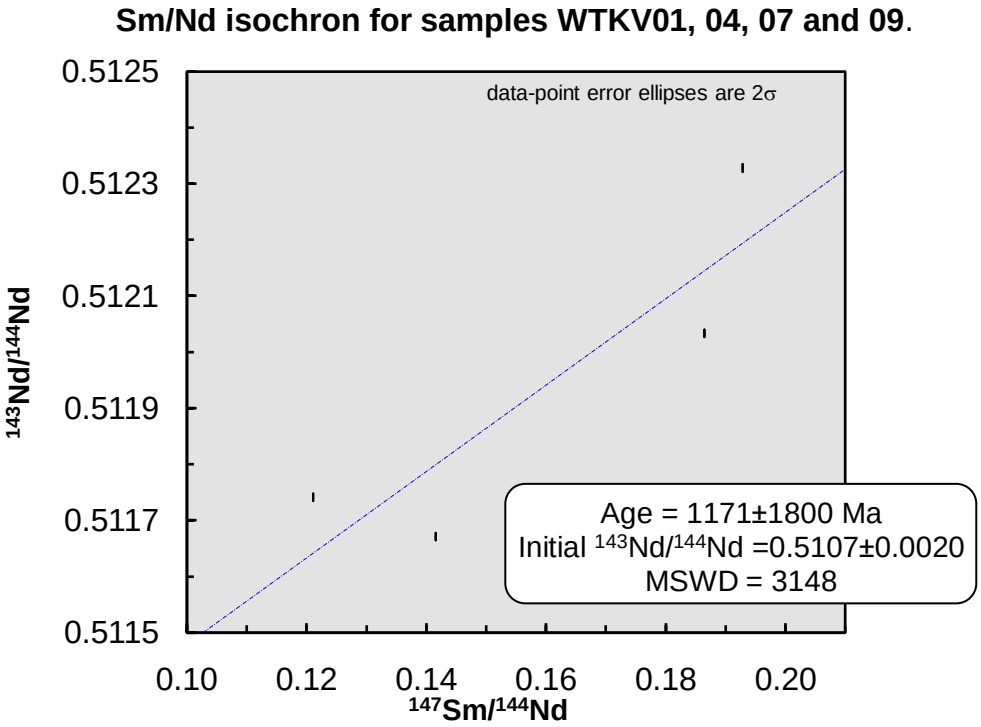

Figure 56. Sm/Nd isochron for igneous samples analysed by TIMS. Plot includes samples WTKV01 and WTKV09 (Hbl/Pl dominated gabbros) and also WTKV04 and WTKV07 (Opx/Cpx dominated gabbros). Note data appears to form two separate, sub-parallel isochrons of two points each. Insufficient data points restrict the accuracy of this data.

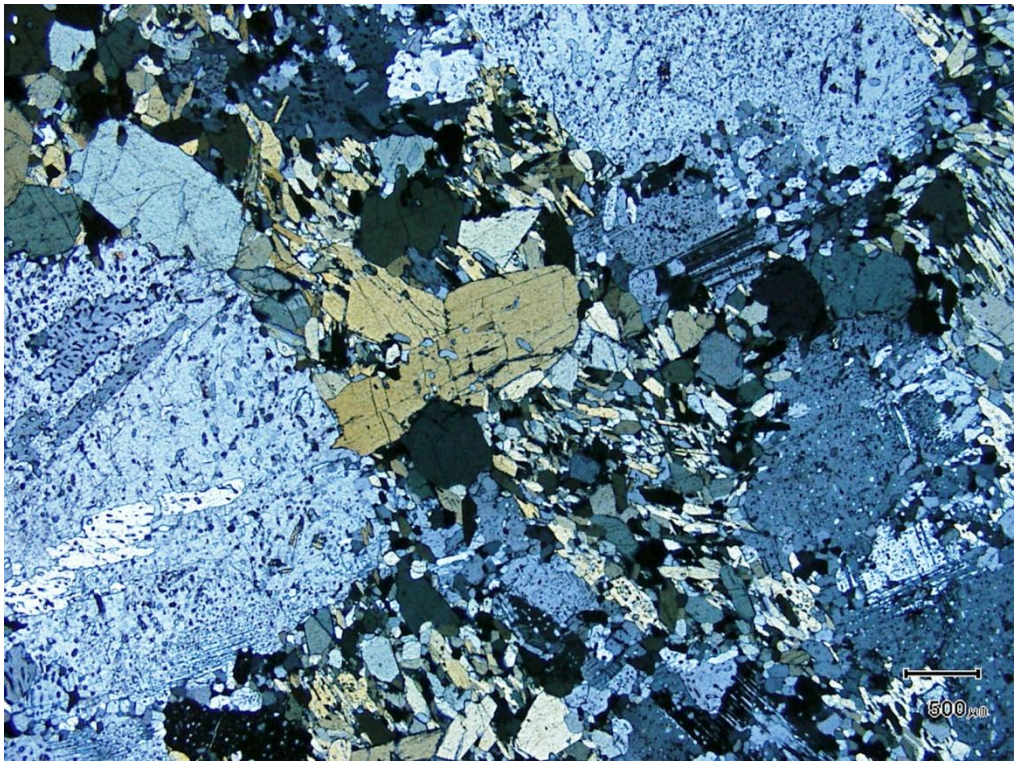

Figure 57. WTKV01. General textural view showing poikilitic plagioclase, hornblende and recrystallised variants of each. Mag. x20; scale bar = 500µm; crossed nicols.

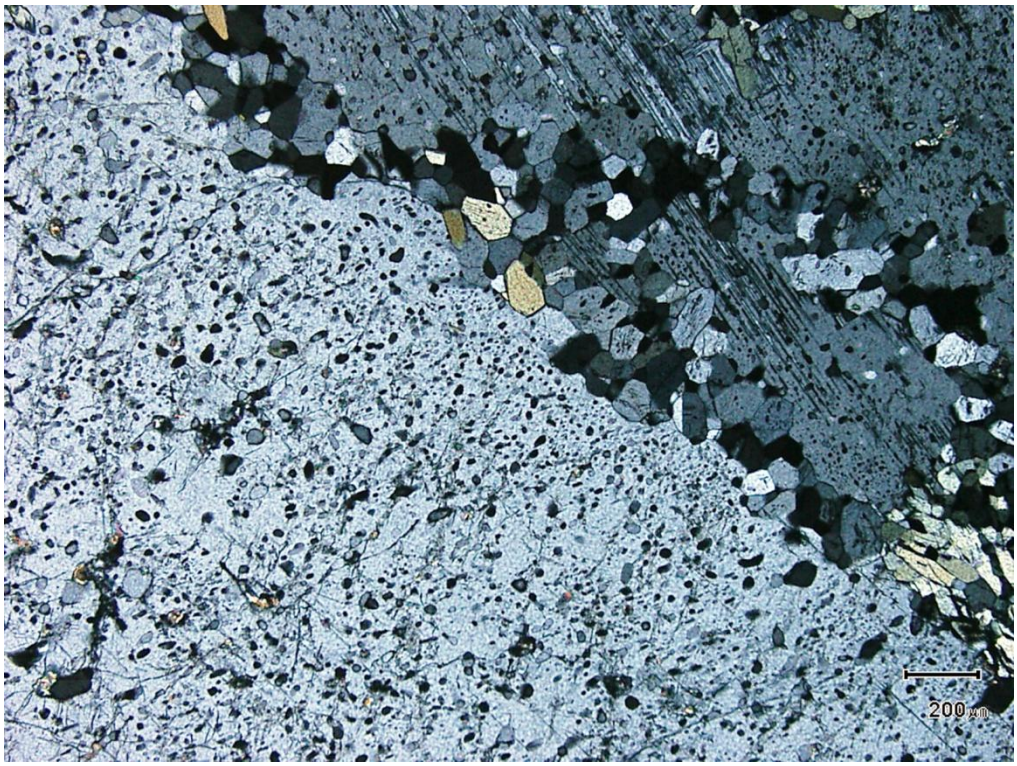

Figure 58. WTKV01. Higher magnification view of Figure X (above) showing highly poikiloblastic plagioclase with polygonal grain aggregates developed along grain boundaries. Mag. x 50; scale bar = 200 µm; plane polarised light.

Figure 59. WTKV01, plane polarised light. Pseudo-polygonal aggregate of recrystallised hornblende. Mag. x 200; scale bar = 50 µm; plane polarised light.

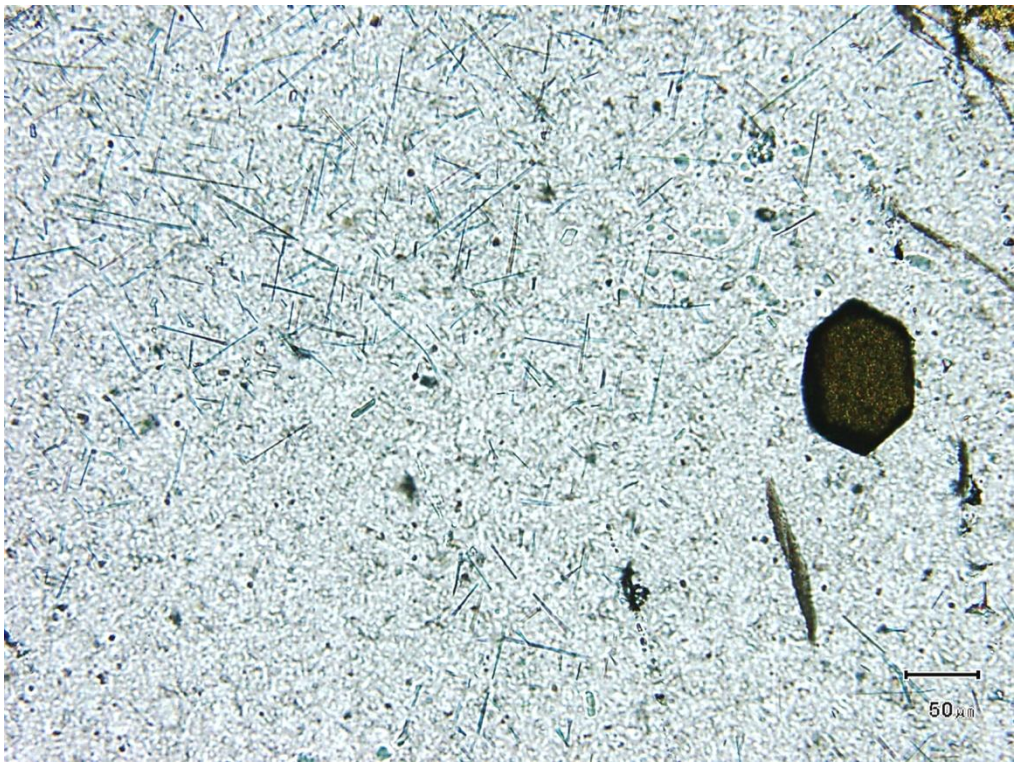

Figure 60. WTKV02, Crystallographically oriented rutile needles in quartz. Note the large rutile crystal RHS of photomicrograph. Mag. x 200; Scale bar = 50 µm; plane polarised light.

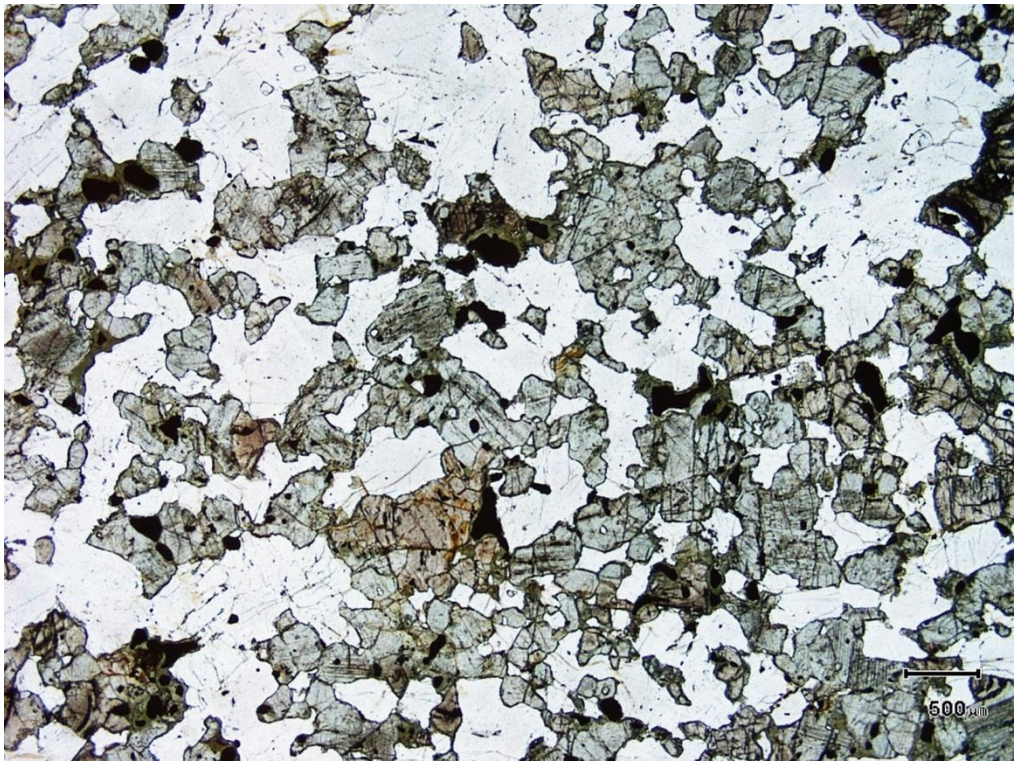

Figure 61. WTKV04, General textural view of a gabbro containing hornblende, clinopyroxene, orthopyroxene, plagioclase and ilmenite. Mag. x 200; Scale bar = 500 µm; plane polarised light.

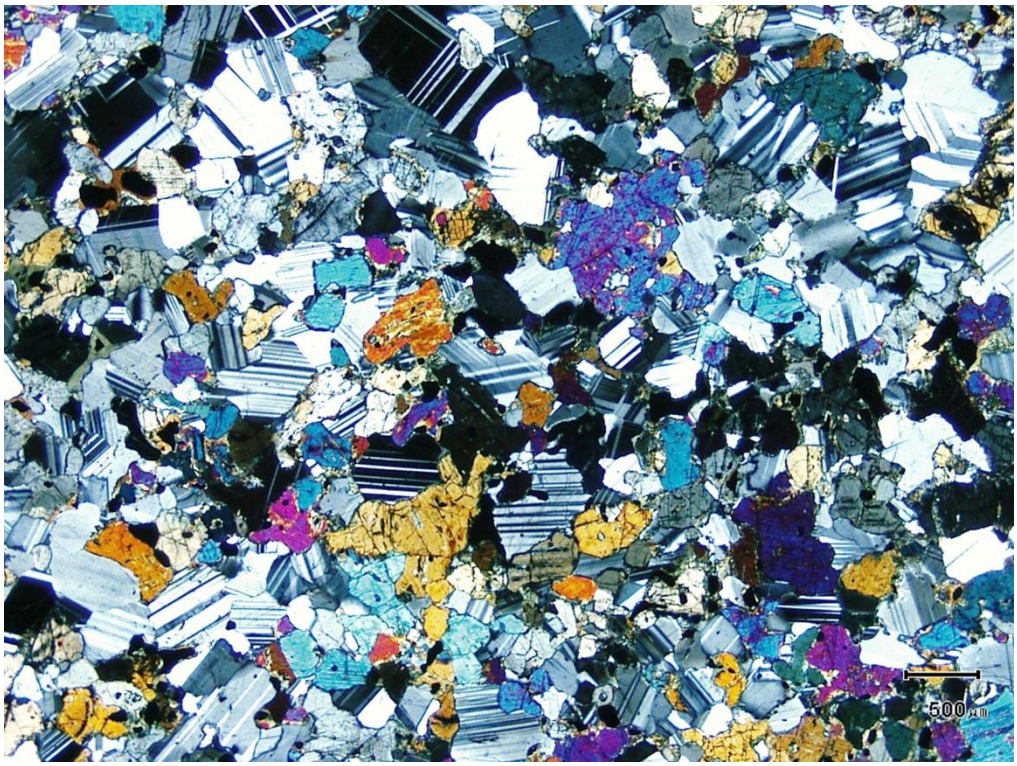

Figure 62. WTKV04, cross nicols view of Figure 61(above).

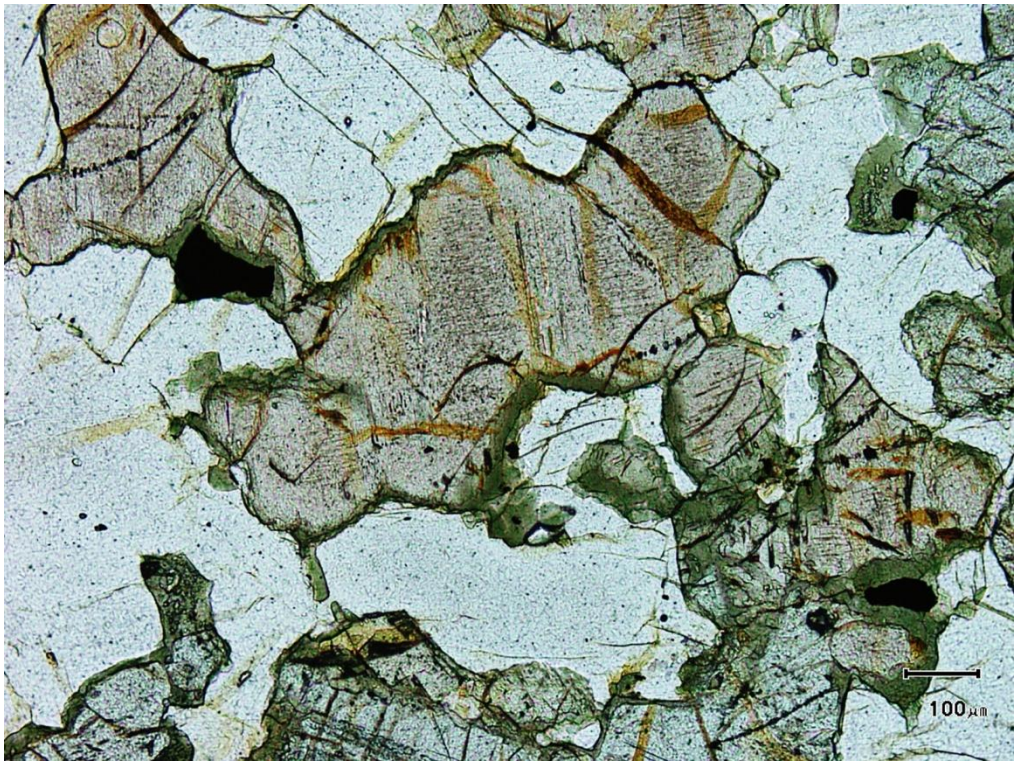

Figure 63. WTKV04, This photomicrograph shows hornblende rimming orthopyroxene. Mag. x 100; Scale bar = 100 µm; plane polarised light.

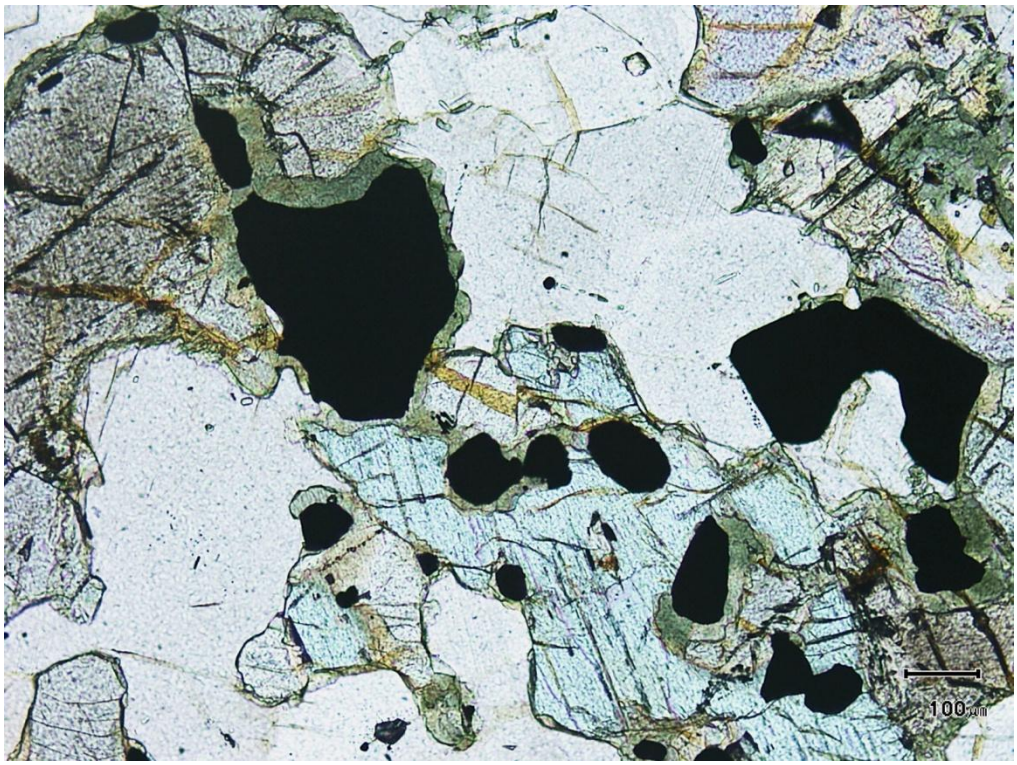

Figure 64. WTKV04, This photomicrograph shows hornblende rimming ilmenite. This may be a deuteric feature or a function of later metamorphism. Mag. x 100; Scale bar = 100 µm; plane polarised light.

Figure 65. WTKV05, General textural view of a pyroxene absent and hornblende bearing gabbro. Mag. x 20; Scale bar = 500 µm; plane polarised light.

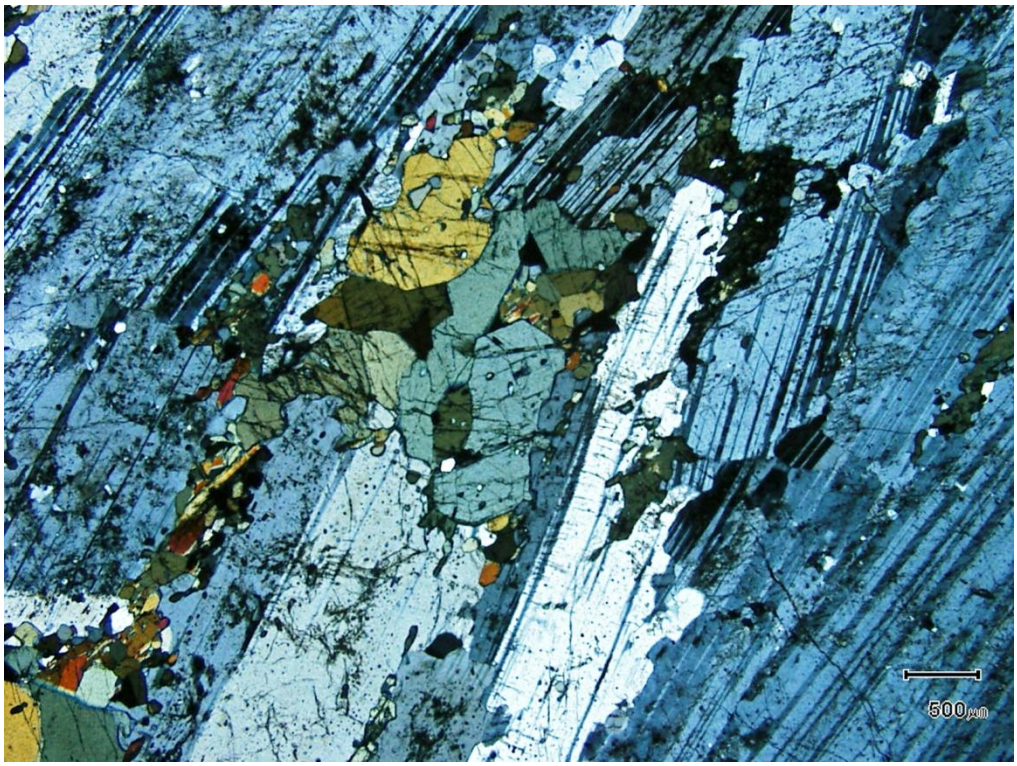

Figure 66. WTKV05, cross nicols view of Figure X (above). Note the preferred orientation of the plagioclase grains. Mag. x 20; Scale bar = 500 µm; crossed nicols.

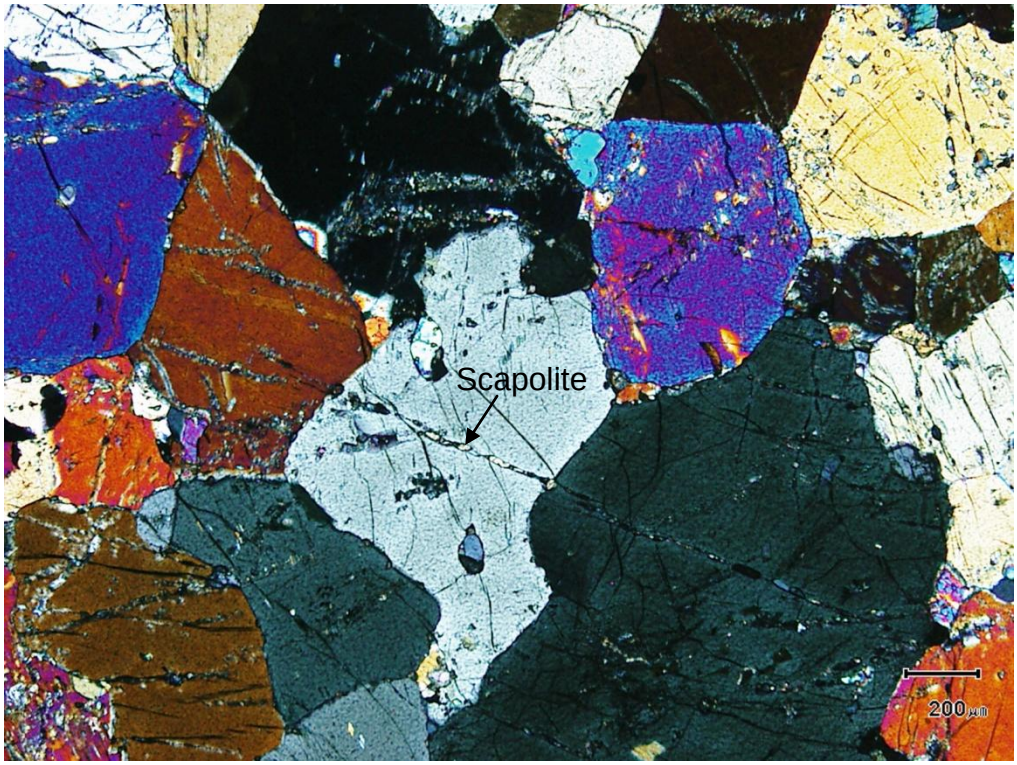

Figure 67. WTKV06, Scapolite with clinopyroxene showing general polygonal texture. Note the scapolite “trails” which crosscut the general texture. Mag. x 50; Scale bar = 200 µm; crossed nicols.

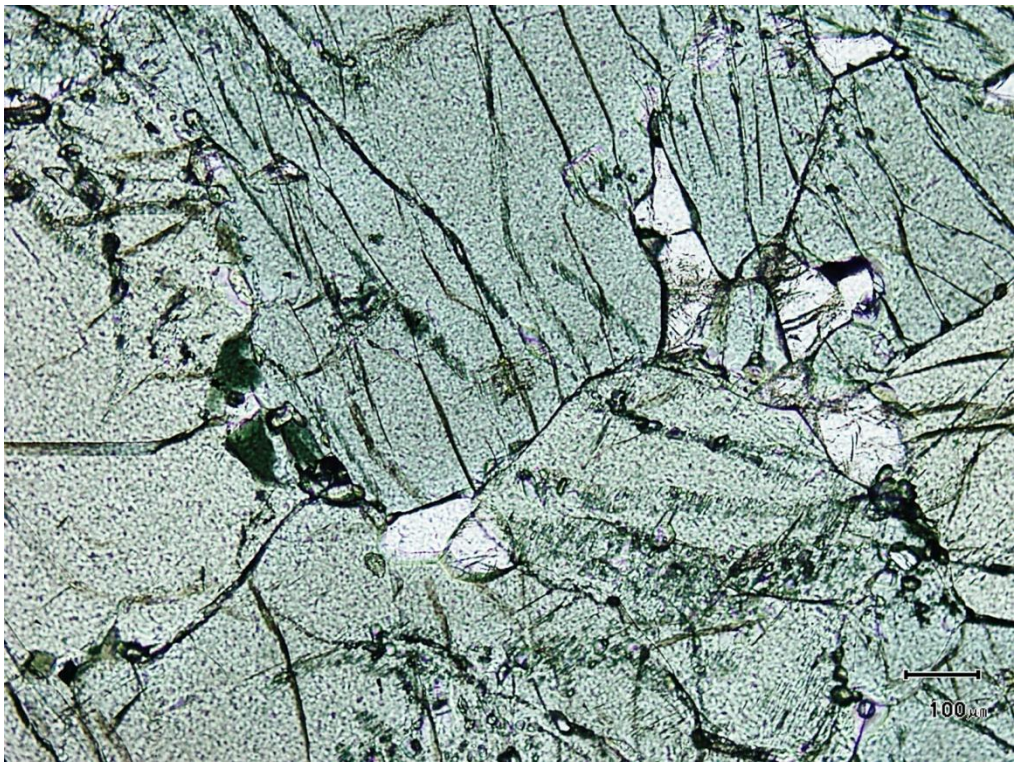

Figure 68. WTKV06, Ferrohastingsite (green) and scapolite (colourless) sitting within hedenbergite. The ferrohastingsite replaces hedenbergite. Mag. x 10; Scale bar = 100 µm; plane polarised light.

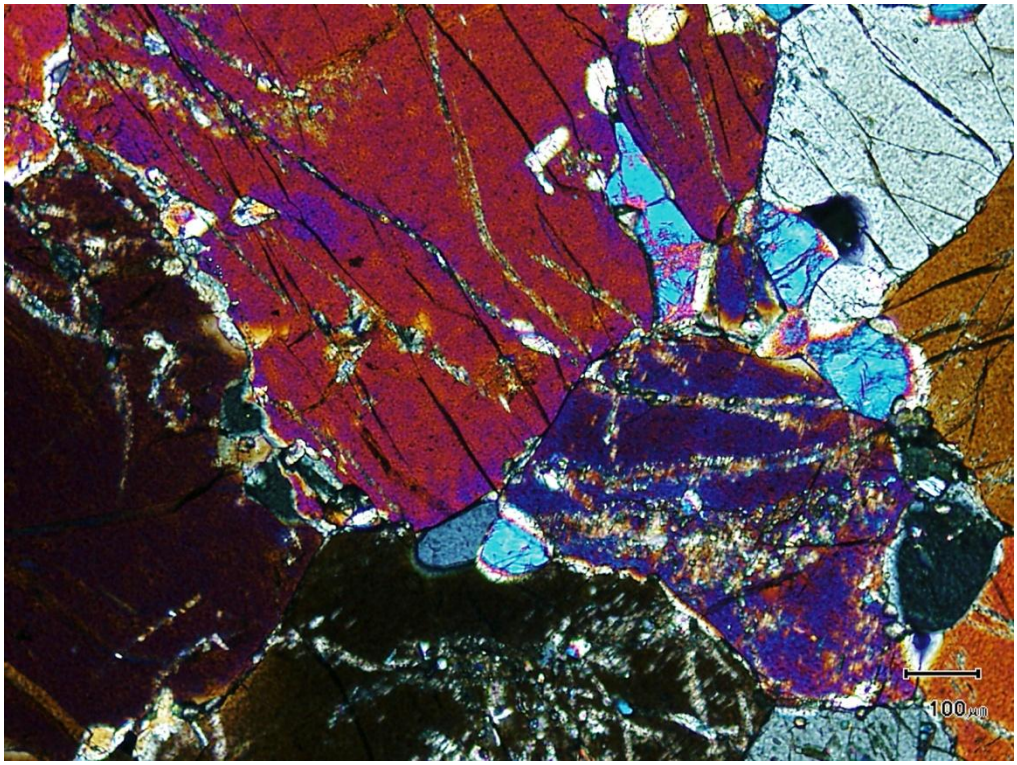

Figure 69. WTKV06, cross nicols view of Figure 68. Small scapolite trails are more easily observed. Mag. x 100; Scale bar = 100 µm; crossed nicols.

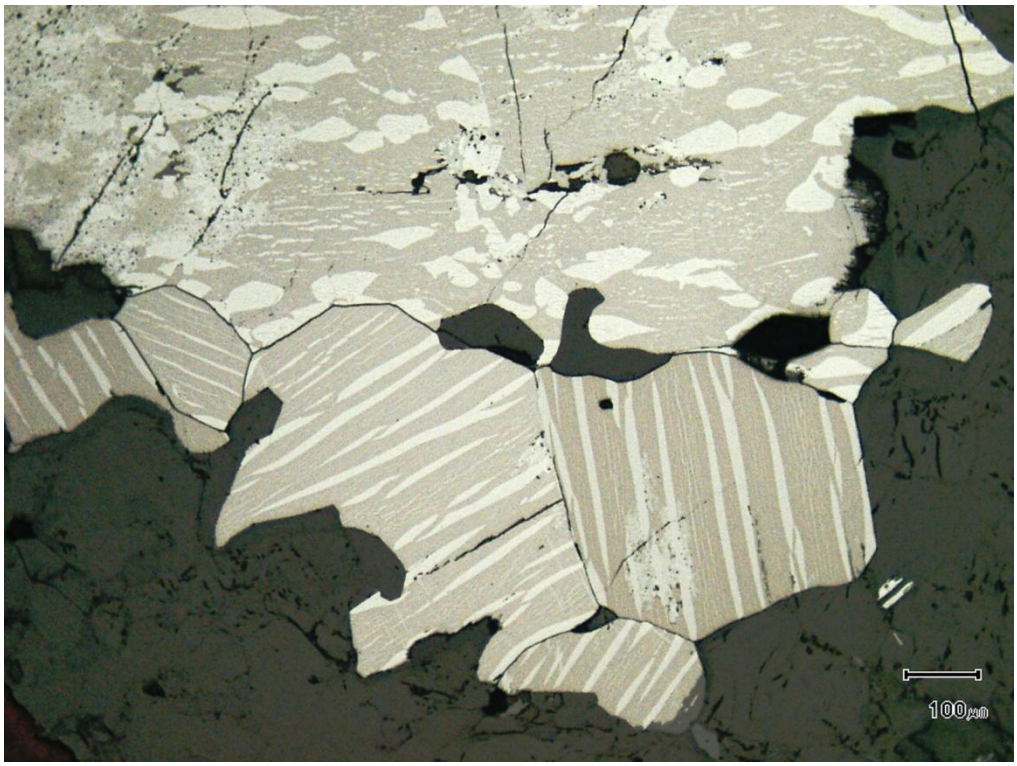

Figure 70. WTKV08, Titan-hematite (white) exsolving from ferrian-ilmenite (grey), with original larger grain being recrystallised. Mag. x 100; Scale bar = 100 µm; reflected light.

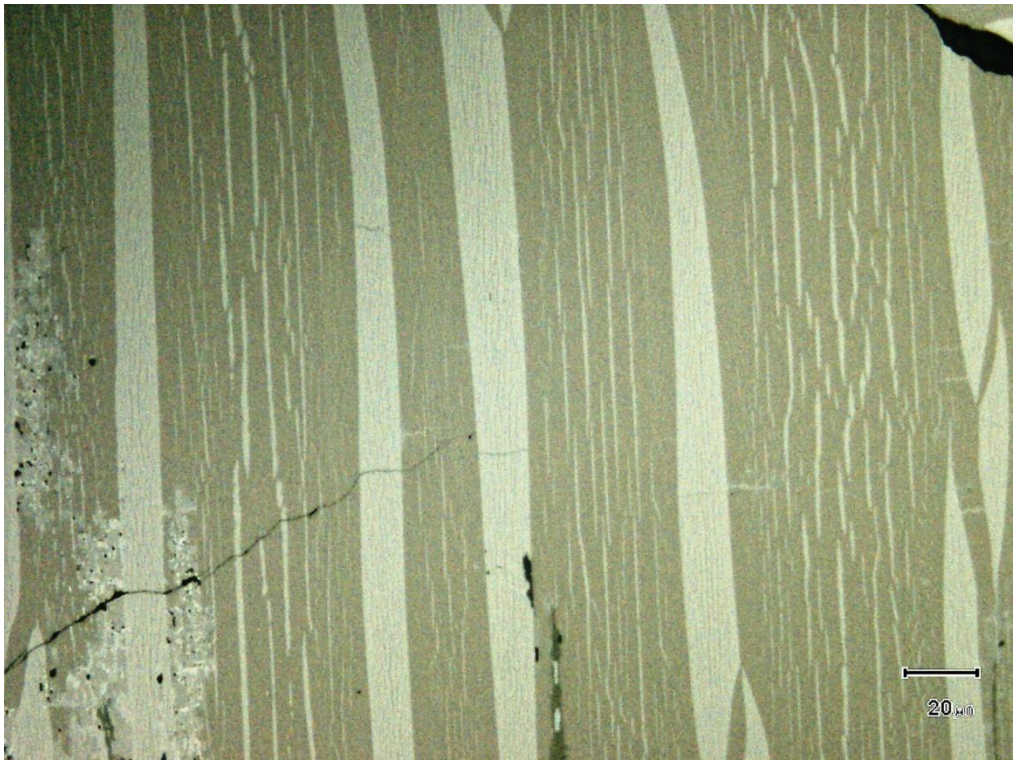

Figure 71. WTKV08, Higher mag. view of part of Figure X (above). Note the complex exsolution within the coarser exsolution bands. Mag. x 500; Scale bar = 20 µm; reflected light.

Figure 72. WTKV08, reflected light. Hematite (former magnetite) rimming goethite (former pyrite). This suggests high oxygen fugacities. Mag. x 200; Scale bar = 50 µm; slightly crossed nicols.

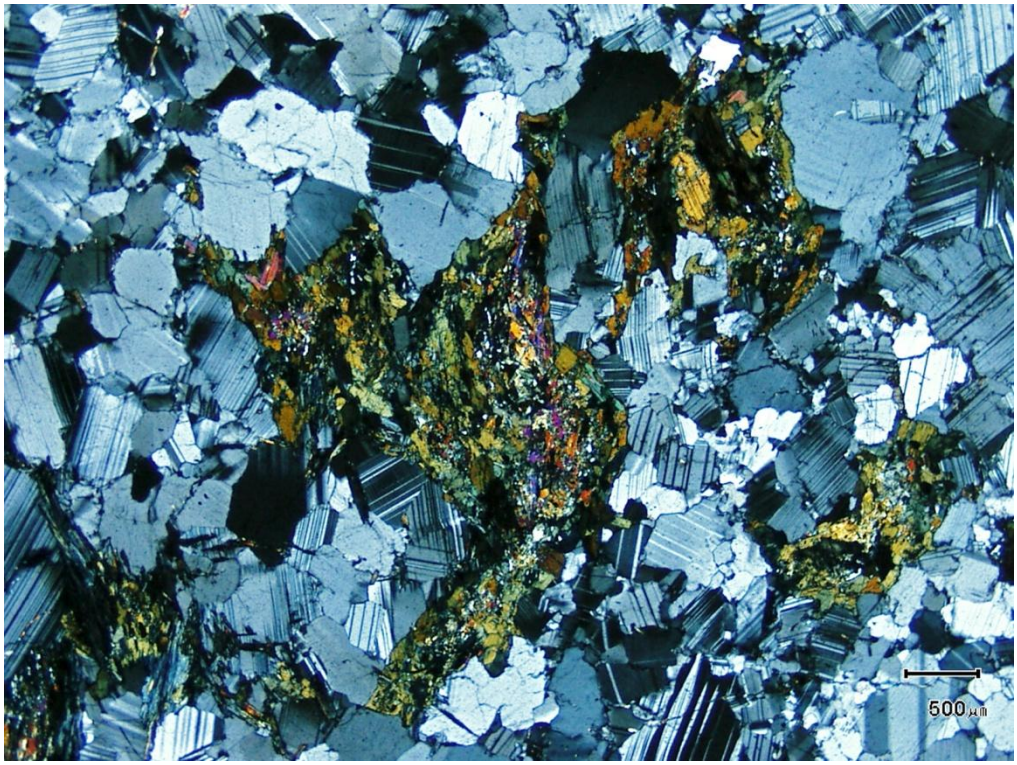

Figure 73. WTKV09, General textural view of a hornblende-plagioclase dominated, pyroxene absent gabbro. Mag. x 20; Scale bar = 500 µm; cross polarised light.

Figure 74. WTKV11, Strongly myrmekitic texture development in plagioclase associated with poikiloblastic hornblende. Mag. x 50; Scale bar = 200 µm; plane polarised light.

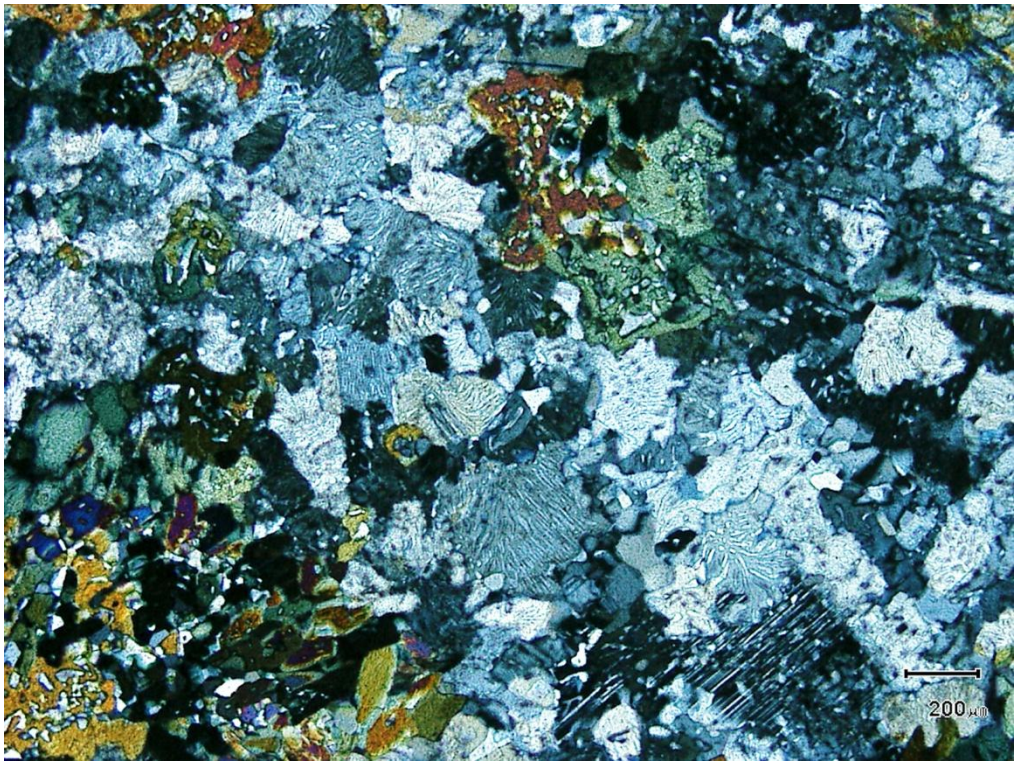

Figure 75. WTKV11, cross nicols view of Figure X (above). Mag. x 50; Scale bar = 200 µm.

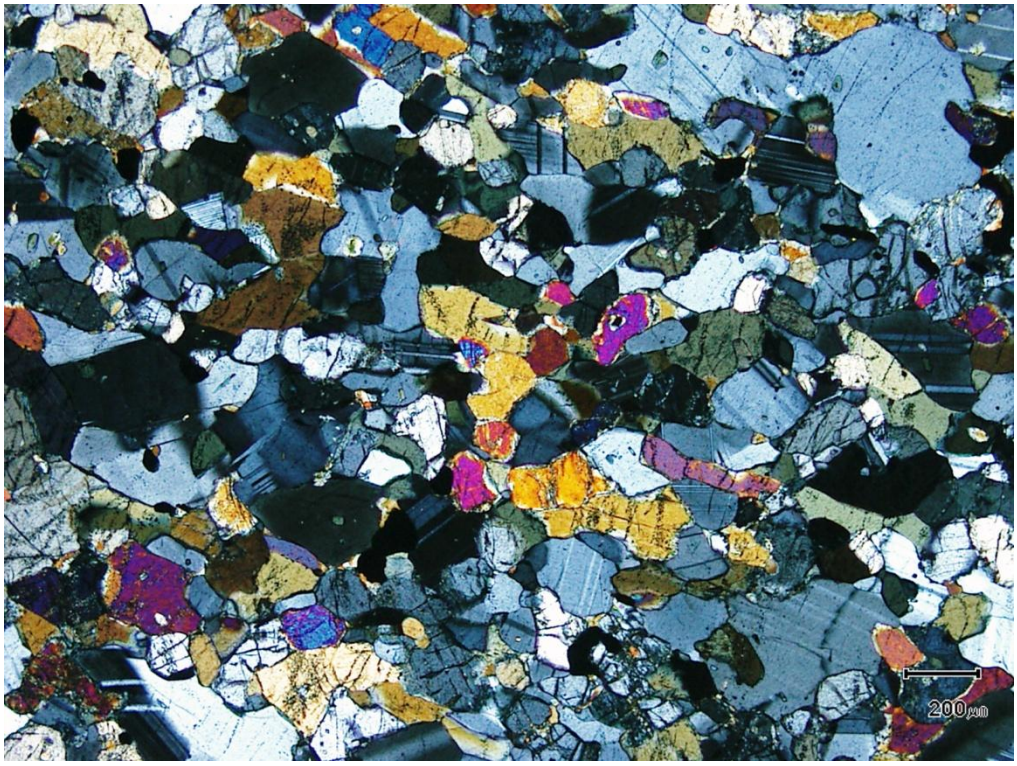

Figure 76. WTKV12, General textural view of a pyroxene bearing gabbro. Mag. x 50; Scale bar = 200 µm; crossed nicols.

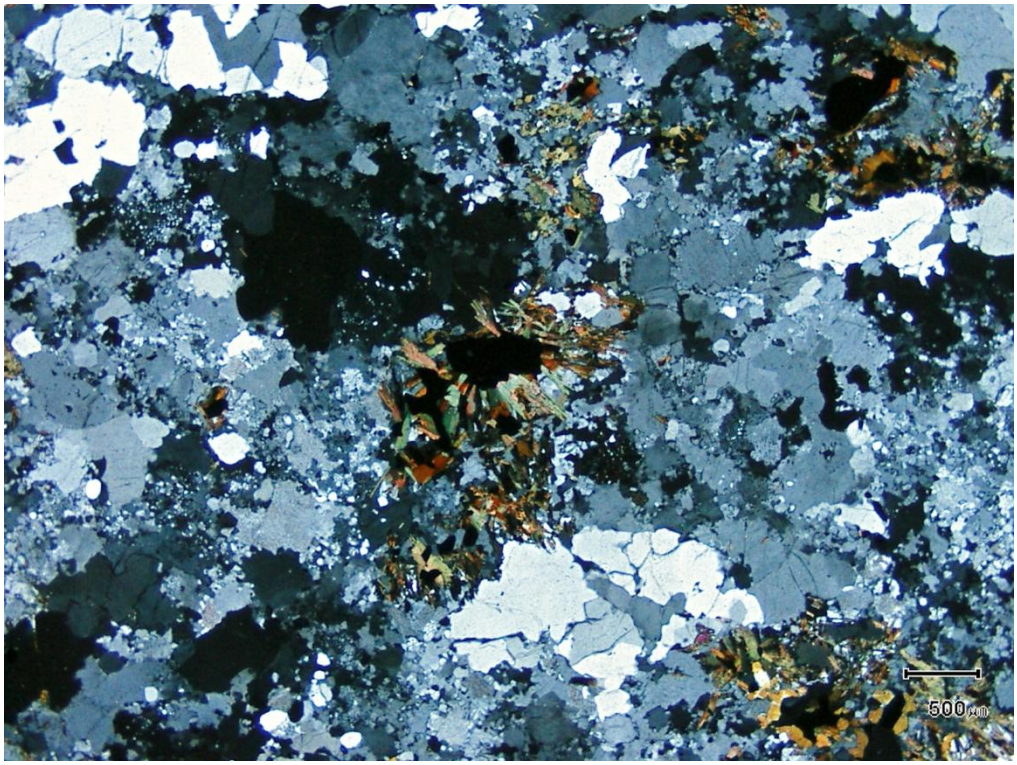

Figure 77. WTKV13, General textural view of the felsic gneiss. No pyroxenes are present as they have been replaced by randomly oriented biotite and hornblende. Mag. x 20; Scale bar = 500 µm; cross nicols.

Figure 78. WTKV13, This photomicrograph shows strongly perthitic (high temperature) K-feldspar. Mag. x 20; Scale bar = 500 µm; plane polarised light.

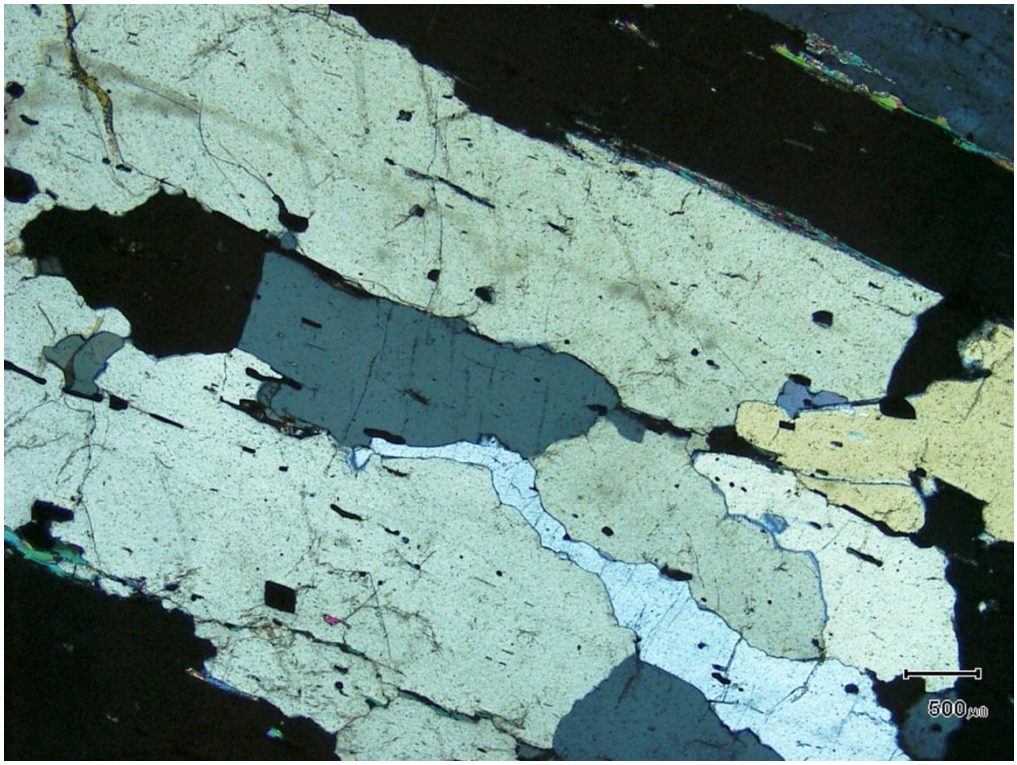

Figure 79. WTKV15, This photomicrograph shows sillimanite and muscovite pinning quartz growth. Note the elongate nature of the quartz grains which parallels the strong fabric. Mag. x 20; Scale bar = 500 µm; crossed nicols.

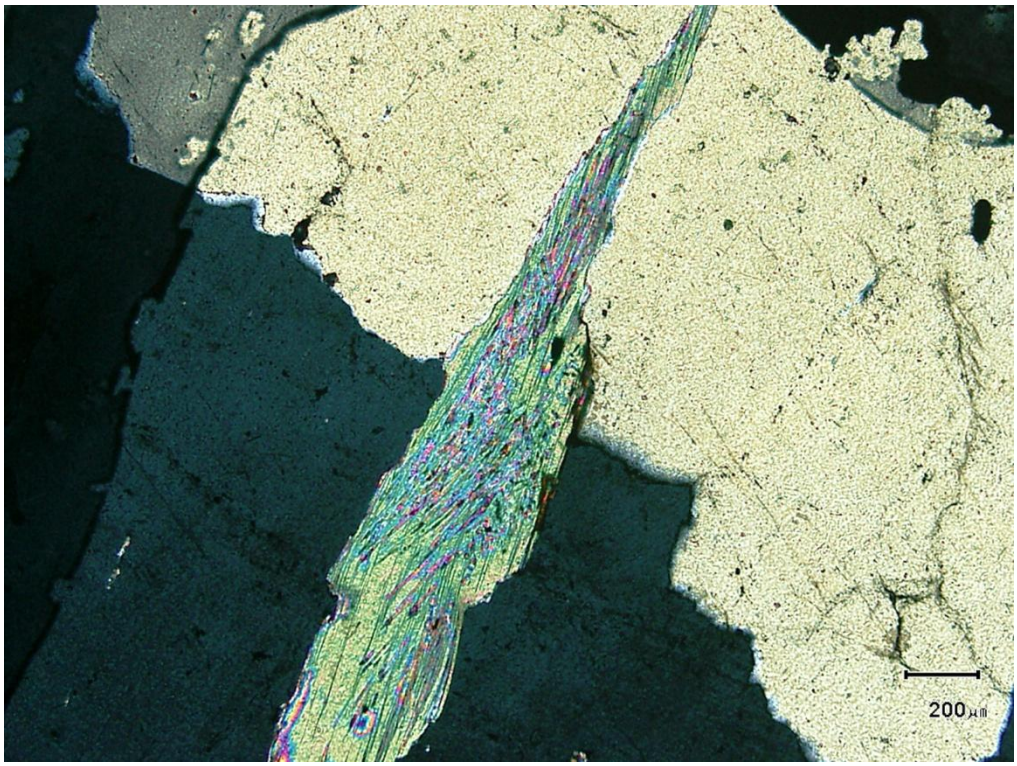

Figure 80. WTKV15, This photomicrograph shows retrograde muscovite grain containing fibrolitic sillimanite. Mag. x 50; Scale bar = 200 µm; crossed nicols.

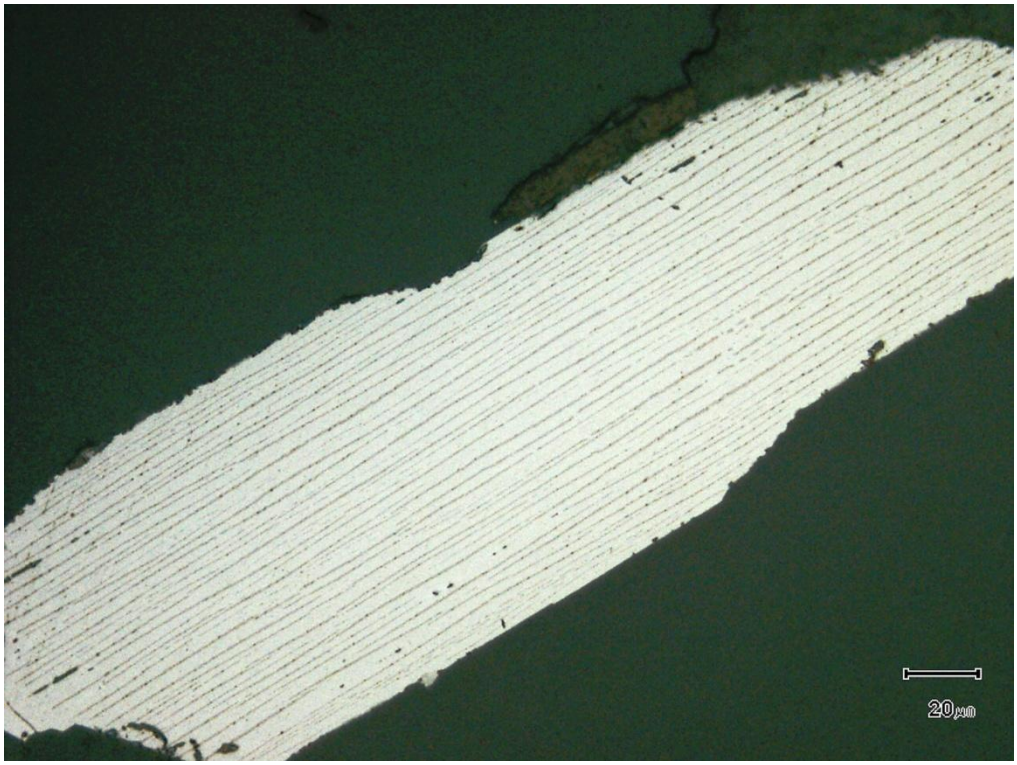

Figure 81. WTKV15, This photomicrograph shows titan-hematite exsolving ferrian-ilmenite. These two minerals occur not only in the quartzite but are also present in the hornblende bearing (pyroxene absent) gabbros. Mag. x 500; Scale bar = 20 µm; reflected light.

Tables:

Table 1. Sample locations and minerals present. Abbreviations after Siivola, S and Schmid, R. 2007, after Kretz, 1983.

Sample name	Northing	Easting	Minerals present (Max. to trace, left to right)
WTKV01	10°36'7.70"N	78°12'53.70"E	Pl, Hbl, Qtz, Ilm, Cb,Rt, Chl.
WTKV02	10°34'45.20"N	78°15'8.40"E	Qtz, Sil, Ilm, Ms, Bt, Crd, Zrn, Mnz, Tur.
WTKV03	10°34'41.50"N	78°15'8.40"E	Qtz, Bt, Rt, Ms, Zrn, Mnz.
WTKV04	10°35'58.70"N	78° 9'39.20"E	Pl, Opx, Cpx, Hbl, Ilm, Gt, Py, Ccp, Ap.
WTKV05	10°35'34.50"N	78°10'21.70"E	Pl, Hbl, Qtz, Rt, Chl, Gt, Bt, Czo, Cb, Ser.
WTKV06	10°33'22.70"N	78° 9'34.80"E	Hbl, Scp, Cb, Fe-Hs, Pl, Sph, Ap, Ccp.
WTKV07	10°33'23.30"N	78° 9'40.60"E	Hbl, Pl, Cpx, Opx, Ilm, Py, Ccp, Po, Gt.
WTKV08	10°34'52.00"N	78°11'4.00"E	Pl, Hbl, Fe-Ilm, Ti-Hem, Bt, Chl, Py, Ant, Gt, Ep, Qtz.
WTKV09	10°34'3.80"N	78°10'9.40"E	Pl, Hbl, Qtz, Ser, Cpx, Chl, Bt, Ilm, Cb, Ep, Czo, Zrn, Hem, Ap, Cum.
WTKV10	10°34'11.40"N	78° 9'49.00"E	Pl, Hbl, Cb, Fe-Ilm, Bt, Chl, Ti-Hem, Mag, Gt, Py, Ccp.
WTKV11	10°34'10.90"N	78° 9'45.70"E	Pl, Hbl, Qtz, Fe-Ilm, Ti-Hem, Gt, Py, Bt.
WTKV12	10°36'3.60"N	78° 9'49.60"E	Pl, Hbl, Cpx, Opx, Ilm.
WTKV13	10°35'10.50"N	78°14'42.90"E	Qtz, K-Fsp, Pl, Bt, Hbl, Mag, Ilm, Py, Zrn, Ap.
WTKV14	10°34'10.30"N	78°11'25.10"E	Qtz, Ms, Zrn, Rt, Ti-Hem, Fe-Ilm, Clays
WTKV15	10°35'27.20"N	78° 9'45.40"E	Qtz, Ms, Ti-Hem, Hem, Fe-Ilm, Mag, Sil, Bt, Gt, Rt, Tur, Zrn, Mnz.

Table 2. Sample and spike weights for TIMS samples.

Sample name	Sample weight	Spike weight
WTKV01	0.51966	0.42067
WTKV02	0.20391	0.52607
WTKV04	0.23119	0.41837
WTKV07	0.18561	0.40619
WTKV09	0.2469	0.40229
BHV0-2	0.08242	0.42067

Table 3. Major element analysis results (wt%).

		SiO2	TiO2	Al2O3	Fe2O3(t)	MnO	MgO	CaO	Na2O	K2O	P2O5	LOI	S	Total
Opx/Cpx dominated Gabbros/gabbro-norite														
	WTKV04	47.7	1.4	14.5	14.3	0.19	7.82	11.9	1.99	0.15	0.1	0.55	0.04	100.64
	WTKV07	50.4	0.765	14.8	9.28	0.11	8.94	12.4	3.26	0.12	0.01	0.54	0.04	100.665
	WTKV12	48.9	1.505	14.5	11.2	0.17	9.01	11.7	2.34	0.28	0.24	0.55	0.04	100.435
Hbl/Pl dominated grabbros/anorthositic gabbros														
	WTKV01	51.9	0.335	23.7	4.48	0.06	4.31	12.9	1.8	0.2	<0.01	1.1	0.04	100.825
	WTKV05	52.4	0.5	26.8	2.53	0.04	2.16	11.6	3.71	0.14	0.03	0.99	0.04	100.94
	WTKV08	52.3	0.595	25.4	4	0.04	1.9	11.3	3.36	0.21	<0.01	1.01	0.03	100.145
	WTKV09	53.8	0.33	25.5	3.11	0.04	0.85	10.8	3.85	0.53	0.05	1.41	0.02	100.29
	WTKV10	51	0.42	27.3	2.82	0.03	1.07	12	3.79	0.35	0.03	1.67	0.04	100.52
	WTKV11	51.9	0.545	17	9.58	0.14	6.86	10.8	2.36	0.26	0.05	1.02	0.02	100.535
Hedenbergite/scapolite calc-silicate														
	WTKV06	47	0.975	6.21	10.4	0.16	9.77	24.1	0.8	0.08	0.11	0.76	0.01	100.375
Felsic gneiss														
	WTKV13	70.3	0.38	13.8	3.36	0.03	0.59	2.08	3.4	4.31	0.1	0.15	0.03	98.53
Quartzites														
	WTKV02	96.6	0.105	1.4	1.12	<0.01	0.04	<0.01	0.01	<0.01	0.01	0.38	0.03	99.695
	WTKV03	99.5	0.08	0.16	0.25	<0.01	0.16	<0.01	<0.01	<0.01	0.01	0.21	0.02	100.39
	WTKV14	98.6	0.07	0.25	0.51	<0.01	<0.01	<0.01	0.02	0.02	0.02	0.1	0.02	99.61
	WTKV15	98.1	0.145	0.52	1.38	<0.01	0.01	0.02	0.01	0.06	0.02	0.22	0.04	100.525

Table 4. Rare earth element analysis results (ppm).

		La	Ce	Pr	Nd	Sm	Eu	Gd	Tb	Dy	Ho	Er	Tm	Yb	Lu
Opx/Cpx dominated Gabbros/gabbro-norite															
	WTKV04	3	9	1.5	8.5	2.5	0.98	2.9	0.52	3.4	0.7	2.1	0.3	1.95	0.3
	WTKV07	5	15	2.3	11	2.6	0.88	2.6	0.44	2.7	0.54	1.6	0.2	1.45	0.22
	WTKV12	11	27	3.6	17	4	1.4	4.1	0.64	3.6	0.72	1.9	0.25	1.7	0.26
Hbl/Pl dominated grabbros/anorthositic gabbros															
	WTKV01	1.5	3	0.5	2.6	0.74	0.58	0.9	0.16	1	0.2	0.55	0.1	0.5	0.08
	WTKV05	2.5	5	0.65	2.9	0.72	0.42	0.75	0.14	0.86	0.16	0.45	0.05	0.45	0.06
	WTKV08	1.5	3	0.45	2.2	0.56	0.64	0.6	0.1	0.66	0.14	0.4	<0.05	0.35	0.06
	WTKV09	7.5	15	1.85	8	1.65	1.65	1.6	0.24	1.45	0.28	0.7	0.1	0.75	0.16
	WTKV10	3.5	7	0.8	3.4	0.64	0.56	0.6	0.08	0.52	0.1	0.25	<0.05	0.25	0.26
	WTKV11	5	11	1.6	8	2.1	0.84	2.3	0.38	2.3	0.46	1.25	0.15	1.2	0.2
Hedenbergite/scapolite calc-silicate															
	WTKV06	7	18.5	2.5	11.5	2.6	0.7	2.6	0.42	2.5	0.5	1.45	0.2	1.7	0.32
Felsic gneiss															
	WTKV13	22	33.5	3.9	15	2.5	1.55	2.3	0.32	1.8	0.36	1	0.15	0.9	0.14
Quartzites															
	WTKV02	13.5	26.5	3.1	12.5	2.1	0.46	1.6	0.2	0.9	0.14	0.3	<0.05	0.15	0.02
	WTKV03	<0.5	0.5	0.05	0.2	0.04	<0.02	<0.05	<0.02	0.04	<0.02	<0.05	<0.05	0.05	0.02
	WTKV14	2	3.5	0.4	1.6	0.24	0.04	0.2	0.02	0.1	<0.02	<0.05	<0.05	0.05	<0.02
	WTKV15	4.5	7.5	0.85	3.3	0.48	0.1	0.4	0.04	0.2	0.04	0.1	<0.05	0.05	<0.02

Table 5. Sm/Nd isotope TIMS analysis results

Sample #	Nd conc. (ppm)	Sm conc. (ppm)	143Nd/ 144Nd	147Sm/ 144Nd	εNd	143Nd/ 144Nd (T)	εNd (T)	TDM	TCHUR
WTKV01	3.495431967	1.114506192	0.51232839	0.192745113	-6.039544776	0.51144398	-5.704541794	5668.346721	11812.50811
WTKV02	2.427770044	0.411701988	0.511102499	0.102552925	-29.95293551	0.510631935	-21.5729784	2771.354111	2476.313804
WTKV04	8.209512846	2.530489364	0.512033923	0.18633301	-11.78369388	0.511178935	-10.88387371	5941.697745	8741.736168
WTKV07	10.43899655	2.443800809	0.511671817	0.141528176	-18.84727435	0.511022416	-13.94246741	3066.430877	2659.316691
WTKV09	8.933950881	1.788882847	0.511741999	0.121055221	-17.47824227	0.511186538	-10.73530839	2286.749806	1802.866231
BHVO-2 (#18)	24.21027181	5.909124669	0.512931114	0.147553933	5.717755759	0.512254063	-10.12556517	499.1216133	-916.5484814

Table 6. LA-MC-ICPMS results for Lu/Hf isotope analysis.

Analysis No.	Interf. Corr. Meth.	Total Hf beam (V)	$^{176}Hf/^{177}Hf$	2 se	exp. factor[1]	2 se	$^{178}Hf/^{177}Hf$	2 se	$^{176}Yb/^{177}Hf$	$^{176}Lu/^{177}Hf$	Age (Ma)	$^{176}Hf/^{177}Hf$ Initial	$\varepsilon_{Hf}(t)$	T_{DM} (Ga)	T_{DM} Crustal	$^{176}Hf/^{177}Hf$ corr. Using Hf corr.	2 se
WTKV02_12_Hf	Yb	4.90418005	0.281454753	4.42864E-05	0.93119799	0.004585528	1.467206848	6.63382E-05	0.095605739	0.001714407	2018.1	0.281388997	-3.894240942	2.561733773	2.902535224	0.281576947	2.55781E-05
WTKV02_15_Hf	Yb	4.504539967	0.281518032	4.10033E-05	0.879379316	0.004077526	1.467235521	5.28396E-05	0.09562803	0.001616348	2423.6	0.281443297	7.338036835	2.467043726	2.497318688	0.281537519	2.22485E-05
WTKV02_20_Hf	Yb	7.290528297	0.281225351	2.77698E-05	0.919549282	0.003225126	1.4672757	5.16666E-05	0.038399797	0.000676737	2423.3	0.281194065	-1.530857007	2.803235589	3.064826709	0.281249067	1.72546E-05
WTKV02_23_Hf	Yb	10.16661072	0.281133497	4.04577E-05	0.906103214	0.004454282	1.467265673	8.26842E-05	0.091792371	0.0013902	2492.1	0.281067359	-4.45111118	2.981887923	3.30344963	0.281208799	2.55561E-05
WTKV02_28_Hf	Yb	8.391489983	0.281079846	2.86966E-05	0.909827267	0.003446738	1.467272831	6.68833E-05	0.06616614	0.001056018	2481	0.281029836	-6.041398436	3.028777206	3.395732985	0.281171889	1.92707E-05
WTKV02_33_Hf	Yb	5.424170017	0.281562257	5.60621E-05	0.911882786	0.003798696	1.467315993	6.05048E-05	0.359811671	0.0049403	2033.3	0.281371319	-4.17519826	2.638612858	2.932099842	0.282055167	3.32275E-05
WTKV02_39_Hf	Yb	8.70407486	0.281372214	2.88665E-05	0.905411135	0.004334417	1.467280743	6.88182E-05	0.05516396	0.000913406	2076.3	0.28133615	-4.442209355	2.620803344	2.982244066	0.281421516	1.9763E-05
WTKV02_40_Hf	Yb	7.83155632	0.281345136	2.30775E-05	0.87571194	0.003366851	1.467286416	5.06123E-05	0.050011605	0.000865276	2213.6	0.281308667	-2.275672337	2.654348968	2.950619463	0.281396741	1.51521E-05
WTKV02_42_Hf	Yb	8.847873688	0.281121898	2.683E-05	0.875309604	0.003943238	1.467253807	7.00897E-05	0.048670597	0.000818544	2437	0.281083837	-5.134796105	2.953413743	3.304379974	0.281178778	1.9744E-05
WTKV02_50_Hf	Yb	7.526063919	0.281403303	2.09522E-05	0.869519773	0.003196604	1.467299293	4.87418E-05	0.019466671	0.000333503	2033.5	0.281390412	-3.492331382	2.540074898	2.88892337	0.28141872	1.39409E-05
WTKV02_51_Hf	Yb	8.527490616	0.281224435	3.22546E-05	0.853797697	0.004054185	1.467283356	5.96875E-05	0.086508176	0.001335562	2428.9	0.281162544	-2.522670074	2.853018022	3.132257984	0.281308966	2.44277E-05
WTKV02_52_Hf	Yb	6.511441231	0.281229064	2.44581E-05	0.877431318	0.003465508	1.467306303	5.10153E-05	0.011094532	0.00017807	2470.3	0.281220668	0.498224382	2.762643769	2.971639375	0.281240388	1.69137E-05
WTKV02_57_Hf	Yb	9.733557701	0.281143962	2.74474E-05	0.865655864	0.003519377	1.467277	6.53133E-05	0.039472678	0.000623029	2461.7	0.281114691	-3.468632864	2.908885437	3.217651705	0.281171498	2.0972E-05
WTKV03_09_Hf	Yb	5.762994766	0.281347146	2.84266E-05	0.789529806	0.004117919	1.467293156	6.2613E-05	0.04294597	0.000750567	2040.2	0.281318037	-5.910493477	2.643733143	3.047385805	0.281374516	1.75077E-05
WTKV03_12_Hf	Yb	6.206089973	0.281198641	2.87036E-05	0.775680742	0.003942444	1.467259181	6.41734E-05	0.055761913	0.000959981	2414.4	0.281154426	-3.145224716	2.860172768	3.160670789	0.281271404	1.86271E-05
WTKV03_19_Hf	Yb	5.641706944	0.281308832	3.0506E-05	0.801928635	0.003354808	1.467266038	5.76142E-05	0.001185851	0.281308832	2326	0.281256258	-1.558293756	2.726390788	2.991623132	0.281348512	1.85767E-05
WTKV03_20_Hf	Yb	6.916255474	0.281412178	2.70404E-05	0.847972205	0.003436054	1.467278424	5.52642E-05	0.052799653	0.000903929	2424.1	0.281370374	4.756643953	2.565705386	2.663571366	0.281469511	1.78648E-05
WTKV03_34_Hf	Yb	6.28439188	0.281210301	2.57967E-05	0.801205662	0.003550018	1.467286359	6.23046E-05	0.02359847	0.000431668	2307.1	0.281191322	-4.300897961	2.805778162	3.151369548	0.281266568	1.70499E-05
WTKV03_36_Hf	Yb	6.532585144	0.280988467	3.08347E-05	0.870630159	0.003655076	1.467236991	5.5814E-05	0.101373751	0.001688376	3020.5	0.280890627	1.514728936	3.205345127	3.329234001	0.281066736	1.87714E-05
WTKV03_46_Hf	Yb	5.459497929	0.281056778	3.3172E-05	0.772041975	0.004037219	1.467246186	6.89878E-05	0.044188624	0.000754154	2470.9	0.281021212	-6.580823302	3.036215117	3.422110819	0.28111893	2.08417E-05
WTKV03_64_Hf	Yb	7.880396366	0.280967153	2.26625E-05	0.814780165	0.003017572	1.467283405	6.39429E-05	0.031233831	0.000506604	2494.5	0.280943028	-8.81734368	3.136675226	3.581690442	0.280984047	1.52026E-05
WTKV03_67_Hf	Yb	7.082185745	0.281187184	2.6418E-05	0.821565022	0.003353803	1.467304342	5.80483E-05	0.042508126	0.0007266	2305.6	0.281155259	-5.617290525	2.858376984	3.233677552	0.281257996	1.69952E-05
WTKV03_69_Hf	Yb	5.183476925	0.281529709	4.71295E-05	0.760267492	0.00416599	1.467209893	6.31677E-05	0.18853841	0.003139785	2103.6	0.28140408	-1.404379947	2.55418982	2.810325446	0.281797299	2.80668E-05
WTKV14_11_Hf	Yb	7.414367199	0.280964972	2.75841E-05	0.793060494	0.002971518	1.467291494	5.38319E-05	0.104348825	0.001708559	2695.9	0.280876872	-6.51833689	3.239387791	3.591366287	0.281067932	1.61517E-05
WTKV14_14_Hf	Yb	7.831250668	0.281801467	2.3844E-05	0.763793965	0.003083388	1.467212098	5.49413E-05	0.046662656	0.000878009	835.5	0.281787679	-16.4019114	2.031012262	2.771401953	0.281830787	1.60352E-05
WTKV14_16_Hf	Yb	6.750782013	0.281659941	3.46247E-05	0.782846119	0.003090675	1.467251126	5.48561E-05	0.10948361	0.001952507	2025.9	0.281584758	3.238217969	2.289608486	2.45409248	0.281730613	2.38586E-05
WTKV14_21_Hf	Yb	6.183230877	0.281697342	2.80806E-05	0.746811643	0.003493348	1.467193876	6.30982E-05	0.044618125	0.000844153	825.5	0.281684246	-20.28883736	2.172164852	3.005525173	0.281775425	1.78346E-05
WTKV14_32_Hf	Yb	6.492120743	0.281737161	3.00919E-05	0.763896779	0.003567825	1.467253862	5.63182E-05	0.068866191	0.001335837	838.3	0.281716112	-18.87520793	2.145080406	2.927654722	0.281789231	1.88175E-05
WTKV14_33_Hf	Yb	5.154439926	0.281328791	3.17482E-05	0.764020598	0.003844325	1.467255487	6.1953E-05	0.05329599	0.000976881	1996.2	0.281291737	-7.849033313	2.684351966	3.135944684	0.281401324	2.09336E-05
WTKV14_37_Hf	Yb	4.738110065	0.281649043	3.6562E-05	0.759116841	0.00412854	1.467294675	5.89449E-05	0.049352054	0.000935704	776.9	0.281635387	-23.09951947	2.243701217	3.141830789	0.281698297	2.34601E-05
WTKV14_48_Hf	Yb	7.979174614	0.281385726	2.07299E-05	0.775726797	0.003016381	1.467269193	5.63348E-05	0.013197195	0.000260071	2081.9	0.281375429	-2.918626123	2.558862488	2.889863552	0.281398668	1.38243E-05
WTKV14_50_Hf	Yb	6.553607464	0.281481352	3.46166E-05	0.747352786	0.004528935	1.467245589	8.00217E-05	0.080793666	0.001477361	2070.9	0.281423177	-1.473692143	2.508822346	2.789498794	0.281582747	2.07195E-05
WTKV14_58_Hf	Yb	5.757136345	0.281380957	3.10152E-05	0.777598018	0.003556283	1.46722979	6.11244E-05	0.025923962	0.000432968	2187	0.281362932	-0.956891958	2.576660188	2.846174521	0.281398511	1.97912E-05
WTKV14_65_Hf	Yb	4.202592373	0.28133203	3.70158E-05	0.751013339	0.004407544	1.467185694	6.21852E-05	0.045684919	0.000820496	2401	0.281294455	1.525091279	2.669057075	2.852714801	0.281397778	2.31389E-05
WTKV14_75_Hf	Yb	6.068590164	0.281435524	2.78792E-05	0.753277513	0.003955836	1.467258854	5.61145E-05	0.013920571	0.000213994	2039.8	0.281427227	-2.040561084	2.489135823	2.801549997	0.281446591	2.0078E-05
WTKV14_78_Hf	Yb	4.71923542	0.280905785	3.52862E-05	0.764988495	0.00423748	1.46724854	6.71166E-05	0.026021356	0.000461539	2458.3	0.280884132	-11.74567889	3.214804273	3.738354174	0.280938913	2.18039E-05
WTKV09_05_Hf	Yb	6.533898354	0.281941249	2.58297E-05	0.788614171	0.003599751	1.467349329	6.03884E-05	0.025528972	0.000453886	814	0.281934306	-11.68536537	1.81813805	2.459604037	0.281977432	1.67926E-05
WTKV09_12_Hf	Yb	5.96057415	0.282007756	3.13557E-05	0.787101332	0.00384494	1.467206262	6.18794E-05	0.05467243	0.000950755	839.2	0.281992758	-9.053665939	1.749764566	2.313914851	0.282084479	1.9387E-05
WTKV09_30_Hf	Yb	6.457593918	0.28193481	2.99307E-05	0.826013837	0.003510943	1.467269829	6.00485E-05	0.044544202	0.000786423	826.3	0.281922597	-11.82656984	1.84281102	2.478048664	0.282015996	1.81776E-05
WTKV09_32_Hf	Yb	8.697278976	0.28200091	2.5327E-05	0.816298768	0.003300337	1.46729282	5.46127E-05	0.054916997	0.000884743	860.1	0.281986604	-8.806327465	1.756205329	2.314631969	0.282058789	1.63273E-05
WTKV09_35_Hf	Yb	6.155326366	0.281945194	2.8294E-05	0.811357676	0.003338825	1.467302987	5.2763E-05	0.032157073	0.000594062	773.2	0.281936565	-12.51253458	1.819358222	2.479647719	0.28198171	1.83041E-05
WTKV09_36_Hf	Yb	6.404765606	0.281961163	2.64676E-05	0.790949316	0.003717027	1.46734773	5.9818E-05	0.036177978	0.000651909	841.1	0.281950856	-10.4959706	1.800170223	2.406069303	0.282005654	1.73608E-05
WTKV09_39_Hf	Yb	9.111807823	0.281983938	2.99288E-05	0.852808483	0.003858248	1.467295079	6.63809E-05	0.051783287	0.000837787	816.3	0.281971086	-10.33115632	1.777487173	2.37638818	0.282060183	2.03743E-05
WTKV09_42_Hf	Yb	8.28867054	0.282036157	2.69799E-05	0.837916998	0.003386095	1.467282875	5.07803E-05	0.076001321	0.001209851	777.6	0.282018483	-9.512799338	1.722118034	2.294788866	0.282138849	1.72379E-05
WTKV09_43_Hf	Yb	8.596906662	0.282032584	2.85533E-05	0.880489023	0.00371998	1.467300899	5.41964E-05	0.073222193	0.001207224	827	0.28201382	-8.579063663	1.726986629	2.274539297	0.282144988	1.84218E-05
WTKV09_44_Hf	Yb	8.960089684	0.28193783	1.95362E-05	0.904619359	0.003561621	1.467266313	4.53017E-05	0.023299943	0.000424975	782.1	0.281931586	-12.49111241	1.821443859	2.485246024	0.281971351	1.40011E-05
WTKV09_47_Hf	Yb	8.10559082	0.281992093	2.43455E-05	0.840458389	0.003338938	1.467319604	4.6835E-05	0.037199534	0.000647163	849.6	0.281981757	-9.211889916	1.757451647	2.331972297	0.28203509	1.62131E-05
WTKV09_49_Hf	Yb	6.739668369	0.28196607	3.01741E-05	0.821551234	0.003461623	1.467243688	5.36122E-05	0.04755247	0.000823144	839.9	0.281953075	-10.44406692	1.801465869	2.401873763	0.282034827	1.90341E-05

Table 6 (continued).

Analysis No.	Interf. Corr. Meth.	Total Hf beam (V)	$^{176}Hf/^{177}Hf$	2 se	exp. factor[1]	2 se	$^{178}Hf/^{177}Hf$	2 se	$^{176}Yb/^{177}Hf$	$^{176}Lu/^{177}Hf$	Age (Ma)	$^{176}Hf/^{177}Hf$ Initial	$\varepsilon_{Hf}(t)$	T_{DM} (Ga)	T_{DM} Crustal	$^{176}Hf/^{177}Hf$ corr. Using Hf corr.	2 se
WTKV13_03_Hf	Yb	6.577444553	0.281515786	3.3994E-05	0.929353133	0.004431505	1.46720223	7.05451E-05	0.082497398	0.001369064	1765.7	0.281469952	-6.765651579	2.454046892	2.889186491	0.281594405	2.29578E-05
WTKV13_18_Hf	Yb	4.811900616	0.281619389	3.59124E-05	0.922287932	0.00745713	1.467349601	7.88263E-05	0.040232521	0.000717971	766.6	0.28160905	-24.26114198	2.271464387	3.205632223	0.281652175	2.26483E-05
WTKV13_19_Hf	Yb	5.435736656	0.281576837	3.65166E-05	0.926972795	0.004512004	1.467332507	8.20034E-05	0.032805435	0.000570528	783.7	0.281568437	-25.32024564	2.320584026	3.284415416	0.281606404	2.32845E-05
WTKV13_24_Hf	Yb	5.060310364	0.281669329	3.89338E-05	0.925467898	0.004693678	1.467355432	9.30291E-05	0.030009173	0.000537841	832.6	0.281660912	-20.95766684	2.193035658	3.052585575	0.28164915	2.59927E-05
WTKV13_29_Hf	Yb	9.004891396	0.281719838	3.21413E-05	0.900320624	0.004130917	1.467332897	7.82035E-05	0.089685907	0.001673165	1726.6	0.281665084	-0.725668735	2.188674241	2.475838317	0.281801245	2.21521E-05
WTKV13_37_Hf	Yb	4.624092102	0.281692469	4.91876E-05	0.972918632	0.00736913	1.467321573	0.000105426	0.05481259	0.00098495	794.8	0.28167776	-21.20086727	2.186880466	3.038165082	0.281659303	2.89364E-05
WTKV13_55_Hf	Yb	8.752171516	0.281593635	3.36752E-05	0.937591876	0.003821838	1.46732155	7.60243E-05	0.050893842	0.001009898	1786.7	0.281559416	-3.11228904	2.324203012	2.674033833	0.28161262	1.9617E-05
WTKV13_58_Hf	Yb	6.613681793	0.281554708	5.76556E-05	0.868934128	0.007654782	1.467262153	0.000118885	0.111828887	0.002118276	1791	0.281482758	-5.736397653	2.448632897	2.843676596	0.281725347	3.62298E-05
WTKV13_63_Hf	Yb	3.659977674	0.281500203	0.000135766	0.90278976	0.01284056	1.467754006	0.000587393	0.069554812	0.001641967	1832.2	0.281443127	-6.207220118	2.493555233	2.905344401	0.281572029	7.5303E-05

Table 7. Oxygen isotope data for zircon areas analysed in sample WTKV09. Oxygen isotope ratios normalised relative to Temora (3) = 7.59 ‰. Uncertainty in the Temora analyses was ± 0.2739 ‰ (2 s.e.) for the analytical session. Spot locations match the U/Pb LA-ICPMS analyses laser holes. CL images were used to analyse as near as possible to those holes but within the same CL zone.

Analysis #	corrected ratio	± 2 se	$\delta^{18}O$ ‰	± 2 σ internal	± 2 σ external
1	0.0020380	0.0000002	6.1764	0.0878	0.2876
2	0.0020376	0.0000003	5.9956	0.1293	0.3028
17	0.0020374	0.0000002	5.9234	0.0805	0.2855
19	0.0020383	0.0000001	6.3245	0.0628	0.2810
20	0.0020391	0.0000002	6.7400	0.0941	0.2896
21	0.0020380	0.0000001	6.1745	0.0672	0.2820
22	0.0020381	0.0000001	6.2487	0.0498	0.2783
24	0.0020386	0.0000001	6.5073	0.0543	0.2793
25	0.0020379	0.0000001	6.1582	0.0661	0.2818
30	0.0020372	0.0000001	5.8165	0.0487	0.2782
37	0.0020390	0.0000002	6.7045	0.1045	0.2931
42	0.0020376	0.0000001	5.9998	0.0714	0.2831
43	0.0020381	0.0000002	6.2242	0.0845	0.2866
44	0.0020375	0.0000002	5.9272	0.0758	0.2841
45	0.0020385	0.0000002	6.4175	0.1027	0.2925
47	0.0020376	0.0000001	6.0037	0.0564	0.2797
48	0.0020383	0.0000002	6.3453	0.0957	0.2901
49	0.0020385	0.0000002	6.4517	0.0765	0.2844

Table 8. LA-ICPMS U/Pb concordia data for WTKV02, a quartzite (detrital zircons)

	Isotope Ratios						Ages			
Analysis #	Pb207/ U235	1σ error	Pb206/ U238	1σ error	rho	Conc. %	Pb207/ Pb206	± Ma	Pb206/ U238	± Ma
WTKV02_01	6.95608	0.088	0.37008	0.00478	0.979235407	93	2181.6	17.11	2029.8	22.49
WTKV02_02	5.56691	0.0706	0.31632	0.00408	0.982955694	86	2066.2	17.47	1771.7	19.96
WTKV02_03	10.43545	0.1333	0.44102	0.00573	0.983008935	91	2574	16.57	2355.2	25.64
WTKV02_04	5.64217	0.0735	0.31984	0.00418	0.997047447	86	2070.5	18.08	1788.9	20.41
WTKV02_05	6.19778	0.0799	0.34922	0.00455	0.989831722	93	2081	17.69	1930.9	21.72
WTKV02_06	9.73317	0.1289	0.4354	0.00577	0.999490337	94	2478.5	17.5	2330	25.93
WTKV02_07	12.77056	0.1697	0.49859	0.00661	0.997844293	96	2705.4	17.31	2607.8	28.45
WTKV02_08	9.85227	0.1287	0.44002	0.00581	0.989554569	95	2481.1	16.93	2350.7	26
WTKV02_09	9.56075	0.1258	0.43562	0.00579	0.990275409	95	2447.3	16.99	2331	26
WTKV02_10	5.55523	0.0747	0.32391	0.00433	0.994533539	90	2020.3	18.53	1808.8	21.07
WTKV02_11	7.45031	0.098	0.38895	0.00515	0.993128194	96	2213.5	17.66	2118	23.92
WTKV02_12	6.04124	0.0851	0.3526	0.00474	0.95454112	96	2018.1	20.72	1947	22.6
WTKV02_13	7.72223	0.0997	0.34617	0.00455	0.982663133	77	2474.3	16.7	1916.3	21.81
WTKV02_14	7.25863	0.0938	0.32919	0.00435	0.977716504	75	2454.6	16.52	1834.5	21.09
WTKV02_15	10.16768	0.1331	0.46963	0.00622	0.988523246	102	2423.6	17.1	2481.9	27.3
WTKV02_16	16.53389	0.3061	0.54279	0.00896	0.891578344	94	2987.5	27.88	2795.1	37.42
WTKV02_17	18.90956	0.2521	0.58847	0.0079	0.993208292	97	3073	16.79	2983.2	32.06
WTKV02_18	9.50865	0.1324	0.38628	0.00526	0.978092675	80	2639.1	18.85	2105.6	24.47
WTKV02_19	9.21214	0.1198	0.41599	0.0055	0.983841711	91	2461.9	16.89	2242.3	25.02
WTKV02_20	9.97144	0.1311	0.46069	0.00608	0.996207982	101	2423.3	17.62	2442.6	26.82
WTKV02_21	5.85282	0.076	0.33649	0.00441	0.991181974	91	2044.9	17.89	1869.7	21.29
WTKV02_22	8.24411	0.1086	0.38276	0.00507	0.994041776	87	2415	17.49	2089.2	23.63
WTKV02_23	10.42664	0.1351	0.46251	0.0061	0.982140587	98	2492.1	16.69	2450.6	26.9
WTKV02_24	7.20559	0.0953	0.3523	0.00468	0.995194163	84	2326.8	17.66	1945.6	22.33
WTKV02_25	5.85539	0.0769	0.34098	0.00453	0.988298764	94	2022.3	17.84	1891.4	21.78
WTKV02_26	9.52402	0.1227	0.43425	0.00564	0.991858206	95	2446	17.3	2324.8	25.37
WTKV02_27	8.21336	0.1023	0.34242	0.0043	0.991654822	73	2596.7	16.82	1898.3	20.66
WTKV02_28	10.85189	0.1384	0.48473	0.00614	0.993058905	103	2481	17.7	2547.9	26.67
WTKV02_29	5.43495	0.0692	0.32628	0.00411	0.989329199	92	1968.8	18.61	1820.3	19.99
WTKV02_30	5.75533	0.0847	0.33668	0.00443	0.894284675	93	2014.8	23.1	1870.7	21.36
WTKV02_31	6.11287	0.0787	0.27943	0.00354	0.983512719	65	2441.9	18.16	1588.5	17.83
WTKV02_32	7.81762	0.0984	0.38136	0.00481	0.997447096	89	2331.1	17.41	2082.6	22.46
WTKV02_33	6.26833	0.0823	0.36287	0.00462	0.96959454	98	2033.3	19.32	1995.8	21.87
WTKV02_34	10.17176	0.1341	0.45472	0.00584	0.973955178	97	2479.5	18.57	2416.2	25.86
WTKV02_35	8.86219	0.1165	0.41127	0.00526	0.973246799	92	2416.2	18.56	2220.7	24.04
WTKV02_36	9.73231	0.1259	0.40579	0.00517	0.984714701	85	2596.3	17.78	2195.6	23.71
WTKV02_37	6.59276	0.0868	0.37096	0.00477	0.977100013	98	2083.3	18.91	2033.9	22.43
WTKV02_38	10.33811	0.1318	0.42874	0.00548	0.99774484	88	2605.2	16.92	2300	24.74
WTKV02_39	6.6852	0.0858	0.37766	0.00484	0.998903115	99	2076.3	18.01	2065.3	22.66
WTKV02_40	7.68728	0.1055	0.40148	0.00525	0.953101476	98	2213.6	19.98	2175.9	24.14
WTKV02_41	5.68424	0.0729	0.32375	0.00415	0.999912405	88	2062	18.01	1808	20.22

WTKV02_42	10.0143	0.1312	0.45909	0.00595	0.989174233	100	2437	17.98	2435.6	26.3
WTKV02_43	14.407	0.1825	0.53034	0.00679	0.989133524	98	2802.2	16.29	2742.9	28.62
WTKV02_44	5.7746	0.0731	0.29317	0.00376	0.986482632	73	2262.6	17.07	1657.3	18.76
WTKV02_45	8.37815	0.1062	0.39938	0.00513	0.987022637	91	2370.6	16.92	2166.2	23.64
WTKV02_46	7.05319	0.0899	0.38115	0.00491	0.989327837	97	2154.4	17.47	2081.6	22.92
WTKV02_47	13.19791	0.1741	0.52308	0.00689	0.998521679	101	2681.1	17.59	2712.2	29.17
WTKV02_48	10.99642	0.1417	0.45716	0.00593	0.993277871	93	2601.8	17.1	2427	26.24
WTKV02_49	10.42137	0.1423	0.4775	0.0063	0.966516304	103	2438.5	19.29	2516.3	27.49
WTKV02_50	6.34677	0.0827	0.36744	0.00478	0.997880895	99	2033.5	18.48	2017.3	22.52
WTKV02_51	9.74052	0.1239	0.44878	0.0058	0.983907869	98	2428.9	16.94	2389.8	25.8
WTKV02_52	10.51286	0.1389	0.47266	0.00619	0.991055337	101	2470.3	18.14	2495.2	27.08
WTKV02_53	12.46532	0.1656	0.50412	0.00663	0.989971519	99	2647.4	17.98	2631.5	28.43
WTKV02_54	5.37368	0.0678	0.30494	0.00392	0.981056487	83	2068.7	17.38	1715.7	19.37
WTKV02_55	7.34546	0.0932	0.39671	0.00512	0.983316411	100	2155.4	17.39	2153.9	23.63
WTKV02_56	6.94082	0.0933	0.39737	0.0052	0.974025235	105	2053.2	19.5	2156.9	24.01
WTKV02_57	10.08855	0.1312	0.45577	0.00592	0.999163193	98	2461.7	17.39	2420.9	26.23
WTKV02_58	12.67997	0.1637	0.49969	0.00647	0.996889987	97	2689.9	16.81	2612.4	27.8
WTKV02_59	4.97813	0.0699	0.27861	0.00368	0.941080141	76	2092.7	20.65	1584.4	18.57
WTKV02_60	9.41179	0.126	0.44786	0.00585	0.975542835	101	2373.4	18.51	2385.7	26.04
WTKV02_61	6.28512	0.0825	0.31551	0.00407	0.982506959	77	2281.9	18.13	1767.8	19.96
WTKV02_62	8.64884	0.1126	0.388	0.00502	0.994135929	85	2473.5	17.26	2113.6	23.33
WTKV02_63	8.85267	0.1178	0.40521	0.00526	0.975516399	90	2439.4	18.17	2193	24.15
WTKV02_64	9.01705	0.1212	0.40679	0.0053	0.969000836	89	2463.9	18.49	2200.2	24.27
WTKV02_65	17.40075	0.2296	0.56128	0.00728	0.982901656	95	3016	17	2871.9	30.05
WTKV02_66	6.83559	0.0906	0.37807	0.00487	0.972183805	98	2113.5	18.69	2067.2	22.76
WTKV02_67	8.46224	0.1083	0.37052	0.00479	0.990055087	81	2514.1	16.77	2031.9	22.51
WTKV02_68	5.89608	0.0776	0.34621	0.00451	0.990417942	95	2007.6	18.59	1916.5	21.59
WTKV02_69	6.42351	0.0869	0.37438	0.00494	0.97502788	101	2020.9	19.43	2050	23.15
WTKV02_70	5.76409	0.0743	0.33043	0.0043	0.990799919	90	2050.2	17.75	1840.5	20.84
WTKV02_71	6.28017	0.0819	0.34129	0.00446	0.997567048	88	2144	17.93	1892.9	21.45
WTKV02_72	16.19805	0.2091	0.46484	0.0061	0.983893352	77	3202	15.94	2460.9	26.85
WTKV02_73	22.62658	0.2912	0.6066	0.00797	0.979594564	92	3309.1	15.71	3056.4	31.97
WTKV02_74	5.44508	0.0701	0.31085	0.00407	0.983544706	85	2057.5	17.6	1744.9	20.03
WTKV02_75	10.59993	0.1385	0.4827	0.00637	0.989898261	104	2448.1	17.31	2539	27.7
WTKV02_76	4.59299	0.0749	0.28657	0.004	0.85639662	86	1899.6	26.08	1624.4	20.06

Table 9. LA-ICPMS U/Pb concordia data for WTKV03, a quartzite (detrital zircons).

	Isotope Ratios						Ages			
Analysis #	Pb207/ U235	1σ error	Pb206/ U238	1σ error	rho	Conc. %	Pb207/ Pb206	± Ma	Pb206/ U238	± Ma
WTKV03_01	5.85328	0.16734	0.31842	0.00544	0.59758	83	2143.3	50.63	1782	26.58
WTKV03_02	6.65687	0.24194	0.31209	0.00657	0.57923	73	2399.3	63.94	1751	32.26
WTKV03_03	4.82059	0.2023	0.24654	0.00514	0.49680	63	2250.1	73.82	1420.6	26.58
WTKV03_04	2.04688	0.39423	0.16986	0.00927	0.28336	73	1392.2	341.08	1011.4	51.06
WTKV03_05	7.42674	0.171	0.30474	0.00496	0.70689	65	2623.3	38.8	1714.8	24.51
WTKV03_06	7.68902	0.22194	0.35839	0.00646	0.62447	82	2408.9	49.93	1974.5	30.66
WTKV03_07	9.13989	0.36305	0.37633	0.00848	0.56729	79	2617.5	67.85	2059.1	39.72
WTKV03_08	5.18002	0.56379	0.27806	0.0101	0.33373	73	2165.8	184.02	1581.6	50.92
WTKV03_09	6.58369	0.09416	0.37955	0.00488	0.89899	102	2040.2	22.96	2074.2	22.79
WTKV03_10	1.43646	0.05365	0.14667	0.00235	0.42899	92	958.5	75.7	882.3	13.21
WTKV03_11	4.14351	0.05281	0.24526	0.00301	0.96292	71	1993.7	19.67	1414	15.56
WTKV03_12	9.38774	0.11656	0.43609	0.00529	0.97699	97	2414.4	18.3	2333.1	23.73
WTKV03_13	5.46158	0.06579	0.25334	0.00304	0.99616	60	2416.9	17.47	1455.7	15.62
WTKV03_14	12.73041	0.19352	0.48701	0.00659	0.89015	93	2738.8	23.42	2557.7	28.55
WTKV03_15	8.4894	0.34058	0.32925	0.00764	0.57840	68	2716.3	68.47	1834.8	37.03
WTKV03_16	7.01907	0.24112	0.33186	0.00651	0.57105	77	2384.6	59.71	1847.4	31.5
WTKV03_17	13.41016	0.40492	0.39894	0.00876	0.72721	69	3145.4	50.56	2164.2	40.36
WTKV03_18	5.77106	0.08544	0.31434	0.00405	0.87026	82	2140.3	23.97	1762	19.85
WTKV03_18b	7.34014	0.0915	0.40772	0.00495	0.97393	105	2105.3	18.6	2204.5	22.68
WTKV03_19	8.58975	0.13166	0.42029	0.00557	0.86464	97	2326	24.61	2261.8	25.28
WTKV03_19b	8.5149	0.10427	0.39123	0.00475	0.99147	87	2432.6	17.39	2128.5	21.99
WTKV03_20	9.30003	0.11073	0.42963	0.00516	0.99135	95	2424.1	16.98	2304.1	23.28
WTKV03_20b	6.9843	0.10167	0.38094	0.00484	0.87281	97	2137.3	23.2	2080.7	22.6
WTKV03_21	4.04762	0.05024	0.25786	0.00313	0.97794	79	1861.4	19.02	1478.9	16.03
WTKV03_22	2.55314	0.03188	0.15171	0.00183	0.96604	46	1985.9	19.38	910.5	10.24
WTKV03_23	5.01992	0.06086	0.29998	0.00362	0.99536	86	1976.1	18.13	1691.2	17.96
WTKV03_24	6.78389	0.08333	0.34933	0.00424	0.98811	86	2237.2	18.13	1931.4	20.24
WTKV03_25	5.15765	0.07917	0.28876	0.0037	0.83475	78	2091.1	25.25	1635.3	18.52
WTKV03_26	5.70527	0.0706	0.33389	0.00406	0.98264	92	2013.2	18.73	1857.2	19.63
WTKV03_27	3.22754	0.04846	0.21866	0.00275	0.83763	73	1749.1	25.44	1274.8	14.57
WTKV03_28	12.70403	0.15527	0.46188	0.0054	0.95657	87	2814.7	18.03	2447.9	23.83
WTKV03_29	7.12507	0.08468	0.3425	0.00393	0.96547	81	2346.8	18.2	1898.7	18.87
WTKV03_30	3.03405	0.13435	0.19649	0.00342	0.39307	63	1825.7	80.23	1156.5	18.45
WTKV03_31	5.54403	0.50125	0.26874	0.00878	0.36135	66	2331.6	152.58	1534.4	44.6
WTKV03_32	6.65073	0.65868	0.31907	0.01112	0.35190	76	2351.4	165.24	1785.2	54.33
WTKV03_33	6.23825	0.51906	0.26295	0.00866	0.39581	59	2569.6	138.83	1504.9	44.19
WTKV03_34	8.41081	0.12345	0.41548	0.00508	0.83303	97	2307.1	24.73	2239.9	23.11
WTKV03_35	11.29374	0.19719	0.50296	0.00679	0.77320	106	2484.6	29.5	2626.5	29.13
WTKV03_36	18.09764	0.24333	0.58204	0.00793	0.98686	98	3020.5	16.17	2957.1	32.32
WTKV03_37	1.38595	0.02246	0.10901	0.00153	0.86609	45	1471.6	26.44	667	8.9
WTKV03_38	11.63243	0.16353	0.46769	0.00647	0.98405	93	2656.3	18.17	2473.4	28.43

WTKV03_39	8.43014	0.11621	0.33815	0.00466	0.99970	71	2660.1	17.42	1877.8	22.45
WTKV03_40	8.83313	0.12124	0.41029	0.00564	0.99849	92	2414.1	17.57	2216.2	25.78
WTKV03_41	5.348	0.07594	0.26655	0.0037	0.97756	66	2293.6	18.98	1523.3	18.84
WTKV03_42	18.00655	0.26249	0.51138	0.00729	0.97792	83	3218.2	18.45	2662.5	31.11
WTKV03_43	6.30398	0.08832	0.35563	0.00494	0.99148	94	2078.8	18.98	1961.4	23.47
WTKV03_44	7.36074	0.10121	0.36283	0.00502	0.99381	86	2313.3	17.77	1995.6	23.73
WTKV03_45	5.78578	0.07954	0.31814	0.00439	0.99627	84	2123.8	18.12	1780.6	21.46
WTKV03_46	10.41871	0.16563	0.46813	0.00685	0.92045	100	2470.9	22.72	2475.3	30.1
WTKV03_47	7.59201	0.10395	0.36673	0.00506	0.99235	86	2347.9	17.56	2014	23.85
WTKV03_48	5.30582	0.07202	0.28058	0.00386	0.98667	73	2191.9	17.44	1594.3	19.43
WTKV03_49	7.88022	0.10636	0.37589	0.00516	0.98322	87	2369.4	16.93	2057.1	24.16
WTKV03_50	5.18873	0.07857	0.31471	0.00446	0.93590	90	1950.3	22	1763.8	21.86
WTKV03_51	8.84189	0.12042	0.41821	0.00577	0.98712	94	2383.9	17.07	2252.4	26.22
WTKV03_52	7.57222	0.10393	0.35233	0.00482	0.99674	81	2411.8	17.69	1945.7	22.99
WTKV03_53	8.23394	0.11191	0.38974	0.00537	0.98642	89	2382.7	17	2121.6	24.9
WTKV03_54	4.82506	0.06674	0.28073	0.00383	0.98634	79	2024.7	18.68	1595	19.3
WTKV03_55	9.2279	0.12522	0.42304	0.00575	0.99835	93	2437.4	17.21	2274.2	26.06
WTKV03_56	6.16879	0.08531	0.30746	0.00422	0.99248	75	2294.6	17.87	1728.2	20.82
WTKV03_57	9.70158	0.13232	0.40158	0.00549	0.99766	83	2608.9	16.78	2176.3	25.26
WTKV03_58	4.25304	0.06799	0.20291	0.00294	0.90635	50	2369.7	23.34	1190.9	15.75
WTKV03_59	5.62619	0.07993	0.26922	0.00372	0.97261	65	2364.4	19.03	1536.8	18.9
WTKV03_60	4.23079	0.06337	0.2258	0.00319	0.94320	60	2176.3	21.04	1312.5	16.76
WTKV03_61	4.96079	0.0685	0.24681	0.00339	0.99471	62	2297.9	17.7	1422	17.53
WTKV03_62	12.90996	0.19296	0.46732	0.0068	0.97354	87	2830.7	19.03	2471.8	29.88
WTKV03_63	13.476	0.2026	0.48968	0.00711	0.96578	91	2823.8	19.51	2569.3	30.77
WTKV03_64	10.37778	0.15091	0.45986	0.00646	0.96604	98	2494.5	19.11	2438.9	28.51
WTKV03_65	10.34114	0.14681	0.3923	0.00547	0.98216	78	2752.8	17.79	2133.5	25.31
WTKV03_66	7.83838	0.10908	0.34564	0.00476	0.98961	76	2502.7	17.48	1913.7	22.82
WTKV03_67	8.41425	0.11642	0.41664	0.00573	0.99399	97	2305.6	17.58	2245.2	26.08
WTKV03_68	7.81719	0.11016	0.37103	0.00514	0.98306	86	2378.1	18.12	2034.2	24.18
WTKV03_69	6.70929	0.09233	0.37323	0.00512	0.99684	97	2103.6	17.8	2044.6	24.02
WTKV03_70	1.80286	0.02487	0.10654	0.00145	0.98660	33	1996.7	18.54	652.6	8.44
WTKV03_71	11.44088	0.17669	0.45548	0.00666	0.94679	91	2673.2	20.54	2419.6	29.48
WTKV03_72	5.30733	0.07333	0.28848	0.00396	0.99351	76	2144.1	17.92	1633.9	19.8
WTKV03_73	6.77034	0.10482	0.32627	0.00462	0.91460	77	2352.5	22.37	1820.3	22.46

Table 10. LA-ICPMS U/Pb concordia data for WTKV14, a quartzite (detrital zircons).

	Isotope Ratios						Ages			
Analysis #	Pb207/ U235	1σ error	Pb206/ U238	1σ error	rho	Conc. %	Pb207/ Pb206	± Ma	Pb206/ U238	± Ma
WTKV14_01	5.68626	0.0712	0.33444	0.00426	0.98302	93	2005	17.57	1859.9	20.56
WTKV14_02	6.0528	0.08342	0.30932	0.00403	0.94533	77	2251.2	20.53	1737.4	19.86
WTKV14_03	1.1888	0.01754	0.12711	0.00167	0.89046	89	863.7	26.41	771.4	9.53
WTKV14_04	4.58575	0.05926	0.27416	0.00354	0.99919	79	1975.9	18.5	1561.9	17.89
WTKV14_05	1.19147	0.01683	0.12818	0.00167	0.92235	91	850.9	24.78	777.5	9.55
WTKV14_06	9.15387	0.11486	0.4225	0.00538	0.98539	94	2425.3	16.85	2271.8	24.38
WTKV14_07	1.18991	0.0175	0.12741	0.00166	0.88589	90	860.8	26.52	773.1	9.48
WTKV14_08	8.6545	0.10921	0.41238	0.0053	0.98184	94	2371.1	16.86	2225.8	24.2
WTKV14_09	7.53172	0.09424	0.37769	0.00481	0.98250	90	2283.6	16.95	2065.5	22.5
WTKV14_10	4.32521	0.05504	0.25967	0.00333	0.99231	76	1968.4	18.03	1488.2	17.02
WTKV14_11	13.0726	0.16539	0.51328	0.00659	0.98541	99	2695.9	16.29	2670.6	28.07
WTKV14_12	5.5814	0.07274	0.27395	0.00358	0.99728	67	2320.5	17.61	1560.8	18.09
WTKV14_13	4.19127	0.06155	0.26503	0.00352	0.90441	81	1875.4	23.16	1515.5	17.93
WTKV14_14	1.22676	0.01755	0.13295	0.00174	0.91484	96	835.5	25.02	804.7	9.91
WTKV14_15	5.83358	0.07927	0.32648	0.00427	0.96249	87	2092.7	19.7	1821.3	20.78
WTKV14_16	6.00723	0.07627	0.34917	0.00447	0.99177	95	2025.9	17.63	1930.6	21.35
WTKV14_17	5.50282	0.06994	0.32054	0.0041	0.99366	89	2022	17.71	1792.3	20.01
WTKV14_18	4.25061	0.05369	0.24445	0.00311	0.99282	69	2044.7	17.62	1409.8	16.1
WTKV14_19	1.13178	0.01726	0.12318	0.00158	0.84108	91	826.7	28.47	748.8	9.05
WTKV14_20	5.7115	0.08156	0.33459	0.00446	0.93346	92	2012	21.34	1860.6	21.55
WTKV14_21	1.20007	0.01721	0.13069	0.00171	0.91239	96	825.5	25.12	791.8	9.75
WTKV14_22	4.74416	0.06126	0.28988	0.00375	0.99817	85	1936.9	18.22	1640.9	18.72
WTKV14_23	1.16147	0.01742	0.12364	0.00164	0.88439	86	872.8	26.66	751.5	9.4
WTKV14_24	9.49121	0.12411	0.42473	0.00555	0.99930	92	2477.5	17.49	2281.9	25.11
WTKV14_25	9.9253	0.12751	0.439	0.00571	0.98771	94	2497.2	16.77	2346.2	25.57
WTKV14_26	2.82424	0.03716	0.1708	0.00223	0.99230	52	1955.2	18.6	1016.5	12.3
WTKV14_27	7.81337	0.1021	0.38492	0.00504	0.99799	91	2314	17.62	2099.2	23.45
WTKV14_28	3.79772	0.05007	0.23167	0.00303	0.99201	69	1939.8	18.72	1343.2	15.86
WTKV14_29	5.46609	0.07261	0.32583	0.00431	0.99579	92	1980.9	18.62	1818.2	20.96
WTKV14_30	4.89399	0.06466	0.27107	0.00352	0.98285	73	2110.7	18.76	1546.3	17.83
WTKV14_31	6.87794	0.09069	0.35551	0.00468	0.99837	88	2231.2	17.94	1960.9	22.27
WTKV14_32	1.21989	0.01784	0.13202	0.00175	0.90641	95	838.3	25.63	799.4	9.98
WTKV14_33	5.91807	0.07514	0.34981	0.00451	0.98480	97	1996.2	17.6	1933.7	21.53
WTKV14_34	5.22247	0.06658	0.3192	0.00414	0.98295	92	1936.6	17.68	1785.8	20.24
WTKV14_35	1.73998	0.02387	0.1504	0.00197	0.95480	70	1290.7	21.93	903.2	11.07
WTKV14_36	11.2817	0.14577	0.455	0.00596	0.98641	91	2651.7	16.73	2417.5	26.42
WTKV14_37	1.194	0.0171	0.13309	0.00175	0.91812	104	776.9	25.31	805.5	9.96
WTKV14_38	5.10143	0.06869	0.31371	0.00413	0.97773	91	1925.6	19.66	1759	20.25
WTKV14_39	3.03195	0.04231	0.21755	0.00288	0.94866	77	1644.4	21.61	1268.9	15.22
WTKV14_40	9.04	0.11427	0.4218	0.00546	0.97651	94	2407	16.6	2268.6	24.75
WTKV14_41	4.72729	0.05976	0.25535	0.00326	0.99019	68	2154.9	17.57	1466	16.74

WTKV14_42	2.8985	0.03719	0.18793	0.00237	0.98288	61	1830.5	19.22	1110.1	12.86
WTKV14_43	6.7067	0.08354	0.35368	0.00445	0.99000	89	2197.1	17.33	1952.2	21.19
WTKV14_44	0.97753	0.01476	0.10382	0.00136	0.86756	72	878.4	27.25	636.8	7.96
WTKV14_45	18.6137	0.23007	0.51759	0.00651	0.98272	83	3252.3	15.43	2689	27.66
WTKV14_46	5.97654	0.07402	0.31962	0.00401	0.98716	82	2172.5	17.27	1787.9	19.57
WTKV14_47	1.03882	0.01629	0.10779	0.00139	0.82235	71	926.2	29.11	659.9	8.12
WTKV14_48	6.47832	0.08056	0.36489	0.00458	0.99073	96	2081.9	17.58	2005.3	21.61
WTKV14_49	5.38445	0.06824	0.27647	0.00351	0.99825	70	2243.4	17.66	1573.6	17.72
WTKV14_50	6.44965	0.08047	0.36558	0.00461	0.98942	97	2070.9	17.51	2008.6	21.78
WTKV14_51	1.18598	0.01663	0.12673	0.00162	0.91163	89	865.5	24.91	769.2	9.27
WTKV14_52	2.83077	0.03625	0.16903	0.00219	0.98838	51	1977.7	17.61	1006.8	12.09
WTKV14_53	15.9697	0.21074	0.56142	0.00744	0.99578	100	2876.6	16.87	2872.5	30.73
WTKV14_54	11.8022	0.15171	0.46211	0.00605	0.98184	91	2700.2	16.28	2448.9	26.66
WTKV14_55	1.2359	0.0175	0.13071	0.00173	0.93472	89	885.9	24.12	791.9	9.86
WTKV14_56	7.59245	0.09842	0.39596	0.00521	0.98518	97	2215.6	17.25	2150.4	24.04
WTKV14_57	5.17054	0.06772	0.29123	0.0038	0.99625	79	2081	18.14	1647.7	18.99
WTKV14_58	7.2069	0.09408	0.38208	0.00502	0.99357	95	2187	17.67	2086	23.42
WTKV14_59	3.76035	0.04878	0.17701	0.00233	0.98550	44	2391.6	16.99	1050.6	12.74
WTKV14_60	5.51295	0.07098	0.32276	0.00422	0.98473	90	2012.8	17.6	1803.2	20.56
WTKV14_61	4.73227	0.06498	0.28473	0.00378	0.96683	82	1964.3	19.97	1615.1	18.95
WTKV14_62	8.33521	0.10888	0.40362	0.00535	0.98549	93	2343.4	16.93	2185.7	24.58
WTKV14_63	8.83129	0.1157	0.34265	0.00455	0.98662	70	2715.4	16.36	1899.4	21.85
WTKV14_64	5.12706	0.06965	0.30247	0.00405	0.98564	85	1999.3	18.95	1703.6	20.02
WTKV14_65	9.12598	0.11945	0.42726	0.00566	0.98806	96	2401	16.89	2293.4	25.56
WTKV14_66	5.13421	0.06768	0.30026	0.00398	0.99449	84	2014.9	17.88	1692.6	19.72
WTKV14_67	7.64628	0.10479	0.36853	0.00496	0.98206	86	2351.5	18.54	2022.5	23.35
WTKV14_68	2.52659	0.03344	0.1589	0.00211	0.99672	50	1885.1	18.22	950.7	11.72
WTKV14_69	5.34258	0.07061	0.31745	0.00421	0.99657	89	1986.7	17.91	1777.3	20.62
WTKV14_70	1.2915	0.02066	0.13276	0.00181	0.85227	85	944.8	28.16	803.6	10.32
WTKV14_71	5.66343	0.07511	0.27977	0.00371	0.99990	69	2309.4	17.41	1590.2	18.71
WTKV14_72	11.1286	0.14673	0.41945	0.00557	0.99290	82	2763.2	16.36	2258	25.31
WTKV14_73	9.81547	0.12895	0.41631	0.0055	0.99441	87	2567.8	16.87	2243.7	25.04
WTKV14_74	9.56895	0.13381	0.43229	0.00585	0.96773	94	2461.7	19.21	2316	26.33
WTKV14_75	6.18401	0.08018	0.35665	0.00468	0.98808	96	2039.8	17.46	1966.3	22.26
WTKV14_76	4.73055	0.06127	0.29288	0.00384	0.98786	87	1913.5	17.78	1655.9	19.14
WTKV14_77	2.50876	0.03301	0.15972	0.00211	0.99601	51	1863.2	18.32	955.2	11.73
WTKV14_78	9.7488	0.12825	0.44131	0.00583	0.99582	96	2458.3	17.29	2356.5	26.07
WTKV14_79	8.38437	0.10971	0.41487	0.00545	0.99607	97	2306.6	17.57	2237.1	24.84
WTKV14_80	3.62862	0.0472	0.24198	0.00316	0.99608	79	1778.9	18.5	1397	16.43
WTKV14_81	11.8257	0.15184	0.47559	0.00621	0.98333	94	2656.3	16.44	2508	27.11
WTKV14_82	1.91004	0.02648	0.15808	0.00209	0.95366	69	1374.6	21.88	946.1	11.62

Table 11. LA-ICPMS U/Pb concordia data for WTKV13, a felsic gneiss.

	Isotope Ratios						Ages			
Analysis #	Pb207/ U235	1σ error	Pb206/ U238	1σ error	rho	Conc. %	Pb207/ Pb206	± Ma	Pb206/ U238	± Ma
WTKV13_01	4.15417	0.05372	0.26654	0.0035	0.98480	82	1849	17.94	1523.2	17.8
WTKV13_01A	1.25089	0.03855	0.1268	0.00192	0.49133	79	973.5	62.13	769.6	10.96
WTKV13_02	4.82738	0.06521	0.31547	0.00419	0.98323	97	1815.8	19.52	1767.6	20.53
WTKV13_02A	4.07926	0.0498	0.27962	0.00345	0.98946	92	1728.8	18.35	1589.4	17.4
WTKV13_03	4.78465	0.06521	0.32139	0.0043	0.98168	102	1765.7	19.83	1796.5	20.97
WTKV13_03A	4.17302	0.05143	0.28423	0.00353	0.99234	93	1740.5	18.52	1612.7	17.71
WTKV13_04	4.77913	0.06492	0.30805	0.00411	0.98218	94	1840.7	19.53	1731.1	20.27
WTKV13_04A	4.12568	0.05063	0.28053	0.00348	0.98926	91	1743.7	18.26	1594.1	17.54
WTKV13_05	1.44458	0.05168	0.12901	0.00234	0.50700	64	1226.9	70.13	782.2	13.37
WTKV13_05A	2.04131	0.04403	0.13359	0.00194	0.67327	45	1813.5	38.94	808.3	11.06
WTKV13_06	1.34982	0.0356	0.12721	0.00201	0.59910	69	1120.4	51.52	771.9	11.5
WTKV13_06A	1.21932	0.03419	0.12883	0.0019	0.52596	88	888.5	56.96	781.2	10.86
WTKV13_07	8.67238	0.14404	0.20571	0.00321	0.93952	34	3499.9	24.63	1205.9	17.15
WTKV13_07A	1.90328	0.04268	0.14865	0.00215	0.64499	60	1485.6	41.91	893.4	12.06
WTKV13_08	1.30286	0.0348	0.13479	0.00196	0.54440	87	931.9	53.63	815.1	11.15
WTKV13_09	3.16504	0.04064	0.19113	0.00242	0.98608	58	1958.2	18.93	1127.5	13.08
WTKV13_10	2.56034	0.03509	0.1832	0.00234	0.93198	66	1649.6	21.79	1084.4	12.78
WTKV13_11	4.38111	0.06199	0.29366	0.00383	0.92176	94	1769.4	22.49	1659.8	19.06
WTKV13_12	1.72961	0.07379	0.12835	0.00238	0.43464	49	1581.4	79.79	778.5	13.6
WTKV13_13	1.28915	0.04919	0.12502	0.00208	0.43602	71	1062.9	76.01	759.4	11.9
WTKV13_14	8.52346	0.15168	0.21014	0.00336	0.89850	36	3439.9	27.99	1229.5	17.89
WTKV13_15	1.13953	0.01681	0.12708	0.00164	0.87483	99	775.6	27.18	771.2	9.41
WTKV13_16	1.1307	0.03456	0.12597	0.00185	0.48048	98	778.9	63.25	764.8	10.6
WTKV13_17	2.77423	0.03661	0.20368	0.00257	0.95615	75	1602.2	20.82	1195.1	13.76
WTKV13_18	1.11097	0.0204	0.1245	0.00163	0.71300	99	766.6	36.5	756.4	9.37
WTKV13_19	1.14238	0.05824	0.12696	0.00241	0.37234	98	783.7	105.76	770.5	13.8
WTKV13_20	4.6287	0.05739	0.30438	0.00379	0.99576	95	1805.1	18.21	1713	18.74
WTKV13_21	4.40984	0.05443	0.29188	0.00362	0.99520	92	1793.3	18.21	1650.9	18.05
WTKV13_22	2.74599	0.03716	0.21161	0.00268	0.93588	82	1511.3	21.8	1237.4	14.26
WTKV13_23	1.29899	0.04413	0.13705	0.00222	0.47681	93	892	69.33	828	12.56
WTKV13_24	1.23007	0.04912	0.13353	0.00219	0.41071	97	832.6	82.01	808	12.47
WTKV13_25	3.77384	0.09135	0.23583	0.00374	0.65516	72	1896.8	43.58	1365	19.48
WTKV13_26	5.24369	0.06643	0.34329	0.00438	0.99292	105	1812.5	18.04	1902.5	21
WTKV13_27	1.37042	0.05507	0.14085	0.00238	0.42049	90	945.3	80.95	849.4	13.44
WTKV13_28	4.19528	0.05534	0.27733	0.00363	0.99227	88	1795.2	19.03	1577.9	18.3
WTKV13_29	4.35794	0.05692	0.29906	0.00396	0.98639	98	1726.6	18.23	1686.6	19.66
WTKV13_30	4.34215	0.0574	0.2961	0.00384	0.98104	96	1738.2	19.5	1671.9	19.12
WTKV13_31	4.54887	0.06426	0.29929	0.004	0.94609	94	1803.7	21.28	1687.8	19.85
WTKV13_32	1.84231	0.05214	0.13801	0.00222	0.56837	53	1564.1	52.86	833.4	12.6
WTKV13_33	4.44627	0.09512	0.16853	0.00274	0.75997	36	2753.9	35.53	1004	15.14
WTKV13_34	1.25009	0.04882	0.13306	0.0022	0.42337	92	873.2	79.63	805.3	12.53

WTKV13_35	4.76408	0.06226	0.31143	0.00405	0.99509	96	1815.3	18.79	1747.7	19.91
WTKV13_36	1.27876	0.02932	0.13464	0.00194	0.62842	91	895.5	45.35	814.3	11.01
WTKV13_37	1.18737	0.03972	0.13126	0.00213	0.48509	100	794.8	69.49	795.1	12.11
WTKV13_38	3.98621	0.05119	0.26725	0.00347	0.98904	86	1769.1	18.21	1526.8	17.66
WTKV13_39	4.51011	0.05773	0.3027	0.00391	0.99095	96	1767.1	18.36	1704.7	19.33
WTKV13_40	3.70847	0.04972	0.25609	0.00336	0.97861	86	1714.8	19.73	1469.8	17.27
WTKV13_41	5.3315	0.07588	0.29112	0.00396	0.95575	77	2135.7	20.37	1647.1	19.77
WTKV13_42	5.37605	0.07722	0.29177	0.00402	0.95922	77	2146.5	20.09	1650.4	20.04
WTKV13_43	4.64013	0.06159	0.3059	0.004	0.98515	96	1799.7	19.41	1720.5	19.74
WTKV13_44	4.47996	0.05797	0.29461	0.00381	0.99942	92	1804.3	18.67	1664.5	18.98
WTKV13_45	4.26853	0.05676	0.28614	0.00378	0.99346	92	1769	19.01	1622.2	18.94
WTKV13_46	4.52985	0.05804	0.30572	0.00395	0.99168	98	1756.6	18.3	1719.6	19.51
WTKV13_47	4.28046	0.0592	0.29154	0.00396	0.98212	95	1740	19.33	1649.2	19.79
WTKV13_48	4.47972	0.07102	0.29552	0.0044	0.93915	93	1798.4	22.35	1669.1	21.88
WTKV13_49	4.83365	0.08197	0.31234	0.00467	0.88168	95	1835.8	25.66	1752.2	22.96
WTKV13_50	4.67747	0.06505	0.30988	0.00434	0.99298	97	1790.4	18.17	1740.1	21.33
WTKV13_51	1.53579	0.07193	0.13247	0.00308	0.49643	62	1295.6	92	801.9	17.53
WTKV13_52	4.70619	0.07261	0.30186	0.00453	0.97267	92	1849.8	20.5	1700.5	22.44
WTKV13_53	5.1625	0.08513	0.30628	0.00471	0.93257	87	1989.2	22.88	1722.4	23.24
WTKV13_54	1.24317	0.02495	0.13502	0.00205	0.75651	98	830.6	37.25	816.5	11.65
WTKV13_55	4.6414	0.06527	0.30811	0.00435	0.99605	97	1786.7	18.43	1731.4	21.43
WTKV13_56	4.51107	0.06759	0.29873	0.00444	0.99198	94	1791.8	19.33	1685	22.05
WTKV13_57	1.23747	0.02759	0.12831	0.00201	0.70262	84	927.2	42.29	778.2	11.48
WTKV13_58	4.77995	0.06817	0.31666	0.00451	0.99865	99	1791	18.44	1773.4	22.1
WTKV13_59	4.47956	0.06545	0.30155	0.00432	0.98051	96	1761.8	19.49	1699	21.4
WTKV13_60	4.49582	0.06365	0.3018	0.00428	0.99831	96	1766.8	18.45	1700.2	21.2
WTKV13_61	3.96343	0.05644	0.27251	0.00388	0.99985	90	1723	18.67	1553.6	19.65
WTKV13_62	4.3641	0.06346	0.29646	0.00418	0.96963	96	1745.1	20.38	1673.7	20.77
WTKV13_63	4.93813	0.07171	0.31978	0.00459	0.98843	98	1832.2	19.01	1788.6	22.43
WTKV13_64	4.72887	0.06682	0.31435	0.00444	0.99959	99	1784.7	18.69	1762.1	21.77
WTKV13_65	4.58459	0.06495	0.3072	0.00435	0.99952	98	1770	18.73	1726.9	21.46

Table 12. LA-ICPMS U/Pb concordia data for WTKV09, an anorthositic gabbro.

	Isotope Ratios						Ages			
Analysis #	Pb207/ U235	1σ error	Pb206/ U238	1σ error	rho	Conc. %	Pb207/ Pb206	± Ma	Pb206/ U238	± Ma
WTKV09_01	1.08286	0.02582	0.11715	0.00161	0.57637	85	839.6	48.44	714.2	9.28
WTKV09_02	0.97156	0.02020	0.10525	0.00143	0.70195	78	988	77.53	772.5	11.75
WTKV09_03	1.18395	0.02930	0.12683	0.00177	0.56392	90	860	50.2	769.8	10.1
WTKV09_04	1.22583	0.02417	0.12768	0.00170	0.67527	84	918	38.94	774.6	9.71
WTKV09_05	1.18342	0.02594	0.12960	0.00177	0.62307	97	814	44.27	785.6	10.11
WTKV09_06	0.97681	0.02102	0.10419	0.00143	0.67658	44	1777.9	58.71	785.2	13.69
WTKV09_07	1.34072	0.03237	0.13502	0.00190	0.58284	83	986.7	48.15	816.5	10.79
WTKV09_08	1.35279	0.02548	0.13863	0.00186	0.71234	88	951	36.49	836.9	10.56
WTKV09_09	1.31964	0.03845	0.14021	0.00211	0.51649	97	876.5	59.47	845.9	11.91
WTKV09_10	0.97531	0.02078	0.10449	0.00143	0.68383	64	1400.5	27.78	893.6	10.94
WTKV09_11	0.97643	0.02096	0.10427	0.00143	0.67839	49	1758.9	28.02	858.2	10.73
WTKV09_12	1.24506	0.02195	0.13468	0.00177	0.74546	97	839.2	34.33	814.5	10.05
WTKV09_13	1.26106	0.02622	0.13877	0.00188	0.65158	104	803.5	41.84	837.7	10.67
WTKV09_14	0.97231	0.02032	0.10510	0.00143	0.69833	77	1094.4	28.29	843.1	10.21
WTKV09_15	0.97381	0.02055	0.10480	0.00143	0.69108	74	1201.1	28.14	885.8	10.72
WTKV09_16	0.97606	0.02090	0.10434	0.00143	0.68020	49	1769.2	40.05	875.7	12.05
WTKV09_17	0.97081	0.02008	0.10540	0.00143	0.70557	79	1050.7	33.8	825.6	10.37
WTKV09_18	1.25545	0.03259	0.13672	0.00197	0.55507	100	825.4	53.07	826.1	11.18
WTKV09_19	1.23220	0.02595	0.13209	0.00181	0.65066	93	858.5	42.03	799.8	10.31
WTKV09_20	0.97418	0.02061	0.10472	0.00143	0.68926	70	1197.8	38.84	841.9	10.91
WTKV09_21	1.19262	0.02238	0.13435	0.00179	0.71000	108	754.8	37.41	812.6	10.16
WTKV09_22	1.34356	0.03061	0.13457	0.00190	0.61973	82	997.9	45	813.9	10.77
WTKV09_23	1.31779	0.02030	0.14094	0.00181	0.83367	98	863.3	28.78	850	10.24
WTKV09_24	1.23284	0.02311	0.13302	0.00178	0.71385	95	844.9	36.91	805.1	10.1
WTKV09_25	1.32230	0.03365	0.13936	0.00201	0.56676	94	893.6	51.43	841.1	11.35
WTKV09_26	1.19009	0.02423	0.12937	0.00176	0.66820	95	829.4	40.59	784.2	10.04
WTKV09_27	1.34406	0.03141	0.13765	0.00195	0.60619	87	952.5	46.54	831.4	11.04
WTKV09_28	0.97118	0.02014	0.10533	0.00143	0.70376	78	1046	46.42	817.9	10.96
WTKV09_29	1.26861	0.02395	0.13569	0.00182	0.71047	95	863	36.92	820.2	10.33
WTKV09_30	1.21583	0.03313	0.13235	0.00198	0.54903	97	826.3	56.56	801.3	11.28
WTKV09_31	1.28374	0.02955	0.13720	0.00196	0.62061	96	864.5	46.38	828.8	11.13
WTKV09_32	1.27056	0.02620	0.13608	0.00186	0.66285	96	860.1	41.2	822.5	10.55
WTKV09_33	0.97493	0.02072	0.10457	0.00143	0.68564	68	971.8	24	663.5	8.07
WTKV09_34	0.97343	0.02049	0.10487	0.00143	0.69289	74	1104.9	29.76	817.3	9.98
WTKV09_35	1.16540	0.02363	0.13011	0.00179	0.67851	102	773.2	40.29	788.5	10.19
WTKV09_36	1.26891	0.02824	0.13715	0.00192	0.62903	99	841.1	44.68	828.5	10.87
WTKV09_37	1.13592	0.02121	0.12367	0.00167	0.72320	91	825.8	36.35	751.7	9.59
WTKV09_38	1.23313	0.02488	0.13204	0.00181	0.67941	93	860.5	39.65	799.5	10.32
WTKV09_39	1.21614	0.02157	0.13302	0.00180	0.76294	99	816.3	34.02	805.1	10.27
WTKV09_40	0.97568	0.02084	0.10442	0.00143	0.68201	62	1325.4	29.34	825.8	10.37
WTKV09_41	1.22808	0.02063	0.13143	0.00175	0.79263	92	861.7	31.61	796	9.97

WTKV09_42	1.17935	0.02036	0.13140	0.00175	0.77145	102	777.6	33.12	795.8	9.99
WTKV09_43	1.25181	0.02070	0.13622	0.00181	0.80354	100	827	31.02	823.2	10.28
WTKV09_44	1.19761	0.02105	0.13314	0.00181	0.77345	103	782.1	33.63	805.8	10.28
WTKV09_45	1.22398	0.02359	0.13161	0.00180	0.70963	94	852	37.66	797	10.25
WTKV09_46	1.24157	0.02986	0.13234	0.00191	0.60010	92	869.9	48.58	801.2	10.89
WTKV09_47	1.27859	0.03012	0.13763	0.00197	0.60762	98	849.6	47.23	831.3	11.18
WTKV09_48	1.20801	0.01937	0.13390	0.00177	0.82439	103	788.5	29.96	810	10.07
WTKV09_49	1.24849	0.02969	0.13502	0.00194	0.60420	97	839.9	47.7	816.4	11.02
WTKV09_50	1.25474	0.03247	0.14018	0.00210	0.57890	110	772.1	52.74	845.7	11.89

Table 13. Microprobe FeO and MgO in Opx and Cpx analyses, and calculated temperatures using two pyroxene thermometry. Note very high temperatures, possibly too high.

Mineral	Cpx	Cpx	Cpx	Cpx	Cpx	Cpx	Cpx	Cpx
Analysis #	43	44	48	49	52	53	59	62
FeO	26.5386	26.5869	26.6273	26.0389	26.884	26.6441	26.8689	26.9223
MgO	19.879	20.0067	19.8172	19.6975	19.8411	19.6278	19.6614	19.7769
Mineral	Opx	Opx	Opx	Opx	Opx	Opx	Opx	Opx
Analysis #	45	46	47	50	57	58	60	66
FeO	9.4326	9.578	12.8177	9.6224	9.3525	9.5457	9.3493	9.8787
MgO	13.4459	13.2721	13.8208	13.3023	13.6546	13.2203	13.2103	13.5951
Calculated Temperature (°C)	1456	1435	1251	1431	1478	1443	1460	1440

Table 14. Probe data.

Sample number	Anal. No.	Mineral	SiO2	TiO2	Al2O3	Cr2O3	FeO	MnO	MgO	CaO	Na2O	K2O	Total	Si	Ti	Al	Cr	Fe2+	Mn2+	Mg	Ca	Na	K	Total Cations (S)	Xmg (mg/ (fe+mg))	Xmg (divalent)
WTKV04	43	Cpx	50.135	0.069	1.271	0.051	26.539	0.620	19.879	0.533	0.000	0.009	99.11	1.933	0.002	0.058	0.002	0.856	0.020	1.143	0.022	0.000	0.000	4.035	0.572	0.560
WTKV04	44	Cpx	50.607	0.024	1.206	0.040	26.587	0.634	20.007	0.470	0.000	0.000	99.57	1.940	0.001	0.054	0.001	0.852	0.021	1.143	0.019	0.000	0.000	4.032	0.573	0.562
WTKV04	48	Cpx	50.139	0.092	1.325	0.036	26.627	0.579	19.817	0.576	0.044	0.009	99.24	1.931	0.003	0.060	0.001	0.858	0.019	1.138	0.024	0.003	0.000	4.037	0.570	0.558
WTKV04	49	Cpx	49.024	0.095	1.154	0.000	26.039	0.614	19.698	0.334	0.000	0.019	96.98	1.932	0.003	0.054	0.000	0.858	0.020	1.157	0.014	0.000	0.001	4.039	0.574	0.565
WTKV04	51	Cpx	49.233	0.082	1.241	0.079	26.827	0.602	19.390	0.455	0.003	0.000	97.91	1.928	0.002	0.057	0.002	0.878	0.020	1.132	0.019	0.000	0.000	4.040	0.563	0.552
WTKV04	52	Cpx	51.740	0.087	1.148	0.000	26.884	0.579	19.841	0.654	0.025	0.000	100.96	1.953	0.002	0.051	0.000	0.849	0.019	1.117	0.026	0.002	0.000	4.019	0.568	0.555
WTKV04	53	Cpx	50.821	0.059	1.253	0.000	26.644	0.613	19.628	0.613	0.021	0.016	99.67	1.946	0.002	0.057	0.000	0.853	0.020	1.120	0.025	0.002	0.001	4.025	0.568	0.555
WTKV04	59	Cpx	49.504	0.463	1.286	0.004	26.869	0.712	19.661	0.589	0.047	0.025	99.16	1.916	0.013	0.059	0.000	0.869	0.023	1.134	0.024	0.004	0.001	4.044	0.566	0.553
WTKV04	61	Cpx	51.463	0.282	2.239	0.021	9.735	0.271	13.263	22.406	0.421	0.023	100.12	1.931	0.008	0.099	0.001	0.305	0.009	0.742	0.901	0.031	0.001	4.027	0.708	0.379
WTKV04	62	Cpx	52.153	0.017	1.005	0.004	26.922	0.632	19.777	0.506	0.000	0.000	101.02	1.966	0.000	0.045	0.000	0.849	0.020	1.111	0.020	0.000	0.000	4.011	0.567	0.556
WTKV04	63	Cpx	51.158	0.144	1.418	0.024	26.585	0.587	19.310	1.215	0.127	0.048	100.62	1.942	0.004	0.063	0.001	0.844	0.019	1.093	0.049	0.009	0.002	4.027	0.564	0.545
WTKV04	64	Cpx	51.053	0.025	0.932	0.000	26.945	0.570	19.962	0.434	0.000	0.000	99.92	1.951	0.001	0.042	0.000	0.861	0.018	1.137	0.018	0.000	0.000	4.028	0.569	0.559
WTKV05	78	Cpx	51.943	0.199	2.044	0.000	10.258	0.771	12.589	22.445	0.383	0.092	100.72	1.945	0.006	0.090	0.000	0.321	0.024	0.703	0.900	0.028	0.004	4.021	0.686	0.361
WTKV05	79	Cpx	50.041	0.225	2.803	0.013	11.000	0.614	12.106	21.912	0.344	0.096	99.16	1.912	0.006	0.126	0.000	0.351	0.020	0.690	0.897	0.026	0.005	4.033	0.662	0.352
WTKV05	80	Cpx	52.210	0.098	1.665	0.022	10.169	0.546	12.194	23.152	0.440	0.032	100.53	1.959	0.003	0.074	0.001	0.319	0.017	0.682	0.931	0.032	0.002	4.018	0.681	0.350
WTKV05	81	Cpx	52.022	0.173	1.974	0.000	10.619	0.546	12.065	22.952	0.419	0.022	100.79	1.949	0.005	0.087	0.000	0.333	0.017	0.674	0.921	0.030	0.001	4.018	0.670	0.346
WTKV12	95	Cpx	42.898	1.695	10.976	0.380	14.954	0.139	11.757	11.956	1.588	1.227	97.57	1.677	0.050	0.506	0.012	0.489	0.005	0.685	0.501	0.120	0.061	4.105	0.584	0.408
WTKV12	96	Cpx	53.123	0.172	1.233	0.087	7.765	0.214	14.697	22.868	0.359	0.000	100.52	1.965	0.005	0.054	0.003	0.240	0.007	0.810	0.906	0.026	0.000	4.015	0.771	0.413
WTKV12	97	Cpx	52.228	0.269	2.121	0.065	7.807	0.203	14.212	22.994	0.360	0.000	100.26	1.940	0.008	0.093	0.002	0.242	0.006	0.787	0.915	0.026	0.000	4.018	0.764	0.403
WTKV07	102	Cpx	51.475	0.126	1.913	0.045	21.686	0.411	23.023	0.656	0.008	0.000	99.34	1.929	0.004	0.085	0.001	0.680	0.013	1.286	0.026	0.001	0.000	4.025	0.654	0.641
WTKV07	103	Cpx	52.816	0.059	1.850	0.016	21.742	0.354	22.979	0.350	0.068	0.000	100.23	1.954	0.002	0.081	0.000	0.673	0.011	1.267	0.014	0.005	0.000	4.006	0.653	0.645
WTKV07	106	Cpx	50.435	0.592	3.728	0.048	8.648	0.189	14.768	20.658	0.863	0.003	99.93	1.882	0.017	0.164	0.001	0.270	0.006	0.822	0.826	0.062	0.000	4.050	0.753	0.427
WTKV07	108	Cpx	51.740	0.625	3.664	0.000	7.405	0.226	14.238	22.376	0.675	0.015	100.96	1.903	0.017	0.159	0.000	0.228	0.007	0.781	0.882	0.048	0.001	4.025	0.774	0.412
WTKV06	132	Cpx	47.893	0.912	5.792	0.017	10.134	0.206	10.899	23.602	0.603	0.015	100.07	1.816	0.026	0.259	0.001	0.321	0.007	0.616	0.959	0.044	0.001	4.050	0.657	0.324
WTKV06	133	Cpx	48.929	0.562	4.279	0.000	9.764	0.145	11.503	23.672	0.635	0.000	99.49	1.862	0.016	0.192	0.000	0.311	0.005	0.653	0.965	0.047	0.000	4.050	0.677	0.338
WTKV06	134	Cpx	50.348	0.390	3.398	0.035	9.553	0.171	11.938	23.687	0.541	0.000	100.06	1.898	0.011	0.151	0.001	0.301	0.005	0.671	0.957	0.040	0.000	4.035	0.690	0.347
WTKV06	142	Cpx	48.955	0.555	3.946	0.009	9.556	0.156	11.722	23.860	0.547	0.005	99.31	1.866	0.016	0.177	0.000	0.305	0.005	0.666	0.974	0.040	0.000	4.050	0.686	0.342
WTKV06	143	Cpx	50.649	0.277	2.970	0.031	9.262	0.149	12.225	24.244	0.498	0.009	100.31	1.905	0.008	0.132	0.001	0.291	0.005	0.685	0.977	0.036	0.000	4.040	0.702	0.350
WTKV04	45	Opx	51.826	0.241	1.910	0.000	9.433	0.239	13.446	22.809	0.455	0.014	100.37	1.938	0.007	0.084	0.000	0.295	0.008	0.750	0.914	0.033	0.001	4.029	0.718	0.381
WTKV04	46	Opx	49.317	0.317	2.338	0.021	9.578	0.167	13.272	22.312	0.427	0.000	97.75	1.903	0.009	0.106	0.001	0.309	0.005	0.763	0.922	0.032	0.000	4.051	0.712	0.382
WTKV04	47	Opx	48.796	0.354	2.305	0.072	12.818	0.297	13.821	19.448	0.306	0.000	98.22	1.889	0.010	0.105	0.002	0.415	0.010	0.798	0.807	0.023	0.000	4.059	0.658	0.393
WTKV04	50	Opx	49.797	0.368	2.496	0.034	9.622	0.185	13.302	22.112	0.469	0.000	98.38	1.906	0.011	0.113	0.001	0.308	0.006	0.759	0.907	0.035	0.000	4.044	0.711	0.383
WTKV04	56	Opx	48.744	0.374	2.546	0.068	9.581	0.238	12.863	21.865	0.509	0.031	96.82	1.900	0.011	0.117	0.002	0.312	0.008	0.747	0.913	0.038	0.002	4.050	0.705	0.377
WTKV04	57	Opx	49.711	0.149	1.535	0.013	9.353	0.299	13.655	22.681	0.390	0.004	97.79	1.918	0.004	0.070	0.000	0.302	0.010	0.786	0.938	0.029	0.000	4.057	0.722	0.386
WTKV04	58	Opx	50.325	0.353	2.311	0.009	9.546	0.224	13.220	22.304	0.409	0.000	98.70	1.918	0.010	0.104	0.000	0.304	0.007	0.751	0.911	0.030	0.000	4.035	0.712	0.381
WTKV04	60	Opx	49.837	0.297	2.363	0.000	9.349	0.142	13.210	22.740	0.451	0.000	98.39	1.908	0.009	0.107	0.000	0.299	0.005	0.754	0.933	0.034	0.000	4.047	0.716	0.379
WTKV04	66	Opx	51.407	0.225	2.082	0.103	9.879	0.267	13.595	22.387	0.388	0.003	100.34	1.927	0.006	0.092	0.003	0.310	0.008	0.760	0.899	0.028	0.000	4.033	0.710	0.384
WTKV04	67	Opx	51.096	0.298	2.341	0.137	9.794	0.221	13.018	22.669	0.425	0.011	100.01	1.923	0.008	0.104	0.004	0.308	0.007	0.730	0.914	0.031	0.001	4.030	0.703	0.373
WTKV04	68	Opx	51.377	0.498	2.659	0.004	9.922	0.281	13.246	22.761	0.411	0.015	101.18	1.911	0.014	0.117	0.000	0.309	0.009	0.735	0.907	0.030	0.001	4.032	0.704	0.375
WTKV12	91	Opx	51.297	0.070	0.978	0.041	23.536	0.461	22.096	0.486	0.000	0.000	98.96	1.948	0.002	0.044	0.001	0.747	0.015	1.251	0.020	0.000	0.000	4.028	0.626	0.615
WTKV07	99	Opx	51.629	0.490	3.505	0.000	8.124	0.153	14.757	21.111	0.772	0.000	100.54	1.907	0.014	0.153	0.000	0.251	0.005	0.812	0.835	0.055	0.000	4.031	0.764	0.427
WTKV07	101	Opx	52.054	0.525	3.442	0.035	6.870	0.182	14.468	22.221	0.727	0.003	100.53	1.916	0.015	0.149	0.001	0.211	0.006	0.794	0.876	0.052	0.000	4.020	0.790	0.421
WTKV07	107	Opx	50.217	0.597	3.770	0.087	7.646	0.116	14.178	21.389	0.786	0.017	98.80	1.890	0.017	0.167	0.003	0.241	0.004	0.796	0.862	0.057	0.001	4.037	0.768	0.418
WTKV07	109	Opx	50.264	0.609	3.545	0.053	6.813	0.186	14.096	22.730	0.723	0.019	99.04	1.888	0.017	0.157	0.002	0.214	0.006	0.789	0.915	0.053	0.001	4.042	0.787	0.410
WTKV01	2	Hb	44.089	0.809	10.663	0.067	12.415	0.117	13.398	10.863	0.993	0.257	93.67	6.691	0.092	1.907	0.008	1.576	0.015	3.032	1.766	0.292	0.050	15.430	0.658	0.475
WTKV01	3	Hb	44.533	0.828	10.801	0.131	12.670	0.149	13.562	10.953	1.015	0.254	94.89	6.678	0.093	1.909	0.015	1.589	0.019	3.032	1.760	0.295	0.049	15.438	0.656	0.474
WTKV01	4	Hb	46.323	0.802	10.892	0.038	12.144	0.120	13.993	11.310	1.140	0.280	97.04	6.757	0.088	1.872	0.004	1.481	0.015	3.043	1.768	0.322	0.052	15.403	0.673	0.483
WTKV01	5	Hb	46.133	0.789	10.931	0.000	12.455	0.170	14.011	11.456	1.105	0.239	97.29	6.727	0.087	1.879	0.000	1.519	0.021	3.046	1.790	0.312	0.044	15.425	0.667	0.478
WTKV01	6	Hb	43.421	0.813	10.440	0.084	12.485	0.124	14.036	11.101	1.033	0.290	93.83	6.607	0.093	1.872	0.010	1.588	0.016	3.184	1.809	0.305	0.056	15.540	0.667	0.483
WTKV01	7	Hb	43.717	0.720	10.528	0.101	12.433	0.173	13.951	11.331	1.214	0.249	94.42	6.612	0.082	1.877	0.012	1.573	0.022	3.146	1.836	0.356	0.048	15.563	0.667	0.478
WTKV01	8	Hb	43.450	0.605	10.072	0.063	11.853	0.159	13.939	11.260	0.985	0.172	92.56	6.678	0.070	1.824	0.008	1.523	0.021	3.194	1.854	0.294	0.034	15.499	0.677	0.485
WTKV01	9	Hb	42.885	0.827	10.500	0.071	12.200	0.177	13.881	11.179	1.135	0.216	93.07	6.579	0.095	1.898	0.009	1.565	0.023	3.175	1.837	0.338	0.042	15.562	0.670	0.481
WTKV01	10	Hb	43.352	0.681	9.955	0.063	12.004	0.293	14.159	11.297	1.152	0.229	93.18	6.640	0.078	1.797	0.008	1.538	0.038	3.233	1.854	0.342	0.045	15.572	0.678	0.485
WTKV01	11	Hb	42.908	0.754	10.350	0.000	12.133	0.198	13.900	11.204	1.025	0.211	92.68	6.605	0.087	1.878	0.000	1.562	0.026	3.190	1.848	0.306	0.041	15.543	0.671	0.481
WTKV01	12	Hb	43.715	0.669	10.268	0.042	11.716	0.177	14.067	11.422	1.172	0.202	93.45	6.656	0.077	1.842	0.005	1.492	0.023	3.193	1.863	0.346	0.039	15.536	0.682	0.486
WTKV01	13	Hb	44.085	0.815	10.774	0.143	12.636	0.223	13.944	11.464	1.018	0.243	95.34	6.602	0.092	1.902	0.017	1.582	0.028	3.113	1.839	0.296	0.046	15.518	0.663	0.474

Table 14. (continued)

Sample number	Anal. No.	Mineral	SiO2	TiO2	Al2O3	Cr2O3	FeO	MnO	MgO	CaO	Na2O	K2O	Total	Si	Ti	Al	Cr	Fe2+	Mn2+	Mg	Ca	Na	K	Total Cations (S)	Xmg (mg/ (fe+mg))	Xmg (divalent)
WTKV01	21	Hb	44.724	0.633	11.142	0.101	11.745	0.226	13.281	10.883	1.095	0.237	94.07	6.728	0.072	1.975	0.012	1.477	0.029	2.978	1.754	0.319	0.045	15.390	0.668	0.477
WTKV01	22	Hb	45.985	0.703	10.685	0.105	12.317	0.279	13.824	11.299	1.125	0.232	96.55	6.757	0.078	1.850	0.012	1.513	0.035	3.028	1.779	0.320	0.044	15.416	0.667	0.477
WTKV01	23	Hb	44.109	0.884	11.278	0.046	12.214	0.215	13.621	11.475	1.141	0.297	95.28	6.595	0.099	1.987	0.005	1.527	0.027	3.036	1.838	0.331	0.057	15.503	0.665	0.472
WTKV01	24	Hb	44.931	0.534	10.389	0.042	12.135	0.219	14.084	11.660	1.070	0.169	95.23	6.708	0.060	1.828	0.005	1.515	0.028	3.135	1.865	0.310	0.032	15.486	0.674	0.479
WTKV01	25	Hb	44.629	0.681	10.564	0.122	11.835	0.202	13.926	11.093	1.081	0.212	94.35	6.709	0.077	1.872	0.014	1.488	0.026	3.121	1.787	0.315	0.041	15.449	0.677	0.486
WTKV01	26	Hb	45.283	0.841	10.991	0.105	12.280	0.194	13.973	11.003	1.043	0.209	95.92	6.694	0.093	1.915	0.012	1.518	0.024	3.080	1.743	0.299	0.039	15.418	0.670	0.484
WTKV01	27	Hb	45.991	0.557	10.933	0.063	12.209	0.173	14.291	11.594	1.057	0.190	97.06	6.718	0.061	1.882	0.007	1.491	0.021	3.112	1.814	0.299	0.035	15.443	0.676	0.483
WTKV01	28	Hb	43.747	0.659	10.284	0.084	11.885	0.237	14.088	11.529	1.106	0.196	93.82	6.643	0.075	1.841	0.010	1.509	0.030	3.189	1.876	0.326	0.038	15.538	0.679	0.483
WTKV01	29	Hb	46.360	0.646	10.793	0.071	12.232	0.173	13.889	11.311	1.101	0.243	96.82	6.780	0.071	1.860	0.008	1.496	0.021	3.028	1.772	0.312	0.045	15.394	0.669	0.479
WTKV01	30	Hb	45.042	0.566	10.563	0.067	11.977	0.191	14.171	11.180	1.002	0.204	94.96	6.724	0.064	1.858	0.008	1.495	0.024	3.154	1.788	0.290	0.039	15.444	0.678	0.488
WTKV01	35	Hb	43.297	0.675	10.142	0.076	11.928	0.184	13.927	11.262	1.153	0.201	92.84	6.646	0.078	1.835	0.009	1.531	0.024	3.187	1.852	0.343	0.039	15.545	0.675	0.483
WTKV04	54	Hb	46.053	1.224	8.516	0.067	14.083	0.088	13.055	11.796	1.078	0.459	96.42	6.862	0.137	1.495	0.008	1.755	0.011	2.900	1.883	0.311	0.087	15.449	0.623	0.443
WTKV04	55	Hb	45.397	1.037	7.582	0.176	13.277	0.056	14.180	12.033	1.007	0.398	95.14	6.852	0.118	1.349	0.021	1.676	0.007	3.191	1.946	0.295	0.077	15.531	0.656	0.468
WTKV04	65	Hb	45.635	1.016	8.789	0.092	14.375	0.014	13.346	11.972	1.227	0.488	96.95	6.785	0.114	1.540	0.011	1.787	0.002	2.958	1.907	0.354	0.092	15.549	0.623	0.445
WTKV04	69	Hb	45.119	0.922	12.169	0.017	11.620	0.163	14.313	11.147	1.342	0.205	97.02	6.579	0.101	2.091	0.002	1.417	0.020	3.112	1.742	0.379	0.038	15.481	0.687	0.495
WTKV04	70	Hb	45.460	0.796	11.580	0.034	11.870	0.198	14.724	10.556	1.166	0.239	96.62	6.649	0.088	1.996	0.004	1.452	0.025	3.210	1.654	0.331	0.045	15.452	0.689	0.506
WTKV04	71	Hb	46.307	0.742	10.752	0.042	11.949	0.202	14.946	11.129	1.080	0.221	97.37	6.726	0.081	1.841	0.005	1.451	0.025	3.236	1.732	0.304	0.041	15.442	0.690	0.502
WTKV04	72	Hb	46.953	0.777	10.022	0.063	12.943	0.187	15.848	9.982	0.959	0.260	97.99	6.781	0.084	1.706	0.007	1.563	0.023	3.412	1.544	0.269	0.048	15.437	0.686	0.522
WTKV04	73	Hb	47.244	0.759	9.987	0.096	13.073	0.208	15.742	9.377	0.986	0.211	97.68	6.829	0.082	1.701	0.011	1.580	0.026	3.392	1.452	0.276	0.039	15.390	0.682	0.526
WTKV05	74	Hb	41.075	1.099	11.339	0.000	20.701	0.344	8.020	11.683	0.915	1.482	96.66	6.394	0.129	2.080	0.000	2.694	0.045	1.861	1.948	0.276	0.294	15.722	0.409	0.284
WTKV05	75	Hb	42.728	0.656	11.021	0.017	19.139	0.572	9.446	11.701	1.008	1.360	97.65	6.513	0.075	1.980	0.002	2.439	0.074	2.146	1.911	0.298	0.264	15.702	0.468	0.327
WTKV05	82	Hb	45.898	0.632	7.392	0.000	16.456	0.339	11.586	12.365	0.444	0.680	95.79	6.980	0.072	1.325	0.000	2.093	0.044	2.627	2.015	0.131	0.132	15.417	0.557	0.388
WTKV05	83	Hb	43.971	0.457	10.006	0.004	19.259	0.426	10.053	12.094	0.692	1.122	98.08	6.648	0.052	1.783	0.001	2.435	0.055	2.266	1.959	0.203	0.216	15.618	0.482	0.337
WTKV10	87	Hb	51.348	0.181	1.864	0.000	8.741	0.420	12.998	23.149	0.393	0.018	99.11	7.451	0.020	0.319	0.000	1.061	0.052	2.812	3.599	0.111	0.003	15.427	0.726	0.374
WTKV10	88	Hb	51.762	0.297	2.832	0.026	9.641	0.347	13.065	21.895	0.414	0.084	100.36	7.406	0.032	0.478	0.003	1.153	0.042	2.787	3.356	0.115	0.015	15.387	0.707	0.380
WTKV10	89	Hb	43.902	0.479	9.580	0.017	16.048	0.299	11.571	11.987	0.776	0.970	95.63	6.704	0.055	1.724	0.002	2.049	0.039	2.634	1.961	0.230	0.189	15.587	0.562	0.394
WTKV10	90	Hb	42.844	0.958	10.107	0.000	16.073	0.274	11.064	12.265	0.792	1.130	95.51	6.579	0.111	1.829	0.000	2.064	0.036	2.533	2.018	0.236	0.221	15.625	0.551	0.381
WTKV12	93	Hb	42.190	1.782	11.596	0.148	15.390	0.121	11.612	11.894	1.559	1.363	97.66	6.336	0.201	2.052	0.018	1.933	0.015	2.600	1.914	0.454	0.261	15.785	0.574	0.402
WTKV12	94	Hb	42.014	1.880	11.035	0.178	14.673	0.071	11.272	11.462	1.569	1.264	95.42	6.429	0.216	1.990	0.021	1.877	0.009	2.571	1.879	0.465	0.247	15.705	0.578	0.406
WTKV07	98	Hb	43.667	1.823	11.448	0.013	12.945	0.043	13.322	11.622	2.279	0.535	97.70	6.436	0.202	1.988	0.001	1.595	0.005	2.927	1.835	0.651	0.101	15.743	0.647	0.460
WTKV07	104	Hb	39.420	2.041	13.508	0.017	13.209	0.097	12.116	11.533	2.591	0.696	95.23	6.032	0.235	2.436	0.002	1.690	0.013	2.764	1.891	0.769	0.136	15.967	0.621	0.435
WTKV07	105	Hb	42.572	1.824	12.079	0.043	12.466	0.147	13.316	11.728	2.330	0.548	97.05	6.323	0.204	2.114	0.005	1.548	0.019	2.948	1.866	0.671	0.104	15.801	0.656	0.462
WTKV11	116	Hb	45.542	0.658	10.489	0.025	15.056	0.251	12.166	11.540	1.059	0.284	97.07	6.751	0.073	1.832	0.003	1.866	0.031	2.689	1.833	0.304	0.054	15.437	0.590	0.419
WTKV11	117	Hb	44.535	0.530	10.490	0.038	14.641	0.233	12.405	11.492	1.119	0.314	95.80	6.695	0.060	1.859	0.005	1.841	0.030	2.780	1.851	0.326	0.060	15.506	0.602	0.428
WTKV11	118	Hb	44.786	0.638	10.399	0.042	14.684	0.308	12.258	11.592	1.059	0.246	96.01	6.716	0.072	1.838	0.005	1.841	0.039	2.740	1.862	0.308	0.047	15.468	0.598	0.423
WTKV13	125	Hb	41.092	1.674	3.901	0.000	20.151	0.000	3.839	11.396	0.076	1.143	83.27	7.431	0.228	0.831	0.000	3.047	0.000	1.035	2.208	0.027	0.264	15.071	0.254	0.165
WTKV13	126	Hb	42.495	1.875	9.544	0.081	20.833	0.414	8.554	11.253	1.436	1.025	97.51	6.542	0.217	1.731	0.010	2.682	0.054	1.963	1.856	0.429	0.201	15.685	0.423	0.300
WTKV13	127	Hb	42.674	1.829	9.626	0.000	20.339	0.351	8.604	11.118	1.561	1.235	97.34	6.567	0.212	1.746	0.000	2.617	0.046	1.974	1.833	0.466	0.242	15.702	0.430	0.305
WTKV06	130	Hb	38.378	0.874	13.515	0.042	19.012	0.160	8.699	11.744	1.633	1.992	96.05	6.027	0.103	2.501	0.005	2.497	0.021	2.037	1.976	0.497	0.399	16.064	0.449	0.312
WTKV06	131	Hb	37.591	0.646	13.277	0.084	19.072	0.156	8.667	12.099	1.711	1.866	95.17	5.982	0.077	2.490	0.011	2.538	0.021	2.056	2.063	0.528	0.379	16.144	0.448	0.308
WTKV06	135	Hb	37.604	0.832	13.348	0.096	18.705	0.132	8.737	11.737	1.639	1.935	94.76	5.992	0.100	2.507	0.012	2.492	0.018	2.075	2.004	0.506	0.393	16.099	0.454	0.315
WTKV06	136	Hb	37.080	0.811	13.447	0.063	18.557	0.085	8.728	11.986	1.701	1.962	94.42	5.940	0.098	2.539	0.008	2.486	0.012	2.085	2.057	0.528	0.401	16.153	0.456	0.314
WTKV06	140	Hb	38.248	0.559	13.520	0.059	19.541	0.135	8.623	11.753	1.879	1.987	96.30	6.013	0.066	2.505	0.007	2.569	0.018	2.021	1.980	0.573	0.399	16.150	0.440	0.307
WTKV01	14	Pl	43.345	0.037	32.141	0.000	0.074	0.072	0.000	17.744	1.416	0.000	94.83	2.114	0.001	1.847	0.000	0.003	0.003	0.000	0.927	0.134	0.000	5.029	0.005	0.000
WTKV01	15	Pl	45.629	0.000	33.096	0.061	0.034	0.018	0.000	17.805	1.695	0.007	98.35	2.140	0.000	1.829	0.002	0.001	0.001	0.000	0.894	0.154	0.000	5.022	0.010	0.000
WTKV01	16	Pl	46.261	0.000	32.708	0.009	0.048	0.051	0.000	17.167	1.980	0.035	98.26	2.167	0.000	1.806	0.000	0.002	0.002	0.000	0.862	0.180	0.002	5.021	0.007	0.000
WTKV01	17	Pl	45.595	0.013	32.102	0.004	0.056	0.018	0.000	16.971	1.885	0.015	96.66	2.171	0.000	1.801	0.000	0.002	0.001	0.000	0.866	0.174	0.001	5.016	0.006	0.000
WTKV01	18	Pl	45.594	0.007	32.551	0.000	0.055	0.000	0.000	17.190	1.848	0.035	97.28	2.158	0.000	1.816	0.000	0.002	0.000	0.000	0.872	0.170	0.002	5.020	0.006	0.000
WTKV01	19	Pl	44.772	0.742	10.717	0.067	11.900	0.191	14.231	11.458	1.116	0.208	95.40	2.318	0.029	0.654	0.003	0.515	0.008	1.099	0.636	0.112	0.014	5.387	0.681	0.487
WTKV01	20	Pl	89.167	0.084	6.666	0.000	0.000	0.000	0.014	3.233	0.679	0.016	99.86	3.669	0.003	0.323	0.000	0.000	0.000	0.001	0.143	0.054	0.001	4.194	0.992	0.006
WTKV01	31	Pl	98.137	0.013	0.001	0.000	0.086	0.000	0.020	0.012	0.039	0.000	98.31	3.996	0.000	0.000	0.000	0.003	0.000	0.001	0.001	0.003	0.000	4.005	0.288	0.255
WTKV01	32	Pl	44.719	0.024	32.419	0.000	0.037	0.000	0.000	17.545	1.591	0.039	96.37	2.140	0.001	1.828	0.000	0.001	0.000	0.000	0.899	0.148	0.002	5.020	0.010	0.000
WTKV01	33	Pl	44.681	0.045	32.399	0.013	0.100	0.022	0.000	17.430	1.825	0.000	96.51	2.137	0.002	1.826	0.000	0.004	0.001	0.000	0.893	0.169	0.000	5.033	0.004	0.000
WTKV01	34	Pl	44.856	0.000	32.110	0.000	0.019	0.000	0.000	17.109	1.870	0.020	95.99	2.153	0.000	1.817	0.000	0.001	0.000	0.000	0.880	0.174	0.001	5.026	0.018	0.000
WTKV01	36	Pl	45.517	0.000	32.640	0.039	0.113	0.022	0.000	17.606	1.592	0.018	97.55	2.151	0.000	1.818	0.001	0.004	0.001	0.000	0.891	0.146	0.001	5.013	0.003	0.000
WTKV01	37	Pl	46.191	0.052	32.893	0.079	0.024	0.025	0.000	16.954	2.034	0.000	98.25	2.163	0.002	1.815	0.003	0.001	0.001	0.000	0.850	0.185	0.000	5.019	0.015	0.000

Table 14. (continued)

Sample number	Anal. No.	Mineral	SiO2	TiO2	Al2O3	Cr2O3	FeO	MnO	MgO	CaO	Na2O	K2O	Total	Si	Ti	Al	Cr	Fe2+	Mn2+	Mg	Ca	Na	K	Total Cations (S)	Xmg (mg/(fe+mg))	Xmg (divalent)
WTKV01	38	Pl	45.359	0.000	32.803	0.048	0.116	0.069	0.000	17.835	1.705	0.016	97.95	2.138	0.000	1.823	0.002	0.005	0.003	0.000	0.901	0.156	0.001	5.028	0.003	0.000
WTKV01	39	Pl	54.149	0.038	27.085	0.022	0.042	0.018	0.005	10.206	4.632	1.855	98.05	2.505	0.001	1.477	0.001	0.002	0.001	0.000	0.506	0.415	0.109	5.017	0.184	0.001
WTKV01	40	Pl	45.995	0.000	32.193	0.035	0.325	0.000	0.098	16.359	2.003	0.054	97.06	2.179	0.000	1.797	0.001	0.013	0.000	0.007	0.830	0.184	0.003	5.015	0.349	0.008
WTKV01	41	Pl	45.633	0.000	32.531	0.000	0.034	0.000	0.000	17.402	1.836	0.023	97.46	2.157	0.000	1.812	0.000	0.001	0.000	0.000	0.881	0.168	0.001	5.022	0.010	0.000
WTKV01	42	Pl	96.218	0.000	0.010	0.066	0.003	0.000	0.000	0.027	0.003	0.019	96.35	3.997	0.000	0.000	0.002	0.000	0.000	0.000	0.001	0.000	0.001	4.002	0.098	0.009
WTKV05	76	Pl	54.415	0.016	27.132	0.000	0.090	0.000	0.000	11.521	5.111	0.244	98.53	2.497	0.001	1.467	0.000	0.003	0.000	0.000	0.566	0.455	0.014	5.003	0.006	0.000
WTKV05	77	Pl	55.188	0.042	27.107	0.071	0.133	0.000	0.000	10.435	5.284	0.277	98.54	2.522	0.001	1.460	0.003	0.005	0.000	0.000	0.511	0.468	0.016	4.987	0.004	0.000
WTKV05	84	Pl	101.644	0.000	0.019	0.000	0.012	0.000	0.004	0.010	0.000	0.010	101.70	3.999	0.000	0.001	0.000	0.000	0.000	0.000	0.000	0.000	0.000	4.001	0.392	0.236
WTKV10	85	Pl	54.170	0.000	27.574	0.005	0.056	0.037	0.000	11.131	5.175	0.226	98.37	2.487	0.000	1.492	0.000	0.002	0.001	0.000	0.547	0.461	0.013	5.004	0.009	0.000
WTKV10	86	Pl	52.552	0.000	28.804	0.022	0.144	0.000	0.003	12.220	4.643	0.204	98.59	2.418	0.000	1.562	0.001	0.006	0.000	0.000	0.602	0.414	0.012	5.014	0.038	0.000
WTKV12	92	Pl	53.457	0.101	28.624	0.036	0.238	0.000	0.000	12.201	4.710	0.178	99.54	2.435	0.003	1.536	0.001	0.009	0.000	0.000	0.595	0.416	0.010	5.006	0.002	0.000
WTKV07	100	Pl	56.326	0.089	25.863	0.000	0.393	0.033	0.331	9.153	6.198	0.107	98.49	2.571	0.003	1.391	0.000	0.015	0.001	0.023	0.448	0.549	0.006	5.007	0.601	0.046
WTKV11	110	Pl	54.159	0.018	28.119	0.058	0.043	0.000	0.000	11.089	5.532	0.071	99.09	2.470	0.001	1.511	0.002	0.002	0.000	0.000	0.542	0.489	0.004	5.020	0.012	0.000
WTKV11	111	Pl	55.732	0.000	27.268	0.000	0.118	0.037	0.000	9.870	6.278	0.014	99.32	2.527	0.000	1.457	0.000	0.004	0.001	0.000	0.479	0.552	0.001	5.021	0.004	0.000
WTKV11	112	Pl	54.653	0.004	27.705	0.013	0.115	0.000	0.000	10.577	5.737	0.048	98.85	2.494	0.000	1.490	0.000	0.004	0.000	0.000	0.517	0.507	0.003	5.016	0.005	0.000
WTKV11	113	Pl	46.248	0.284	10.223	0.000	14.559	0.179	12.770	11.520	1.099	0.227	97.11	2.373	0.011	0.618	0.000	0.625	0.008	0.977	0.633	0.109	0.015	5.369	0.610	0.436
WTKV11	114	Pl	45.787	0.404	10.369	0.000	14.628	0.244	12.679	11.386	1.068	0.223	96.79	2.360	0.016	0.630	0.000	0.630	0.011	0.974	0.629	0.107	0.015	5.370	0.607	0.434
WTKV11	115	Pl	46.550	0.250	9.690	0.000	14.344	0.248	13.149	11.364	1.062	0.224	96.88	2.391	0.010	0.587	0.000	0.616	0.011	1.007	0.625	0.106	0.015	5.366	0.620	0.446
WTKV11	119	Pl	52.702	0.000	28.428	0.013	0.089	0.000	0.011	11.992	4.915	0.058	98.21	2.431	0.000	1.546	0.000	0.003	0.000	0.001	0.593	0.440	0.003	5.017	0.180	0.001
WTKV11	120	Pl	53.625	0.000	27.846	0.005	0.063	0.000	0.000	11.172	5.230	0.028	97.97	2.471	0.000	1.512	0.000	0.002	0.000	0.000	0.552	0.467	0.002	5.007	0.008	0.000
WTKV11	121	Pl	54.526	0.106	27.327	0.009	0.094	0.037	0.000	10.432	5.544	0.059	98.13	2.504	0.004	1.479	0.000	0.004	0.001	0.000	0.513	0.494	0.003	5.002	0.006	0.000
WTKV13	122	Bi	35.402	4.469	13.278	0.012	22.264	0.172	10.022	0.000	0.019	9.183	94.82	2.770	0.263	1.224	0.001	1.457	0.011	1.169	0.000	0.003	0.916	7.814	0.445	0.443
WTKV13	123	Bi	36.059	4.655	13.433	0.000	22.175	0.225	10.014	0.032	0.043	8.898	95.53	2.788	0.271	1.224	0.000	1.434	0.015	1.154	0.003	0.006	0.877	7.771	0.446	0.443
WTKV13	124	Bi	33.751	5.047	12.625	0.041	21.956	0.186	9.400	0.028	0.081	8.955	92.07	2.734	0.307	1.205	0.003	1.487	0.013	1.135	0.002	0.013	0.925	7.824	0.433	0.430

9. Appendix

Petrological Descriptions

Sample Number: WTKV 01

Sample Locality: 10°36'7.70"N, 78°12'53.70"E

Rock Type: meta-gabbro

Sample Description:

The sample is dominated by large plagioclase grains (up to 7.5mm in length) and lenticular to tabular hornblende grains (avg. 0.5mmin length).

A visual estimate of the minerals present is:

Plagioclase	~53%
Hornblende	~42%
Quartz	~ 4%
Ilmenite	trace
Carbonate (calcite?)	trace
Rutile	trace
Chlorite	trace

The plagioclase is highly poikiloblastic (sieve textured) containing rounded inclusions of quartz up to 70 µm in diameter and rare rounded rutile of roughly the same size. Minor retrograde chlorite and carbonate are also present. The poikiloblastic plagioclase has been recrystallised into finer grained polygonal aggregates along grain boundaries (see Vernon, 1976 p 137).

Hornblende seems to have replaced igneous pyroxene. It is pleochroic from pale yellow green to pale green and major element geochemistry suggests that it is intermediate in composition and pseudo-polygonal.

Ilmenite occurs as acicular grains up to 0.5mm in length and as xenoblastic grains up to 0.2mm in diameter. The ilmenites have been oxidised with hematite inclusions present as small, blebby grains. In the xenoblastic ilmenite grains the hematite can outline grain boundaries.

Sample Number: WTKV 02

Sample Locality: 10°34'45.20"N, 78°15'8.40"E

Rock Type: Quartzite

Sample Description:

The sample is dominated by coarse grained quartz, with grains up to 1.8cm in length. The larger grains exhibit undulose extinction and sub-grain development with finer grained recrystallised quartz developing along quartz-quartz grain boundaries. Quartz grains are lenticular and are parallel with sillimanite which exhibits a strong preferred orientation and is fabric forming.

A visual estimate of the minerals present is:

Quartz	~90%
Sillimanite	~ 7%
Ilmenite	~ 2%
Muscovite	trace
Biotite	trace
Cordierite	trace
Zircon	trace
Monazite	trace
Tourmaline	trace

The sillimanite grains reach lengths of up to 1mm and fibrolitic and prismatic variants are present. Pinitised cordierite grains are rare and can be up to 1mm in length and contain inclusions of sillimanite. Biotite is also rare and is pleochroic from pale yellow to a mid-brown/green colour. Ilmenite grains tend to be rounded, included in quartz and range in size up to 0.4mm.

Detrital accessories include tourmaline, monazite and zircon, and rare retrograde muscovite (sericite) is also present.

Sample Number: WTKV 03

Sample Locality: 10°34'41.50"N, 78°15'8.40"E

Rock Type: Quartzite

Sample Description:

The sample is dominated by quartz with grains reaching up to 1.2cm in length. It is dissimilar to WTKV02 in that sillimanite is absent and there is abundant ragged and oxidised biotite which can be associated with muscovite. The quartz grains exhibit undulose extinction, sub-grain development and minor recrystallisation. Sutured grain boundaries are common.

A visual estimate of the minerals present is:

Quartz	~ 98%
Biotite	~ 1%
Rutile	trace
Muscovite	trace
Zircon	trace
Monazite	trace

The detrital accessory phases are relatively course grained and generally range in size up to 0.25mm in diameter.

Sample Number: WTKV 04

Sample Locality: 10°35'58.70"N, 78° 9'39.20"E

Rock Type: Layered gabbro

Sample Description:

The sample is dominated by plagioclase (labradorite) and two pyroxenes and has an average grain size of 0.25mm. Plagioclase grains are randomly oriented and there is no fabric developed in the sample.

A visual estimate of the minerals present is:

Plagioclase (labradorite)	~ 33%
Orthopyroxene	~ 20%
Clinopyroxene	~ 20%
Hornblende	~ 20%
Ilmenite	~ 2%
Goethite	trace
Pyrite	trace
Chalcopyrite	trace
Apatite	trace

The layering is caused by linear replacement of pyroxenes by fine grained equigranular green hornblende. Associated coarser grained hornblende is highly poikiloblastic. Elsewhere pyroxenes are rimmed by green hornblende which can also rim ilmenite.

The hornblende is mid green in colour. Orthopyroxene is pleochroic from pale green to pale pink. Associated clinopyroxene is a very pale green in colour. Rounded orthopyroxene grains can be present as inclusions in clinopyroxene. Ilmenite can be up to 0.3mm in diameter and tends to occur as inclusions in pyroxenes.

Minor chalcopyrite and pyrite are present and goethite can partially replace both minerals. Trace apatite is present. The sample is gabbroic textured however some polygonal textures can be observed in some ilmenites with pyrite in triple junctions.

Sample Number: WTKV 05

Sample Locality: 10°35'34.50"N, 78°10'21.70"E

Rock Type: Layered anorthositic gabbro

Sample Description:

The sample is dominated by hornblende and plagioclase with the latter being up to 1cm in length. Plagioclase grains can be highly poikiloblastic with rounded quartz inclusions and can be partially replaced by fine grained, retrograde sericite-carbonate-clinozoisite.

A visual estimate of the minerals present is:

Plagioclase	~ 63%
Hornblende	~ 31%
Quartz	~ 2%
Rutile	~ 1%
Chlorite	~ 1%
Goethite	~ 1%
Biotite	trace
Clinozoisite	trace
Carbonate	trace
Sericite	trace

The hornblende is pleochroic from pale green/yellow to mid green. The grains can be polygonal textured and contain rounded to elongate inclusions of plagioclase. Hornblende can be partially replaced by a deep green chlorite.

The sample contains abundant rutile with grains up to 1.2mm in length. The rutile is present as inclusions in hornblende and plagioclase. Trace biotite is present and there is abundant accessory goethite replacing former sulphide. The sample contains no Ilmenite.

Sample Number: WTKV 06

Sample Locality: 10°33'22.70"N, 78° 9'34.80"E

Rock Type: Hedenbergite-scapolite calc silicate

Sample Description:

The sample is dominated by polygonal textured hedenbergite and associated scapolite. It has an average grain size of 1.2mm with scapolite always finer grained.

A visual estimate of the minerals present is:

Hedenbergite	~ 91%
Scapolite	~ 5%
Carbonate	~ 2%
Ferrohastingsite	~ 1%
Plagioclase (anorthite)	trace
Sphene	trace
Apatite	trace
Chalcopyrite	trace

The hedenbergite is a pale green colour and can be partially replaced by a deep emerald green ferrohastingsite which often develops along hedenbergite grain boundaries. The scapolite is colourless, highly birefringent and exhibits parallel extinction.

Trace prograde carbonate (part of the polygonal textured groundmass) is present as well as trace plagioclase, sphene, apatite and chalcopyrite.

Sample Number: WTKV 07

Sample Locality: 10°33'23.30"N, 78° 9'40.60"E

Rock Type: Layered gabbro

Sample Description:

The sample is dominated by plagioclase, pyroxenes and hornblende and has an average grain size of 0.35mm.

A visual estimate of the minerals present is:

Plagioclase	~37 %
Clinopyroxene	~ 23%
Orthopyroxene	~22%
Hornblende	~ 15%
Ilmenite	~2 %
Pyrite	trace
Chalcopyrite	trace
Pyrrhotite	trace
Goethite	trace

Pseudo-polygonal textures are developed in the plagioclase. Mid- to olive green hornblende rims ilmenite. Clinopyroxene and orthopyroxene appear very similar in this sample. Pyrrhotite up to 0.2mm in diameter contains lamellae of chalcopyrite.

Sample Number: WTKV 08

Sample Locality: 10°34'52.00"N, 78°11'4.00"E

Rock Type: Meta-gabbro

Sample Description:

The sample is dominated by plagioclase with grains up to 12.5mm. The plagioclase is poikiloblastic with rounded quartz inclusions.

A visual estimate of the minerals present is:

Plagioclase	~ 72%
Hornblende	~ 20%
Ferrian Ilmenite	~ 2%
Titan hematite	~ 3%
Biotite	~ 1%
Chlorite	~ 1%
Oxidised pyrite	trace
Anatase	trace
Goethite	trace
Epidote	trace
Quartz	trace

Hornblende is also poikiloblastic with pleochroism from mid green to pale yellow. Large grains of ferrian Ilmenite (up to 3.25mm) exsolve titan hematite which in turn exsolves ferrian ilmenite. Biotite is dark brown in colour indicating high TiO_2. Trace epidote is highly birefringent and pleochroic from pale yellow to almost colourless. Chlorite is iron rich and deep green and is associated with epidote, in places replacing epidote.

Sample Number: WTKV 09

Sample Locality: 10°34'3.80"N, 78°10'9.40"E

Rock Type: metamorphosed anorthositic gabbro

Sample Description:

The sample is dominated by plagioclase which contains needles of an unidentified mineral and has grains up to 3.5 mm in diameter. The plagioclase exhibits pericline twinning.

A visual estimate of the minerals present is:

Plagioclase	~ 74%
Hornblende	~ 14
Quartz	~ 3%
Sericite	~ 2%
Clinopyroxene	~ 2%
Chlorite	~ 2%
Biotite	~ 1%
Ilmenite	~ 1%
Carbonate	trace
Epidote/clinozoisite	trace
Zircon	trace
Hematite	trace
Apatite	trace
?Cummingtonite	trace

Hornblende exhibits both pale green to dark blue/green and pale green to pale yellow pleochroism. The hornblende can be intergrown with rare ?cummingtonite. Ilmenite is being altered to hematite along fractures and along grain boundaries. Retrograde sericite, carbonate and epidote/clinozoisite develop in some plagioclase grains. Quartz occurs along recrystallised plagioclase grain boundaries with recrystallised polygonal textured plagioclase. Rare clinopyroxene can be located as relicts within some hornblende.

Sample Number: WTKV 10

Sample Locality: 10°34'11.40"N, 78° 9'49.00"E

Rock Type: Anorthositic gabbro

Sample Description:

The sample is dominated by plagioclase, some of which exhibits pericline twinning. The plagioclase exhibits polygonal textures in recrystallised domains along plagioclase-plagioclase grain boundaries. Grains of up to 4mm remain.

A visual estimate of the minerals present is:

Plagioclase (labradorite)	~ 79%
Hornblende	~ 12%
Carbonate	~ 4%
Ferrian-ilmenite	~ 2%
Biotite	~ 1%
Chlorite	~ 1%
Titan-hematite	trace
Magnetite	trace
Goethite	trace
Pyrite	trace
Chalcopyrite	trace

Hornblende is present as both mid blue/green to pale green in pleochroism and as almost colourless to pale green in pleochroism. Pyrite and chalcopyrite are being replaced by goethite. Carbonate and chlorite replace hornblende. Titan hematite is exsolved by ferrian-ilmenite in some grains. Chalcopyrite occurs both alone and as small (to 12.5µm) rounded inclusions in pyrite. Magnetite is also present and biotite rims several of the oxide grains.

Sample Number: WTKV 11

Sample Locality: 10°34'10.90", N 78° 9'45.70"E

Rock Type: Meta-gabbro

Sample Description:

The sample is dominated by green hornblende and plagioclase. Some grains of hornblende are highly poikiloblastic with rounded inclusions of quartz.

A visual estimate of the minerals present is:

Plagioclase (labradorite)	~ 47%
Hornblende	~ 47%
Quartz	~ 3%
Ferrian-ilmenite	~ 2%
Titan-hematite	trace
Goethite	trace
Pyrite	trace
Biotite	trace

Some plagioclase grains exhibit pericline twinning and myrmekitic textures Hornblende is pleochroic from deep green to pale yellow. Pyrite is being oxidised to goethite. Trace biotite rims ferrian-ilmenite which is exsolving titan hematite.

Sample Number: WTKV 12

Sample Locality: 10°36'3.60"N, 78° 9'49.60"E

Rock Type: Layered gabbro-norite

Sample Description:

The sample is dominated by fine grained plagioclase, hornblende, clinopyroxene and orthopyroxene.

A visual estimate of the minerals present is:

Plagioclase (labradorite)	~ 31%
Hornblende	~ 25%
Orthopyroxene	~ 25%
Clinopyroxene	~ 15%
Ilmenite	~ 4%

Hornblende is pleochroic from mid brown to light green and contains abundant ultra-fine grained Ilmenite inclusions which have exsolved from an original titaniferous magmatic amphibole. Rounded inclusions of hornblende are also present in plagioclase. The largest grains of plagioclase reach 0.75mm in diameter, with pyroxenes and hornblendes generally finer grained.

Clinopyroxene exhibits pleochroism from pale pink to almost colourless. Ilmenite occurs throughout the sample and the larger grains are around 0.5mm, with most grains being finer than this.

Sample Number: WTKV 13

Sample Locality: 10°35'10.50"N, 78°14'42.90"E

Rock Type: Felsic gneiss

Sample Description:

The sample is dominated by K-feldspar, quartz, plagioclase and biotite with quartz grains up to 2.5mm.

A visual estimate of the minerals present is:

Quartz	~ 36%
K-feldspar	~ 32%
Plagioclase	~ 17%
Biotite	~ 6%
Hornblende	~ 5%
Magnetite	~ 2%
Ilmenite	~ 1%
Pyrite	trace
Zircon	trace
Apatite	trace

Quartz grains contain needle-like inclusions and grains reach 2mm in diameter. K-feldspar is strongly perthitic and plagioclase is present as large myrmekitic aggregates. Biotite rims magnetite in places and is present as ragged lenticular aggregates. Hornblende is often poikilitic and often occurs with biotite.

Sutured grain boundaries occur extensively throughout the sample between quartz grains. Quartz can often occur along K-feldspar-K-feldspar grain boundaries. Accessory zircon and apatite are present and the latter is tabular to rounded with grains up to 0.3mm in diameter.

Sample Number: WTKV 14

Sample Locality: 10°34'10.30"N, 78°11'25.10"E

Rock Type: Quartzite

Sample Description:

The sample is dominated by quartz with grains up to 5mm. The quartz in this sample has been recrystallised and is therefore much finer grained when compared to samples WTKV02 and WTKV03.

A visual estimate of the minerals present is:

Quartz	~ 99%
Muscovite	trace
Zircon	trace
Rutile	trace
Titan hematite	trace
Ferrian Ilmenite	trace
Clays	trace

Muscovite often develops as a fringe on opaque oxides. Zircons are up to 90µm in diameter. Rutile is present as an alteration product of Ilmenite and also as rare discreet grains. Ferrian Ilmenite exsolves titan hematite and the latter can exsolve ferrian Ilmenite.

Sample Number: WTKV 15

Sample Locality: 10°35'27.20"N, 78° 9'45.40"E

Rock Type: Quartzite

Sample Description:

The sample is dominated by1 elongate quartz grains up to 0.8cm with grain boundaries pinned by sillimanite and muscovite. The latter replaces sillimanite.

A visual estimate of the minerals present is:

Quartz	~ 93%
Muscovite	~ 2%
Titan-hematite	~ 1%
Hematite	~ 1%
Ferrian ilmenite	~ 1%
Magnetite	~ 1%
Sillimanite	trace
Biotite	trace
Goethite	trace
Rutile	trace
Tourmaline	trace
Zircon	trace
Monazite	trace

Tabular ferrian Ilmenite and titan hematite grains are fabric forming as is trace sillimanite and muscovite. Magnetite grains are present and are often partially replaced by secondary hematite. Trace sillimanite is present in quartz and generally occurs as acicular grains up to 0.1mm. Fibrolitic sillimanite grains contained within muscovite are coarser grained.

Zircons up to 40 µm in diameter are rounded as is monazite which can be up to 0.15mm in diameter. Trace tourmaline, biotite and rutile are also present as accessory phases.